

SHRP-A-335

Binder Characterization and Evaluation by Nuclear Magnetic Resonance Spectroscopy

Principal Investigator: Dr. P.W. Jennings

Co-Principal Investigator: J.A. Pribanic

Research Associates: Dr. M.A. Desando

Dr. M.F. Raub

Researchers: F. Stewart

J. Hoberg

R. Moats

Technical Staff: J.A. Smith

T.M. Mendes

M. McGrane

Department of Chemistry

Montana State University

Bozeman, Montana

Co-Principal Investigators: Dr. B. Fanconi

Dr. D.L. VanderHart

Research Associate: Dr. W.F. Manders

Polymers Division

National Institute of Standards and Technology

Gaithersburg, Maryland



Strategic Highway Research Program

National Research Council

Washington, DC 1993

Publ. No. SHRP-A-335
ISBN 0-309-05252-1
Contract A-002C

Program Manager: *Edward T. Harrigan*
Project Manager: *Jack Youtcheff*
Program Area Secretary: *Juliet Narsiah*
Production Editor: *Katharyn Bine Brosseau*

May 1993

key words:
aliphatic characteristics
aromaticity
asphalt
functional group analysis
materials reference library (MRL)
MRL core asphalts
methylation
micellar model
molecular diffusion
multiple-pulse proton spectra
pi-pi interactions
proton lineshapes
spin diffusion
van der Waals interactions

Strategic Highway Research Program
2101 Constitution Avenue N.W.
Washington, DC 20418

(202) 334-3774

The publication of this report does not necessarily indicate approval or endorsement by the National Academy of Sciences, the United States Government, or the American Association of State Highway and Transportation Officials or its member states of the findings, opinions, conclusions, or recommendations either inferred or specifically expressed herein.

©1993 National Academy of Sciences

Acknowledgments

The research described herein was supported by the Strategic Highway Research Program (SHRP). SHRP is a unit of the National Research Council that was authorized by section 128 of the Surface Transportation and Uniform Relocation Assistance Act of 1987.

Table of Contents

Acknowledgments	iii
List of Figures	ix
List of Tables	xiii
List of Schemes	xv
Abstract	1
Executive Summary	3
1. Solution NMR Characterization of Asphalts	9
Introduction	9
Purpose and organization of the report	10
Results and discussion	11
The hydrocarbon portion of the SHRP core asphalts	11
Aromatic hydrogen	11
Aromatic carbon	12
Description of aliphatic characteristics	13
Description of aromatic characteristics	15
Attempted use of shift reagents to enhance resolution of NMR spectra	17
Summary: Aliphatic and aromatic characteristics of core asphalts	17
Heteroatoms in asphalt structure	18
Functional groups containing oxygen	19
Phase-transfer methylation	19
Methylation using labelled diazomethane	21
Comparison of methylation procedures	22
Other experiments for analysis of heteroatoms	23
Summary of work on heteroatom-containing functional groups	26
Average molecular structures of core asphalts	27
Derivation of average structures	27
Discussion of average structures	29
Summary and ramifications of average structures	30

Effects of oxidation on asphalt chemical characteristics	31
Effects on percentage of aromatic carbon	32
Effects on some oxygen-containing functional groups	33
Summary of oxidation effects	34
Fractions from Ion Exchange Chromatography	35
Summary and Conclusions	36
References	39
 2. Solid State NMR Characterization of SHRP Core Asphalts	75
Introduction	75
General Comments	75
Brief review of the kinds of experiments and the nature of the corresponding information	75
Importance of the micellar model as a theory to be tested	76
Results and Discussion	77
Perspective on the use of ^{13}C versus ^1H NMR techniques	77
Proton FID lineshapes	78
Temperature dependence	78
Spectra of components versus the spectrum of a whole asphalt	81
Influence of temporal aging on the ^1H lineshapes	82
Lineshape changes accompanying oxidation	82
Measurement of changes in molecular mobility upon mixing asphalt and aggregate	84
Sample preparation	84
NMR method	85
Summary of asphalt/aggregate results	85
Multiple-pulse proton spectra: The partial resolution of aromatic and aliphatic protons	86
Spin diffusion measurements and estimates of domain size for motional and compositional heterogeneities	86
Spin diffusion measurements based on mobility gradients	87
Spin diffusion measurements based on chemical aromatic/aliphatic composition	89
Comments on the interpretation of spin diffusion data	91
Miscellaneous experiments testing for the existence of large domains	94
Summary and Concluding Remarks	97

Summary of NMR findings	97
Brief comments on these findings	100
References	101
Appendix A. Solution NMR Spectroscopy	127
¹ H-NMR spectroscopy	127
¹³ C-NMR spectroscopy	127
Purification of tetrahydrofuran	128
Short-term phase-transfer methylation	129
Long-term phase-transfer methylation of asphalt	129
Methylation of asphalt with sodium hydride and [¹³ C]-iodomethane	130
Double methylation of asphalt with sodium hydride and [¹³ C]-iodomethane	130
Methylation of asphalt with [¹³ C]- diazomethane	131
Reduction of asphalt with sodium borohydride	131
Reduction of asphalt with lithium aluminum hydride	131
Asphalt O-methylated with iodomethane, reduced with lithium aluminum hydride, O-methylated with [¹³ C]-iodomethane	132
Methoximation of asphalt	133
Phosphorylation of asphalt with CDMPOPS	133
Phosphorylation of asphalt with ethylene chlorophosphite	133
Appendix B. NMR Basics for Data Interpretation, Solid State NMR Spectroscopy	135
Dipolar interaction	135
Chemical shift	139
Magic angle spinning	139
Magnetization	140
Relaxation	140
Spin diffusion	140
Cross-polarization	141

List of Figures

Part 1

Figure 1. Percentage of aromatic hydrogen in core asphalts	42
Figure 2. Example of ^1H -NMR spectrum of asphalt	43
Figure 3. Percentage of aromatic carbon in core asphalts	43
Figure 4. Typical spectrum from DEPT 135 experiment	44
Figure 5. Typical spectrum from DEPT 90 experiment	44
Figure 6. ^{13}C -NMR spectrum of aliphatic region, showing integration limits for peaks identified by number in Tables 5 and 6	45
Figure 7. Aromatic Substitution Index (ASI) for eight core asphalts	46
Figure 8. Methoxy region of ^{13}C -NMR spectrum of asphalt after phase-transfer methylation treatment	46
Figure 9. Methoxy regions of ^{13}C -NMR spectra after short-term PTM	47
Figure 10. Example of aromatic and hydrolysis-resistant oxygen functionalities	47
Figure 11. Methoxy regions of ^{13}C -NMR spectra after long-term PTM	48
Figure 12. Comparisons of ^{13}C -NMR spectra of methoxy regions of core asphalts after one reaction with diaxomethane and after second reaction	49
Figure 13. ^{13}C -NMR spectra resulting from LAH reduction and subsequent methylation of esters and ketones	50
Figure 14. Comparison of aromatic carbon content before and after POV and TFO/POV oxidation	51

Figure 15. Change in aromatic carbon percentage after POV oxidation	52
Figure 16. Change in aromatic percentage after TFO/POV oxidation	52
Figure 17. Susceptibility to POV and TFO/POV oxidation: change in Wt% O as COOH plus OH	53

Part 2

Figure 1. Carbon-13 non-spinning spectra of AAH-1	103
Figure 2. Temperature-dependent proton spectra of AAG-1	104
Figure 3. 160 kHz spectral displays of core asphalts	105
Figure 4. Full width at half height of proton spectra at various temperatures	106
Figure 5. Illustration of hysteresis in linewidth for asphalts AAC-1 and AAF-1 ...	107
Figure 6. FID proton spectra of the asphalts indicated	108
Figure 7. Spectra showing that malthenes and asphaltenes are not separate phases in asphalts	109
Figure 8. Proton spectra of AAF-1 at 300 K	110
Figure 9. Proton spectra of AAF-1 at 340 K	111
Figure 10. Echo profile showing that D and G have different rates of decay, which is expected based on their linewidth difference	112
Figure 11. Echo decay illustrating that the profile is sensitive to a change in mobility corresponding to a 2° temperature change	112
Figure 12. Echo decays for AAG-1 and several solids including the RJ aggregate ..	113
Figure 13. Echo decays for AAD-1 and its mixtures with various solids	113
Figure 14. Normalized MP proton spectra of AAG-1 and AAD-1 using the MREV-8 sequence	114
Figure 15. Example mobility-based spin-diffusion spectra of AAG-1	115
Figure 16. MP spin-diffusion spectrum of asphalt AAG-1	116

Figure 17. Chemical shift based, MP spin-diffusion spectra of AAC-1	117
Figure 18. Comparison of chemical-shift-based spin diffusion data from a PBI/PEI polymer blend and asphalt AAC-1	118
Figure 19. MP proton spectra as a function of MO spin locking in a $T_{1\rho}$ experiment (A-C)	119
Figure 20. T_1 zero-crossing-spectra for AAG-1 and AAK-1, using MP and FID readouts respectively	120
Figure 21. Proton T_1 -zero-crossing experiment at 200 K for asphalt AAD-1 using cross-polarized ^{13}C signals	121
Figure 22. CP-MAS spectra of the AAD-1 and AAG-1 strong acid fractions	122
Figure B-1. Proton spectra illustrating the influence of proton distribution and motion	136
Figure B-2. Typical proton linewidths versus correlation time for isotropic and particular anisotropic motion	138

List of Tables

Part 1

Table 1. Outline of SHRP A-002C workplans	54
Table 2. Percent aromatic carbon and hydrogen from ^{13}C - and ^1H -NMR spectroscopy	55
Table 3. Resonance assignments for ^1H -NMR spectra	56
Table 4. Approximate ratio of protons between 2 and 5 ppm (including benzylic protons) to all aliphatic protons in core asphalts	56
Table 5. Peak assignments for aliphatic region of ^{13}C spectra of asphalts	57
Table 6. Number of aliphatic carbon atoms per average molecule in each ^{13}C -NMR peak area	58
Table 7. Molecular weights and formulae for SHRP core asphalts	58
Table 8. Data for average structures of core asphalts	59
Table 9. Concentrations of phenols and carboxylic acids from short-term phase transfer methylation	59
Table 10. Concentrations of phenols and carboxylic acids from long-term phase transfer methylation	60
Table 11. Concentrations of aliphatic carboxylic acids from methylation of asphalt using diazomethane	60
Table 12. Concentrations of phenols and carboxylic acids from recommended procedures	61

Table 13. Concentrations of primary alkylamines from ^{31}P -NMR spectra of asphalts phosphorylated with CDMPOPS	61
Table 14. Changes in percent aromatic carbon during oxidation	62
Table 15. Changes in percent aromatic hydrogen during oxidation	62
Table 16. Change in maximum possible ratio of benzylic to all aliphatic protons with oxidation	62
Table 17. Changes in measured OH+COOH after POV and TFO/POV oxidation . .	63
Table 18. Changes in concentrations of oxygen-containing functional groups after POV and TFO/POV oxidation, from short-term PTM	64
Table 19. Possible reactions in TFO/POV for core asphalts	65
Table 20. Percent aromatic carbon in some fractions from ion exchange chromatography	65
Table 21. Percentage of total aromatic carbon supplied by IEC fractions	66

Part 2

Table 1. Viscosities ($\times 10^{-3}$ poises) for the core asphalts at 298 and 333 K and some selected viscosities for oxidized samples	123
Table 2. Ratios of base proton intensities of various asphalts with respect to the base intensity of asphalt	124
Table 3. Times required, at 300 K, for protons to reach internal spin equilibrium following the production of the polarization gradients indicated	124
Table 4. Spin diffusion times for attaining spin equilibrium in a <i>mobility-based</i> experiment at different temperatures using FID-lineshape monitoring . . .	125
Table 5. Proton aromatic fractions ^a (f_{AR}^{H}) and mass fractions ^b ($m(x)$) associated with IEC separations	125

List of Schemes

Scheme I.	Phase-transfer methylation reaction	66
Scheme II.	Derivatization of primary amines	66
Scheme III.	Sodium hydride for deprotonation prior to methylation of -OH and -COOH groups	67
Scheme IV.	Potassium ethoxide and 18-crown-6 ethers for deprotonation	67
Scheme V.	Methoximation reaction for analysis of ketones	67
Scheme VI.	Lithium aluminum hydride reduction	67
Scheme VII.	Sodium borohydride in analysis of ketones	68
Scheme VIII.	Bis (tri-n-butyltin) oxide derivatization	68
Scheme IX.	Formation of trimethylsilyl derivative	68
Scheme X.	Derivatization of sulfides	68
Scheme XI.	Average molecular structures of core asphalts	69 - 72
Scheme XII.	Possible reactions under oxidizing conditions in asphalt	73

Abstract

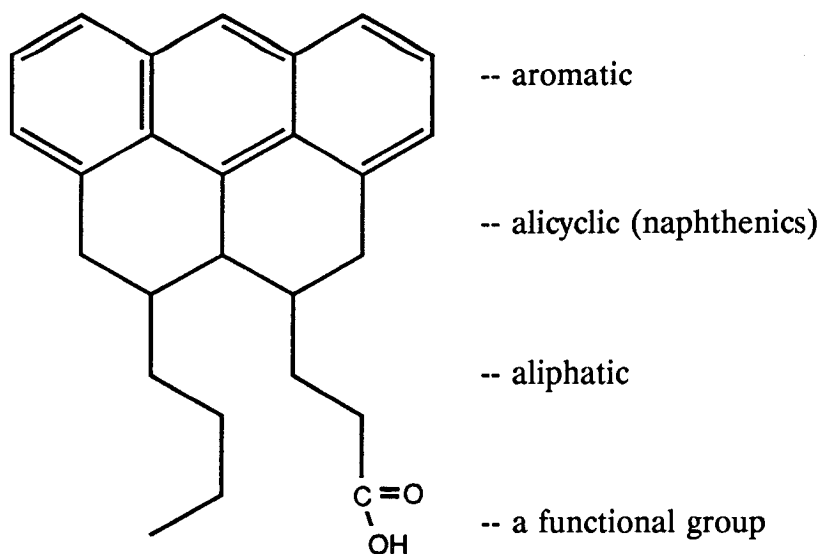
Nuclear magnetic resonance (NMR) spectroscopy was used in solution-state and solid-state experiments on eight asphalt cements. Using a variety of chemical and solution-state NMR spectroscopic techniques, data were obtained about the amounts of aromatic carbon in an average molecule of the asphalt sample, how that carbon is arranged in terms of the size of the average aromatic system and the extent of substitution. The arrangement of the aliphatic portion has also been described in terms of the average number of alicyclic rings, of aliphatic chain length and extent of branching. Concentrations of carboxylic acids and phenols were measured both before and after laboratory oxidative aging. All these data show both surprising similarities and significant differences among the asphalts studied.

By using solid-state NMR spectroscopic techniques, the structure of asphaltic cements was probed on a small-distance scale of a few angstroms to 30 μm . Differences in molecular mobility were found among the asphalts studied. Changes in molecular mobility after laboratory oxidative aging were found to be small. The implications of these data with regard to the "micellar model" of asphalt are discussed. The research results' potential impact on understanding asphalt cement properties is explored.

Executive Summary

Nuclear Magnetic Resonance (NMR) spectroscopy is an analytical tool commonly used to study the molecular structures of chemical compounds. In this project, NMR spectroscopy has been used in two ways: 1) with the asphalt sample in solution ("solution-state"), some details about the overall chemical nature of asphalts have been obtained; 2) Using neat asphalt ("solid-state"), the ability of asphalt molecules to assemble into rigid structures has been investigated.

The solution-state NMR work has concentrated on three characteristics of the asphalts: the aromatic portion, the aliphatic portion (including both alicyclic and chain-type structures) and several functional groups (see sketch below).



These characteristics are important because they are responsible for different kinds of interactions between molecules--interactions which contribute to the behavior of the asphalt. For example, the flat aromatic systems can stack one-above-another to form what are known as pi-pi interactions which can hold molecules together. These interactions are stronger between larger systems with fewer substituents.

Another mode of molecular interaction arises between aliphatic chains. These van der Waals interactions are stronger between longer chains with fewer branches.

Polar interactions, including hydrogen bonding, are also potential contributors to self-assembly in asphalts. These involve heteroatoms such as oxygen, nitrogen or sulfur and could associate two molecules or perhaps two pi-bound stacks. However, concentrations of heteroatoms are very low in asphalts.

Using a variety of chemical and solution-state NMR spectroscopic techniques to study eight SHRP asphalts, data has been obtained about the amounts of aromatic carbon in an average molecule, and how that carbon is arranged in terms of size of the average aromatic system and the extent of substitution. Characteristics of the aliphatic portion may also be described in terms of alicyclic rings, length of average aliphatic chain and extent of branching. Concentrations of phenols and carboxylic acids have also been measured both before and after laboratory oxidative aging. All these data show both surprising similarities and significant differences among these asphalts. These findings alone do not solve the puzzle of asphalt performance but, when combined with results from other SHRP research efforts, they will contribute significantly to understanding the relationships between asphalt chemistry and asphalt properties.

In the remainder of this summary, some of the more important findings from this project will be presented briefly. These paragraphs will describe *average* characteristics of each asphalt and make *relative* comparisons among the core asphalts.

Asphalt AAM-1 is unique among the core asphalts. Although it contains a low percentage of aromatic carbon, that carbon is arranged in the largest aromatic systems with few substituents. Its aliphatic chains are longest and least branched but it has low concentrations of phenols and carboxylic acids (and heteroatoms in general). Furthermore, the measured characteristics change very little on oxidation. Pi-pi and van der Waals interactions are therefore likely to be most important with little contributions from polar interactions and oxidative aging.

Asphalt AAD-1 also has a low percentage of aromatic carbon but these are arranged in the smallest aromatic systems (on average) with little substitution. The average aliphatic chain is shorter and more highly branched. However, it contains more polar functional groups and is very susceptible to formation of phenols and carboxylic acids on oxidation. Therefore, polar interactions are likely to contribute to intermolecular assembly in the neat asphalt and to increase in importance upon aging.

The aromatic portion of asphalt AAG-1 is not unusual except that it is more highly substituted; its aliphatic chains are relatively short but not highly branched. Thus, on average, both pi-pi and van der Waals interactions are limited. Its overall heteroatom content is small but it has the highest concentrations of phenols and carboxylic acids of the core asphalts. However, since these are apparently present as salts, hydrogen

bonding interactions are prevented. It is not susceptible to oxidation as determined by these measures. The authors would expect this asphalt to form so-called "tender mixes."

On average, the interactions in the neat asphalt AAC-1 appear to be dominated by van der Waals interactions since its aliphatic chains are quite long and less branched but its aromatic nucleus is more substituted and it has the lowest concentrations of phenols and carboxylic acids and very few heteroatoms. However, it is very highly susceptible to increases in phenol and carboxylic acid concentrations upon oxidation thus increasing the potential for polar interactions.

Following similar logic, the remaining core asphalts can be described more briefly. In asphalts AAA-1 and AAK-1, all three types of interaction are likely with none predominating. Asphalt AAA-1 changes to a moderate degree upon oxidation, whereas a sharp increase in phenol and carboxylic acid groups is noted in AAK-1. A similar description applies to asphalt AAB-1 except that there are fewer changes in measured parameters upon oxidation.

Asphalt AAF-1 has a higher percentage of aromatic carbon than any of the other asphalts but their arrangement reduces the probability of pi-pi interactions; van der Waals interactions would possibly make a contribution and the high heteroatom content may favor polar interactions. There is little change upon oxidation.

The precise contributions of these factors to performance can be defined only when these and other chemical characteristics are correlated with behavioral traits. However, the authors speculate that:

1. Some minimum level of self-assembly is necessary for acceptable performance;
2. Some balance of all interactive forces is preferable to predominance of one type of force.
3. A certain level of change on oxidation is beneficial.
4. A very high level of change on oxidation may upset the balance of interactive forces.
5. There is a maximum level of self-assembly that is compatible with acceptable performance in a given climate regimen.

It was the intent of the solid state NMR portion of this work to probe structure in asphaltic cements on a small-distance scale ranging from a few angstroms to 30 nm. Solid state NMR techniques can probe motions, especially rotational motions, on timescales shorter than 0.1 ms. Motions of molecular fragments as well as whole molecules can be sensed. Furthermore, the phenomenon of "spin diffusion" (really polarization diffusion) allows one to probe the characteristic distance scales for inhomogeneities in molecular mobility or chemical structure (aromatic/aliphatic ratios). A strong motivation for this work was to test the micellar theory which suggests that asphalt consists of roughly spherical hard cores of asphaltenes (molecules with high polarity and aromaticity) and these cores are suspended in a "peptizing" medium of more fluid, more aliphatic molecules.

The following insights into asphaltic structure were obtained:

- a. Core asphalts differ in molecular mobility at any given temperature: AAG-1 is the most rigid and AAD-1 is the most mobile.
- b. At any given temperature a wide range of correlation times for molecular motion exists; moreover, the more mobile protons have a higher-than-average aliphatic character. This is consistent with the micellar theory. Another implication is that any glass transition phenomena will be found over a broad temperature range.
- c. Large viscosity increases (7- to 40-fold at 333 K) which accompany oxidation, either POV or TFO-POV, decrease the mobility of only a few percent of the protons. The protons which were already more mobile prior to oxidation, if anything, become slightly more mobile. The latter effect is small and hints at oxidation decreasing the overall compatibility of the asphalt components. The combined observations, namely, that the more fluid molecules have slightly enhanced fluidity after oxidation, that the number of more rigid molecules is only slightly enhanced by oxidation, and that the viscosity increases dramatically upon oxidation, is the most serious challenge to the micellar theory. Asphalt, according to hydrodynamic fluid theory, cannot consist of *non-interacting* hard spheres suspended in a fluid medium and still exhibit the properties just cited. If asphalt contains hard spheres, they must be *strongly interacting* spheres. On the other hand, there are reasonable arguments for the position that the more rigid molecules in asphalt form a more continuous phase, e.g. rods or lamellae, but the observations do not favor one or the other of these possibilities.
- d. Temporal aging, under a nitrogen atmosphere, for periods up to 6 months, at various temperatures from 253 K to 333 K produced no measurable change in molecular mobility.
- e. Mixing the asphalt with very fine, magnetically cleaned, aggregate particles produced no measurable change in molecular mobility.
- f. The shortest characteristic distance scale over which changes in molecular mobility or in aromatic/aliphatic composition occur are no larger than a few molecular diameters, i.e. less than about 4 nm in all of the core asphalts. This statement allows for several possibilities including small spheres, thin rods, and thin lamellae. Nevertheless, the distance scale of primary heterogeneities in these aspects of structure are very small and the small size tends to raise questions about the meaning of models for molecular organization.

The principle contributions of the solid state NMR studies are, I believe, an appreciation of the small scale of motional and compositional heterogeneity in all of the asphalt cements investigated and the necessity of invoking a more continuous, structural phase in these materials.

In terms of those observables which varied from asphalt to asphalt, the most obvious one, and an easily measured one, is the proton lineshape at a given temperature. It is my opinion that this measurement will not, by itself, be useful to invoke in terms of writing specifications for asphalt cements because, at any given temperature, one cannot determine the relative strength of molecular associations for those protons which look "rigid". Perhaps, a battery of measurements of lineshapes at a few other elevated temperatures would begin to address the issue of determining the relative strengths of molecular associations. This latter point needs more investigation.

Solution NMR Characterization of Asphalts

Introduction

Nuclear magnetic resonance (NMR) spectroscopy, especially with modern, high resolution instruments and sophisticated software, has become an indispensable tool for elucidating structures of organic compounds. When applied to complex mixtures such as asphalt cements, it cannot, of course, define specific compounds. However, it can provide potentially valuable information about the chemical nature of the material that is available from no other source. It is anticipated that information of this kind will help to explain the properties of asphalt cements.

There are numerous references in the literature to the use of NMR spectroscopy in the study of a variety of complex materials including shale oils (1), tar sand bitumens (2), petroleum crudes (3, 4, 5, 6), coal products (7, 8, 9, 3) as well as petroleum asphalts and asphaltenes (10, 11, 12, 13). C.E. Snape (14) has provided a valuable review of the applications of proton and carbon-13 NMR measurements, in both solution- and solid-state, to the analysis of fossil fuels. A.P. Hagen (15) has published early results on carbon-13 NMR analysis of roadway asphalts. As the subject pavements age, correlations of the data with performance will be attempted.

In most of the studies cited above, emphasis has been placed on characterization of the hydrocarbon portions of the materials. Nevertheless, heteroatoms (oxygen, nitrogen and sulfur) are present and are likely to be important to the performance of asphalt. In their native state, the functional groups and their environments are too varied for relevant NMR signals to be observed. However, some functional groups may be derivatized, thus improving their detectability. K.D. Rose (16, 17, 18) has reported techniques for derivatizations that are particularly important for carboxylic acids, phenols and alcohols through preparation of their carbon-13-enriched methyl esters and ethers. Other derivatizations have been discussed (14, 19, 20, 21, 22, 23, 24, 25) mostly for application to coal products. Some of these have been used in the present study and will be more specifically cited at the appropriate time in this report.

In a number of these papers, emphasis has been placed on the derivation of molecular structures for the materials being studied (1, 2, 3, 4, 9, 10, 11, 14, 15, 26). Speight (26) and Ebert (27) have discussed the relationship between molecular structure and intermolecular interactions.

In the work to be described in this report, it has been possible to characterize the SHRP core asphalts in terms of their true aromaticity, that is, their ratios of aromatic to aliphatic carbon and hydrogen. At a somewhat more sophisticated level, it has been possible to discern details about the aromatic and aliphatic structure. Additional NMR work has provided information about certain functional groups (e.g., carboxylic acids and phenols). Combining these data, average molecular structures have been derived for each of the core asphalts.

At Western Research Institute (WRI), SHRP A-002A contractors have fractionated the core asphalts using ion exchange chromatography (IEC). These fractions have different acid-base properties, obviously, and presumably play different roles in determining the physical and performance properties of the whole asphalt. Some NMR experiments have been conducted on the IEC fractions to provide information about their structures.

Oxidation makes an important contribution to asphalt performance and has thus been given a great deal of attention by SHRP. Core asphalts which have been oxidized by a pressure oxygen vessel (POV) procedure to simulate long-term pavement aging, and asphalts oxidized using thin film oven (TFO) in addition to POV procedures to add the effect of short-term (mix plant) aging, were supplied by WRI. Some NMR studies have been conducted on these samples as well.

Experiments with solid state NMR spectroscopy have been geared to exploration of a new application of these techniques with the potential of demonstrating the presence of heterogeneities in the neat asphalt cement. Such heterogeneities could represent molecular self-assembly and be related, first, to chemical differences among the asphalts and, ultimately, to performance characteristics of the materials.

Purpose and organization of the report

Contractors for SHRP A-002C were charged with the responsibility of elucidating various chemical characteristics of the eight SHRP core asphalts and some of their fractions using both solution and solid state nuclear magnetic resonance (NMR) spectroscopy. This charge included not only the provision of specific information about the core asphalts but also the development of detailed experimental procedures used to obtain this information.

Data was intended to be used by other SHRP contractors, particularly in SHRP A-002A, -002B, and -003, in the construction of a broad picture of the chemical characteristics of

the core asphalts. Documentation of experimental procedures was desired so that further work could be done, both within and outside SHRP.

In SHRP A-002C work plans, the effort was divided into two subtasks and attendant work elements (Table 1). However, in this final report, rather than adhering strictly to the order of work elements, results from these work elements are combined in somewhat different fashion in order to present a more cohesive picture of the chemical nature of the asphalt cements.

Results and Discussion

The hydrocarbon portion of the SHRP core asphalts

Several kinds of NMR experiments were undertaken to elucidate the structure of the hydrocarbon portions of the core asphalts. The simpler experiments provide information about the ratio of aromatic to aliphatic carbon and hydrogen. Results of more complex experiments, when combined with elemental analyses, provide some insight into more specific molecular structure characteristics and, eventually, can be used to visualize an "average molecule" for an asphalt. Experimental methods used may be found in Appendix A.

Aromatic hydrogen Integratable hydrogen [proton, (^1H)] NMR spectra were used to determine the relative contents of aromatic and aliphatic protons in each asphalt, (1, 2, 3, 4, 14) (Appendix A.1). Integration limits for aromatic protons were 6.0-10.0 ppm and -1.0 to 5.0 ppm for aliphatic protons.

$$\frac{H_{\text{aromatic area}}}{H_{\text{aromatic area}} + H_{\text{aliphatic area}}} \times 100 = \% \text{ aromatic H}$$

Table 2 contains the resulting data which is represented graphically in Figure 1.

Murphy's Gap Test (32, 33) was used to determine if asphalts may be distinguished based on differences in values of a parameter or rather if those differences are not statistically significant. Application of Murphy's Gap Test to the aromatic proton data yielded three subgroups:

Subgroup I: F

Subgroup II: B > A = G > D = K

Subgroup III: M = C

(These are ordered with highest values first. Ordering within the groups indicates trends in the data).

In less complex materials such as oils, individual peaks in the aliphatic region of the proton spectrum may be specifically assigned (14). At 1.25 ppm, for example, protons in long methylene chains, $(-\text{CH}_2-)_{\text{n}}$, resonate. About 2 ppm, there is a division between resonances for protons α to an aromatic ring and those in most other aliphatic systems. This division is not absolute, however, since it can shift slightly depending on the proportions of aliphatic substituents present. Also, there are protons adjacent to heteroatoms which may overlap, appearing between 1.8 and 4.2 ppm (Table 3).

The α protons, also called benzylic protons, are of particular interest because they are susceptible to oxidation and could be important in the oxidation of asphalts. Unfortunately, as can be seen in Figure 2, peaks in the aliphatic region of the asphalt spectrum are coalesced because of the wide variety of protons and environments present. This fact, coupled with the interferences noted above, make it impossible to integrate the peaks for benzylic protons clearly. An estimate has been made of the ratio of protons resonating between 2 and 5 ppm (including benzylic protons) to all aliphatic protons. These ratios, presented in Table 4, will be useful in investigation of oxidized samples to be discussed later in this report. It is interesting that there are two groups in this table:

$$(D > B = K > A = F = G) > (C > M)$$

This is related to the fact that aliphatic chains in AAM-1 and AAC-1 are much longer than in the other asphalts, thus increasing the contribution of protons resonating at 1.25 ppm to this ratio. Aliphatic chain length will be discussed later in this report.

Aromatic Carbon

Integratable spectra from ^{13}C NMR experiments (5, 14, 15) (Appendix A.2) provided carbon data which were used to determine the percentage of aromatic carbon in each of the asphalts. Integration limits were 110 to 160 ppm for aromatic and -5 to 66 ppm for aliphatic carbon. The data is included in Table 2 and plotted in Figure 3.

Murphy's Gap Test was applied to the aromatic carbon data to yield three subgroups (ordered from largest value to smallest with trends indicated within the groups):

Subgroup I: $F > B$

Subgroup II: $G > A = C > K > M$

Subgroup III: D

The subgroupings for percent aromatic carbon and percent aromatic hydrogen differ only slightly. When the values are ranked, it appears that only asphalts AAC-1 and AAD-1 are not in similar order by both parameters, reflecting differences in aromatic substitution (as will be discussed later).

Aromatic H $(F) > (B > A = G > D = K) > (M \approx C)$

Aromatic C $(F > B) > (G > A = C > K > M) > (D)$

Phasing the resonance peak, which is an important step in integrating NMR spectra, was thought to be a potential source of statistical error, particularly between operators. However, it has been determined that the difference between two operators' techniques is not statistically significant.

Brief Summary The percentage of hydrogen present in aromatic entities varies from about 6.4 to about 8.7 among the core asphalts. Although three statistically-distinguishable groups emerge, the differences are not large. Aromatic carbon percentages range from near 23 to about 33, a range that is apparently larger but still results in three groupings. However, even at this basic level, it is possible to discern some differences among the materials by this test. For example asphalts AAF-1 and AAD-1 represent the extremes of aromatic carbon content, asphalt AAF-1 having a higher percentage of aromatic carbon than all other core asphalts. This fact could be of importance in the asphalt's compatibility with certain types of polymer additives.

Description of aliphatic characteristics

DEPT experiments (Distortionless Enhancement by Polarization Transfer) (14) can be used to differentiate among methyl (CH_3), methylene (CH_2) and methine (CH) groups. Thus, they were used to clarify the aliphatic region of ^{13}C spectra by making a general characterization of the aliphatic region. The typical DEPT 135 spectrum (Figure 4) will display the methyl (CH_3) and methine (CH) carbons as positive signals, whereas the methylene (CH_2) carbons are "down", or negative signals.

The aliphatic region of the DEPT 135 spectrum is very similar for all eight of the core asphalts and is represented by Figure 4. Characteristic of the region between 10 and 40 ppm is the high degree of congestion on which is superimposed a series of outstanding signals. The outstanding positive signals resonate at 11.4, 14.1, 19.7, 22.7, 27.9, 32.8 and 34.8 ppm (See Table 5 and Figure 6 for assignments of these resonances). The first three of these are attributed to methyl groups and the rest to methine groups. These assignments are confirmed by the DEPT 90 experiment discussed below. Major negative, or methylene signals, are noted at 22.8, 24.5, 29.7, 31.9 and 37.4 ppm. The largest signal in the spectrum by far is that at 29.7 ppm representing methylene groups in long chains. The downfield signal at 37.4 ppm is broad, suggesting the presence of a number of methylene groups with only slightly different magnetic environments. A low, broad positive CH signal extending from 40 ppm to about 60 ppm suggests that the responsible moieties are quite varied in magnetic environments.

Further definition of the aromatic region by DEPT experiments is not anticipated since this region contains only methine and quaternary carbon. The latter is not discriminated by these DEPT experiments.

Since both methyl and methine carbons give positive signals in the DEPT 135 experiment, other means must be found to discriminate between these two carbon types.

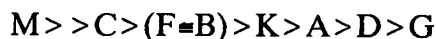
The DEPT 90 experiment and values for model compounds in the literature are helpful. In the DEPT 90 spectrum all methylene and methyl peaks should be nulled, leaving only methine signals as positive peaks. In practice, especially in a complex mixture, the results may not be so clear cut. In the DEPT 90 spectrum of asphalt AAA-1 (Figure 5), methylene peaks at 22.8, 24.5 and 37.4 ppm (from DEPT 135, Figure 4) have been nulled. However, methylene peaks at 31.9 and especially 29.7 ppm appear as positive peaks. This could result from a methine contribution at the same chemical shift or from leakage of the methylene signal. Note that smaller peaks have been nulled but the larger ones, representing higher concentrations, are not. Nevertheless, the resonance at 29.7 ppm is quite uniquely assigned to methylene carbons in long chains and that at 31.9 ppm to methylene carbons β to the end of a long chain (14, 15).

The intensities of resonances at 11.4, 14.1 and 19.7 are considerably reduced relative to other positive peaks in the DEPT 90 spectrum compared to the DEPT 135 spectrum. This indicates that, although not reduced to zero as desired, these resonances are indeed those of methyl groups.

The resonance at 22.7 ppm has apparently increased in intensity in the DEPT 90 spectrum (please note that DEPT spectra are not quantitative). At this chemical shift, there are contributions from both methyl and methylene groups. Because they can not be separated, and because the methylene contribution appears to be stronger, this peak will be assigned to methylene carbons in the overall accounting.

The DEPT experiments show remarkable similarities among the core asphalts. Because the chemical shifts of the various positive and negative peaks are the same, the asphalts must contain the same kinds of aliphatic groups in the same kinds of environments. However, there are some significant differences among the asphalts in the relative numbers of carbon atoms involved in each group. These numbers were obtained by integration of the areas in individual portions of the ^{13}C -NMR spectrum as shown by the identification numbers printed below the spectrum in Figure 6. Table 6 contains the results of this process and should be used in conjunction with Figure 6 and Table 5.

Brief Summary Although these data will be used in the construction of models of average structures later in this paper, some general comments may be made here. The largest differences among the asphalts arise in area 6 (see Table 6), indicating a wide range in the length of methylene chains in the order:



with 27 carbons so involved in asphalt AAM-1, about 15 in AAC-1 and only about 8 in AAD-1.

In the remaining areas only small differences are found because of the difficulty in observing small differences in the small areas inherent in the spectra of such a mixture. However, even small differences may be important. For example, area 3 represents

branching methine groups which could affect van der Waals interactions. As will be seen later, asphalt AAM-1, in spite of having as many as seven branching methine groups still has 14 backbone carbons for every branch. This ratio of backbone carbons to branches decreases in the order:

$$M > (K > F > A > C = D) > (B = G)$$

with the lowest value being 5 to 1 for AAG-1 and AAB-1. This and other consequences of the data will be discussed in the section on average structures.

Description of Aromatic Characteristics

It was anticipated that important differences among the asphalts might be found in the degree to which their aromatic entities were substituted by units other than hydrogen. A means of assessing these differences was devised. First, using the average molecular weight and elemental analysis (Table 7¹) an average molecular formula was calculated for each asphalt. Then, using percentages of aromatic hydrogen and aromatic carbon from the NMR experiments described earlier, the numbers of aromatic protons and carbons in an average molecule were calculated.

$$\text{No. of aromatic carbons} = \frac{\% \text{ aromatic carbon} \times \text{total carbon in average molecule}}{100}$$

$$\text{No. of aromatic hydrogens} = \frac{\% \text{ aromatic hydrogen} \times \text{total hydrogen in average molecule}}{100}$$

Finally, a ratio of the number of aromatic carbons to the number of aromatic hydrogens was determined.

$$\text{Aromatic substitution index} = \frac{\text{No. aromatic carbons}}{\text{No. aromatic hydrogens}}$$

¹ Although not directly related to the subject at hand, some comments on the data in Table 7 should be made. Differences in molecular weight and the number of carbon atoms in the average formulae are obvious with AAM-1 having a large average molecule, AAD-1 a small one. However, the differences in H/C ratio are quite small (1.45 to 1.56). There are insignificant differences with regard to oxygen content. Variation in nitrogen content is somewhat greater and one could place the asphalts into three groups: (G, K, M) > (A, B, D) > (C, F). Sulfur content is more variable. The asphalts can be ranked by sulfur content in the order: (K, D, B, A) > F > (C, M, G). Thus, if the aromatic/aliphatic ratio for sulfur is constant, one would expect sulfur to contribute to oxidation of the asphalts in the same order.

This parameter, called the Aromatic Substitution Index (ASI) is, by definition, the number of aromatic carbons per aromatic hydrogen atom. A higher value for the ASI implies more substitution by non-hydrogen units than does a lower value.

The ASI (Table 8, represented graphically in Figure 7) indicates that there is a relatively narrow range among the core asphalts, from 2.2 carbons per proton to 2.8 carbons per proton. Looking at this number somewhat differently, an ASI value of 2 means that one half the aromatic carbons are substituted and a value of 3 indicates that 2/3 are substituted; i.e., on average, more than half of the aryl carbons are substituted with either another aryl carbon or an aliphatic carbon. Asphalt AAC-1 is the most highly substituted with just under 3 carbons/proton; asphalt AAD-1 is the least substituted with only 2.2 carbons/proton. The remaining six core asphalts have ASI values between 2.5 and 2.7.

It should be noted that this data proposes fractional parts of atoms because of the complications of working with an average molecular formula of a complex material. Clearly, this is not possible and adjustments will be made when suggesting molecular structures.

ASI has further ramifications in light of double bond equivalents (DBE -- sites of unsaturation) as will be discussed below.

The concept of the double bond equivalent (DBE) permits one to determine how many rings and/or double bonds are in a molecule. The DBE is calculated:

$$\text{DBE} = 1 + (\text{number of C atoms} - 0.5 \text{ number of H atoms})$$

A molecule with a formula of C_6H_{14} has no double bond equivalents and, therefore, must be a straight chain, saturated hydrocarbon. A formula C_6H_{12} has one DBE and, therefore, one double bond in a straight chain *or* one saturated ring. A single benzene ring accounts for 4 DBE; each additional catacondensed aromatic ring (i.e., arranged in a straight line) for 3 DBE.

From the elemental analyses and derived chemical formula (Table 7), the number of double bond equivalents in an average molecule of each asphalt was calculated (Table 8). Since there appear to be few if any olefins in the asphalts and the number of carbonyl groups is extremely small, almost all of the DBE's may be accounted for in aromatic structures.

Among the core asphalts, five have 15 DBE, one has 17 DBE. However, asphalt AAD-1 has only 11 whereas AAM-1 has 23 DBE. Thus, the asphalts may be ordered as follows:

$$\text{M} > (\text{F} > \text{A} = \text{B} = \text{C} = \text{G} = \text{K}) > \text{D}$$

The foregoing information will be used in the derivation of average structures which will be discussed in the section titled, "Heteroatoms in asphalt structure."

Attempted use of shift reagents to enhance resolution of NMR spectra

Shift reagents are compounds generally containing a lanthanide element, e.g., europium in $\text{Eu}(\text{fod})_3$ (28, 29). These reagents are designed to interact reversibly and very briefly with heteroatoms such as nitrogen, oxygen or sulfur. Because of this interaction, the resonance of the adjacent proton or carbon-13 is moved from its normal position on the chemical shift axis. In elucidation of the structure of an organic compound, this is very useful in identifying the nature and location of functional groups, even in complex molecules, but simple mixtures.

In asphalt cement it was intended that the resonances of protons or carbon atoms in similar heteroatom environments would be shifted away from the complex group of peaks in the aromatic or aliphatic regions of the respective spectra. In proton spectra two minor peaks were observed to shift downfield (to the left) at different rates with increasing concentrations of $\text{Eu}(\text{fod})_3$. Although the faster-moving resonance is probably that of a proton attached directly to a heteroatom, it was not further identified. Nevertheless, the behavior of all eight core asphalts was the same, that is, no unique characteristics were observed for any asphalt. No significant changes in chemical shift could be induced in ^{13}C -NMR spectra.

After considerable effort, this approach was abandoned. At least two reasons for the lack of significant results may be advanced. First, because of the complex mixture of compounds in asphalt, the shift reagent could have been unable to interact with heteroatoms efficiently perhaps for steric reasons. Second, the molecular environments of the various functional groups may differ to such an extent that too few of any one kind are present to provide a coherent NMR resonance.

Summary: Aliphatic and aromatic characteristics of core asphalts

In terms of the parameters discussed in this section, the core asphalts may be ranked as follows. For each parameter, the identifying letter of the asphalt with the highest value is listed first. Use of parenthesis indicates that, although there may be trends within a group of asphalts, the differences may not be statistically significant.

% Aromatic hydrogen: $\text{F} > (\text{B} > \text{A} = \text{G} > \text{D} = \text{K}) > (\text{M} > \text{C})$

% Aromatic carbon: $(\text{F} > \text{B}) > (\text{G} > \text{A} = \text{C} > \text{K} > \text{M}) > \text{D}$

Aromatic substitution index: $(\text{C} > \text{B} = \text{G} > \text{F} > \text{A} = \text{K} = \text{M}) > \text{D}$

Double bond equivalents: $\text{M} > > \text{F} > \text{C} = \text{G} = \text{B} = \text{A} = \text{K} > > \text{D}$

Number of carbon atoms in long methylene chains:

$\text{M} > > \text{C} > (\text{F} > \text{B} > \text{K} > \text{A}) > (\text{D} > \text{G})$

A few generalizations may be made from these data. The average molecule of asphalt AAD-1 stands out with low aromatic carbon content assembled in the smallest ring systems with the least substitution of all core asphalts. Its methylene chains are relatively short. (Its heteroatom content is highest.)

Asphalt AAM-1 also has a low aromatic carbon content. However, that carbon is assembled in the largest aromatic rings in any of the core asphalts. These rings are not highly substituted, but the average molecule has more carbon in long methylene chains than the other asphalts. It also has the lowest heteroatom content.

Asphalt AAC-1 may be described similarly to AAM-1, except that its aromatic ring systems are considerably smaller and its methylene chains shorter. (Low heteroatom content.)

Asphalt AAG-1 contains the fewest carbons in methylene chains. The remaining asphalts show no particularly distinguishing characteristics at this level.

Heteroatoms in asphalt structure

In the previous section of this paper, study of the hydrocarbon skeleton of asphalt cement by proton and carbon-13 NMR spectroscopy has been discussed. Asphalts also contain low concentrations of heteroatoms (oxygen, nitrogen, sulfur) some in functional groups that may be important to the properties of the asphalt. The detection and quantitation of some of these functional groups was the purpose of this portion of the study.

Hydrogen and carbon atoms adjacent to or even in the environment of heteroatoms such as oxygen, nitrogen or sulfur, resonate at characteristic chemical shifts in the NMR spectrum. Resonances for ketones and carboxylic acids are easily found in individual compounds or simple mixtures. However, in asphalt cements, the concentrations of such functional groups are so low and their molecular environments so varied that their characteristic resonances can not be discerned.

Nevertheless, it is possible to overcome some of these problems by derivatizing the functional groups so that their NMR signals are enhanced and collected into a narrower resonance line of the NMR spectrum. For example, Rose (18) has described a procedure known as phase-transfer methylation (PTM) by which the *acidic hydrogen* atoms attached to nitrogen, oxygen or sulfur in hydroxyl (-OH), carboxylic acid (-COOH), imino (=NH) or thiol (-SH) groups are replaced by methyl groups. These methyl groups are enriched with NMR-active carbon-13, thus enhancing their detectability. These functional groups are important because they can participate in intermolecular hydrogen bonding, a process which may contribute to the behavior of asphalts. For that reason, the phase-transfer methylation reaction has been studied in this project.

Other derivatization reactions were studied. Diazomethane was used to derivatize carboxylic acids exclusively (30). For the detection of ketones, methoximation reactions were effected. Primary amines were sought using a reagent known as "CDMPOPS" (20). In addition, alternatives to phase-transfer methylation were explored. All of these reactions, successful and unsuccessful, will be described in the section to follow.

Functional groups containing oxygen

Phase-Transfer Methylation (Appendix A.4) (16,17,18) Using ^{13}C -enriched reagents, a phase transfer methylation (PTM) procedure converts phenols to methyl ethers and carboxylic acids to methyl esters (Scheme I). Although imines and thiols also reportedly react under these conditions (18), the increased intensity in the 30-46 ppm region for N-methyl derivatives or in the 10-25 ppm region for S-methyl derivatives could not be quantitated. The O-methylated products appear in the NMR spectrum between about 50 and 65 ppm (Figure 8).

This methoxy region consists of three peaks representing, from left to right, the methyl ethers of hindered phenols, the methyl ethers of unhindered phenols and the methyl esters of carboxylic acids.

The peaks for phenolic methyl ethers are expected to be rather broad because the probe atom ($^{13}\text{CH}_3$) is only two bonds away from the structure which influences its chemical shift and those influencing structures are likely to be highly varied in asphalt cement. On the other hand, the resonance for carboxylic acid esters is expected to be sharp, because the probe atom is three bonds removed from the influencing structure.

As this reaction was explored, it was repeated on several samples to ensure that the reaction was complete. It was found that the intensity of the resonance near 51 ppm (for methyl esters of carboxylic acids) continued to increase with the development of a shoulder on the down-field side (the left) of the peak. However, the intensity of the peaks representing phenolic methyl ethers increased with a second PTM procedure and then remained constant. It appears, therefore, that the shoulder immediately downfield of the ester peak is an artifact of the PTM reaction.

Partial spectra showing the methoxyl region resulting from short-term PTM of the core asphalts are shown in Figure 9. The spectra of asphalts AAA-1, AAD-1, AAG-1 and AAK-1 are quite similar if the downfield shoulder on the ester peak is ignored, that is, all have a sharp, substantial ester resonance. On the other hand, asphalts AAB-1, AAC-1, AAF-1 and AAM-1 show little if any distinct ester resonance, suggesting that their concentrations of free carboxylic acid are relatively very low.

By using an integration standard (^{13}C -tetramethylsilane or ^{13}C -acetonitrile), the concentrations of these three functional groups were determined (Table 9). Asphalt AAG-1 has the highest concentration of -OH and -COOH groups (column 4). Asphalts

AAA-1, AAB-1, AAF-1 and AAM-1 appear to be similar to each other with lower concentrations; asphalts AAC-1, AAD-1 and AAK-1 have still lower concentrations. However, given that the base treatment almost certainly results in an artifact which interferes with the ester peak, the values for carboxylic acid concentrations must be regarded as upper limits to free carboxylic acid concentrations.

Phenol concentrations are likely to be adequately represented by this technology.

The final column in Table 9 reports the percentage of the total oxygen found by elemental analysis that is accounted for by the short-term PTM method. This amounts to as much as 50% and as little as 17%. This result is attributable to several factors. First, not all oxygen functionalities are alcohols, phenols or acids. Some oxygen could be held in sulfoxides or ethers, among other groups. Asphalt AAD-1, for example, clearly exhibits resonances about 70 ppm in the ^{13}C -NMR spectrum representing naturally-occurring ethers. These ethers are resistant to the derivatization reactions. Their contribution to baseline intensity of the 50-65 ppm region was negligible in control experiments and did not interfere with the derivatization results. Second, some oxygen-containing groups may be hindered and not be available for derivatization. Third, some oxygen is likely to be present in aromatic (Figure 10, left) and hydrolysis-resistant ester moieties (Figure 10, center and right).

As mentioned earlier, repetition of the PTM reaction was explored and evidence for continued derivatization was found, particularly in the development of a down-field shoulder on the methyl ester peak. Therefore, a long-term PTM procedure was developed (Appendix A.5) and adopted as a means of assuring that all of the functional groups would be uncovered by unfolding structures which might protect them and by complete hydrolysis of native esters, etc. Spectra of the methoxy regions after long-term PTM (Figure 11) show further enhancement of the patterns evident after short-term PTM. Asphalts AAA-1, AAD-1, AAG-1 and AAK-1 remain similar to each other with sharp ester resonances, although the down-field shoulder on that resonance is now more prominent than after short-term PTM. Asphalts AAB-1, AAF-1 and AAM-1 also remain similar to each other with three approximately equal peaks and a subdued resonance at 51 ppm for $\text{RCOO}^{13}\text{CH}_3$ (although the intensity of that peak increased slightly for AAB-1 and AAF-1). The spectrum of asphalt AAC-1 is dramatically different suggesting that extensive base-facilitated processes occurred during long-term PTM. (Repetition of the experiment verified the results.)

There are three significant differences between the spectra from the short-term PTM products and those from the long-term method. First, the three peaks, which are rather distinct in the short-term procedure, begin to coalesce after the long-term reaction. Second, there is an aliphatic methyl ether peak at 58.7 ppm after the long-term method in nearly all asphalts verifying the hydrolysis of aliphatic esters during the derivatization process with the final formation of methyl ethers. However, the major difference observed between the methodologies is the appearance of a broad resonance to the left (down-field) of the sharp $\text{RCOO}^{13}\text{CH}_3$ resonance (51 ppm) after long-term PTM. The

origin of this broad resonance has not been fully determined and, therefore, its value in the integration is suspect.

Integration of the ^{13}C -NMR peaks from long-term PTM products showed dramatic increases in the concentrations of the functional groups compared to the short-term reaction (Table 10). Asphalts AAC-1 and AAD-1 contain much higher concentrations of these groups than any of the other asphalts; asphalts AAA-1, AAB-1, AAG-1 and AAK-1 are similar; asphalts AAM-1 and AAF-1 display similar low concentrations.

The concentrations of phenols increase after a second PTM procedure and then remain fairly constant. Nevertheless, the changes in the peak patterns (e.g., coalescence) and the appearance of an aliphatic methyl ether peak indicate that the reactions involved there may be complicated by repeated exposures to base and, therefore, that the short-term PTM provides more reliable data for concentrations of phenols in asphalt.

As a consequence, the long-term PTM is suspect because it generates artifacts which obscure the results which it was designed to supply. This is particularly evident in the last column of Table 11 which shows that the final oxygen content of the long-term PTM products is in some cases higher than in the original asphalt. Therefore, the authors do not recommend reliance on the long-term PTM technique unless the results are corroborated by other approaches.

Methylation using labelled diazomethane Reaction of the asphalts with ^{13}C -diazomethane (30) (Appendix A.8) was selected for use because the reagent reacts specifically with free carboxylic acids to form esters and not with phenols or alcohols (to form ethers). Moreover, it does not involve the use of base and, therefore, should not create artifacts which will interfere with the analysis of the resulting esters. The reaction was carried out once and then a second time (on the same sample) on the SHRP core asphalts to ensure complete methylation. In Figure 12 there are two spectra for each asphalt. The lower spectrum, *a*, results after one reaction; the upper, *b*, after the second reaction. These spectra show that, although sufficient reagents are present to complete the methylation in the first reaction, further methylation does occur during a second reaction. This is particularly true for asphalt AAG-1 wherein the carboxylic acids are present as salts. These salts apparently are protonated during workup of the first reaction and thus are available for methylation during the second reaction.

The spectra (Figure 12) are quite "clean", indicating that the predominant reaction was formation of methyl esters (~ 51 ppm). Minor downfield peaks probably result from impurities and a very minor amount of phenol methyl ether. Following the second reaction asphalts AAD-1, AAG-1 and AAK-1 have similar spectra (as they did after short-term PTM). Likewise, asphalts AAB-1, AAC-1, AAF-1 and AAM-1 are similar, and show little evidence for free carboxylic acids. The spectrum of asphalt AAA-1 appears to be intermediate between the two types in this experiment.

Concentrations of free carboxylic acids in the core asphalts obtained from integration of the diazomethane-derived spectra (Table 11) appear to vary widely. Asphalt AAG-1 has the highest concentration (about 30×10^{-6} mol/g), followed by AAD-1, AAK-1 and then AAA-1 (about 5×10^{-6} mol/g). The remaining asphalts are similar to each other with 2×10^{-6} mol/g of COOH or less. It must be emphasized that, even at their highest, these concentrations are very low and account for a relatively small portion of the oxygen content (last column, Table 11). In essence, asphalts AAD-1, AAG-1 and AAK-1 contain free carboxylic acids, the remaining asphalts contain very little free COOH.

Comparison of methylation procedures Of the reactions described above, methylation with ^{13}C -labelled diazomethane is the most simple and clean. Only the esterification of carboxylic acids occurs, however. The fact that a second reaction of the same sample was required to complete the esterification could result from the presence of metal carboxylates. Another explanation may be that some carboxylic acids are hindered or enclosed within large folded structures and are, therefore, not readily available to the first reaction. The authors favor the former explanation.

Phenols and alcohols are not derivatized by diazomethane because their protons are not adequately acidic. Phase-transfer methylation procedures using strong base readily promote the derivatization of all acidic protons. The fact that repeated PTM procedures on the same sample resulted in increased methylation could be explained, as with diazomethane, as resulting from slow opening of folded structures to expose the reactive functional groups. However, the procedure can also hydrolyze esters and other functional groups naturally available in the asphalt. The resulting acids and alcohols would then be available for reaction with the labelled reagent. That appears to be the case, especially in the long-term PTM reaction, as evidenced by the appearance of the aliphatic methyl ether peak at 58.7 ppm. Again, the increase in intensity of the shoulder downfield on the methyl ester peak at 51 ppm appears to be an artifact. It may seem that the long-term PTM procedure is too harsh and, therefore, unrealistic and unnecessary. However, it is conceivable that certain conditions in the service life of an asphalt cement (e.g., contact with certain aggregates at high temperatures) might result in similar reactions. For that reason, further study of this reaction may be warranted if evidence is found for such complex chemistry in field samples.

Brief Summary of Methylation Procedures Because of the limitations discussed above, the authors recommend use of diazomethane methylation procedure for analysis of free carboxylic acids and the short-term phase-transfer methylation for analysis of phenols. Data from these reactions are collected in Table 12.

The asphalts may be ranked as follows:

unhindered phenols - $G > (F = B) > (M > A > D > C > K)$
hindered phenols - $F > (G = B) > (M = A) > (K > D > C)$
combined phenols - $(G > F) > B > (M > A) > (D > K > C)$
free carboxylic acids - $G > D > K > A > (M > C = B = F)$

total OH + COOH - G > > F > B > (D ■ A ■ M) > K > C
 susceptibility to long-term PTM (as defined by the ratio of total OH +
 COOH by LT-PTM to total OH + COOH by recommended
 procedures) C > > D > (B > A > K) > (M > F = G)

Although the concentrations of these functional groups in the whole asphalts are very low, they do vary. Asphalts AAG-1 and AAF-1 are highest in phenol content but AAG-1 has the highest carboxylic acid content and AAF-1 the lowest.

Asphalt AAC-1 has the lowest combined concentration of OH and COOH. Only seven percent of its total oxygen is represented by these groups. However, it is the most highly susceptible to change in the long-term PTM treatment indicating that much of its oxygen in the native state may be present in base susceptible functional groups.

There are also differences in concentrations of free carboxylic acids. Asphalts AAG-1, AAD-1 and AAK-1 may be regarded as having modest amounts of free COOH. The remaining core asphalts have virtually none.

These procedures may be summarized as follows:

- a. Diazomethane Available COOH with no hydrolysis--recommended for COOH.
- b. Short-term PTM Available COOH, phenols and some hydrolysis products--*recommended for phenols*.
- c. Long-term PTM All COOH, phenols and alcohols plus products from extensive hydrolysis and possibly other unknown reactions. *Not recommended at this time*.

Other experiments for analysis of heteroatoms

CDMPOPS for analysis of primary amines Nitrogen-containing functional groups are perceived to be of importance to asphalt behavior, particularly with regard to interactions with aggregate. Like oxygen-containing groups, they must be derivatized for NMR spectroscopic analysis.

The reagent CDMPOPS [(2R,4R,5S)-2-chloro-3,4-dimethyl-5-phenyl-1,3,2-oxazaphospholidine-2-sulfide] reacts specifically with primary amines and secondary alcohols (20) (Appendix A.14). Reactions with model compounds confirmed this specificity (Scheme II). The derivatized primary alkyl amine produced a resonance peak at 80.7 ppm in the ³¹P-NMR spectrum; other alkyl amines will resonate between 80 and 85 ppm.

Reaction products of CDMPOPS with the core asphalts confirmed the presence of alkylamine derivatives with resonances between 80 and 85 ppm in all except asphalt AAK-1.

Reproducibility of this reaction in terms of quantitation was found to be less than ideal. Nevertheless, as data in Table 13 show, concentrations of primary alkyl amines are extremely low.

Suitable derivatization reactions for analysis of other nitrogen-containing functionalities were not found.

¹⁴N- and ¹⁵N-NMR Both of these nitrogen isotopes resonate in NMR experiments but neither nucleus is particularly sensitive (¹⁵N is not adequately abundant. While ¹⁴N is sufficiently abundant, it is quadrupolar, making it impossible to measure in this case.) Both ¹⁴N- and ¹⁵N-NMR spectra were obtained for asphalt AAG-1 which contains more nitrogen (2.0%) than any other SHRP core asphalt. If the nitrogen were present at sufficient concentrations in a given group, a characteristic resonance would be expected. However, no discernable resonances were found probably because of not only the low sensitivity of the nitrogen nucleus but also the low concentration of functional groups and the variety of their molecular or magnetic environments. Therefore, this approach was abandoned.

Sodium hydride as an alternative to tetrabutylammonium hydroxide (TBAH) in the methylation reaction (22,23), (Appendix A.6,7). Because TBAH is likely to cause hydrolysis of native esters (and perhaps other reactions) and thus interfere with the analysis of carboxylic acids by methylation, the reaction using sodium hydride (NaH) in Scheme III was tried. With asphalt AAG-1, methyl ether formation occurred but less esterification than in the phase- transfer methylation. Stoochnoff and Benoiton (22) reported that this reaction methylates weakly acidic and sterically hindered phenols in preference to more acidic phenols and acids. This was confirmed in this laboratory with model compounds. The reaction clearly produced a different mixture of methylated products than PTM reactions. However, the specificity did not appear to warrant further study at the time. In retrospect this procedure may be superior to that using TBAH as it may not cause serious side reactions.

Potassium ethoxide and a crown ether in the methylation reaction (25) This reaction, shown in Scheme IV, takes advantage of the fact that 18-crown-6 ether readily complexes the potassium ion and thus facilitates the formation of anions which should then react readily with methyl iodide.

With asphalt there was evidence for reaction at ROH sites but little with carboxylic acids. As a result, the reaction appeared not to warrant further study.

Methoximation reaction for analysis of ketones (Appendix A.12) Both ketones and aldehydes are subject to the reaction in Scheme V. However, since aldehydes oxidize

readily to acids, they are not likely to be present in asphalt. Evidence for the product was found about 61 ppm in the ^{13}C -NMR spectrum of asphalt AAG-1. However, time did not permit further work with this reaction.

Lithium aluminum hydride reduction (Appendix A.10) The reaction of lithium aluminum hydride (LAH) (Step 2 in Scheme VI) was used to verify the assignment of the resonance about 51 ppm in the ^{13}C -NMR spectrum of phase-transfer methylated asphalt to ^{13}C methyl esters. Since LAH reduces esters to alcohols but does not affect ethers, the gradual disappearance of the 51 ppm peak after successive LAH treatments confirmed the assignment. Furthermore, chemical shift correlations with known compounds establish that esters of aliphatic carboxylic acids represent the major contributors to this resonance.

However, the fact that this resonance could not be completely eliminated leads to the suspicion, mentioned earlier, that there are other unknown contributors to the resonance than esters alone.

As shown in Scheme VI, LAH will also reduce ketones to alcohols. This fact seemed to hold promise for the analysis of this elusive functional group by NMR spectroscopy. The content of carboxylic acids would first be determined by phase-transfer methylation as previously described. A separate sample of the asphalt would be methylated using $^{12}\text{CH}_3\text{I}$ (Step 1) which will not be observed in the NMR spectrum, thus removing any interference from the peaks in the methoxy region which result from methylation using $^{13}\text{CH}_3\text{I}$. If this sample is then reduced with LAH (Step 2), ketones and esters would be reduced to alcohols which could be methylated using $^{13}\text{CH}_3\text{I}$ (Step 3). An example of this methylated product is shown in Figure 13, spectrum *B*. In comparing *B* to spectrum *A* (from the standard PTM reaction using $^{13}\text{CH}_3\text{I}$ on the same asphalt) it can be seen that there is a new peak about 58.7 ppm which represents the $^{13}\text{CH}_3$ ethers of the alcohols resulting from both ketones and esters. There remains a peak about 51 ppm which indicates that not all esters were reduced by the LAH. A second reduction and methylation (spectrum *C*) further increased the ratio between the ether resonance and that for esters, indicating that more esters had been reduced by the second LAH reaction but the reduction was still not complete. This complicates the process of analyzing for ketones which would, ideally, be measured by subtracting the known contribution of carboxylic acids to the ether peak leaving the contribution from ketones. Time did not permit the work needed to optimize this reaction series to analyze ketones; however, it remains as a possible solution to this problem.

Sodium borohydride for analysis of ketones (Appendix A.9) Sodium borohydride reacts specifically with aldehydes and ketones to form the corresponding alcohols. Since aldehydes are unlikely to be present in asphalt (they are readily oxidized to carboxylic acids) only ketones are shown in Scheme VII. When the resulting alcohols are methylated via standard phase transfer methylation reaction, the product shows two new peaks in the ^{13}C -NMR spectrum, at 57 ppm and 53.5 ppm, for ketone derivatives. The difference in chemical shift for the two peaks indicates distinctly different molecular

environments for the original ketones. In asphalt AAG-1 a total of 4.9×10^{-5} moles/gram of ketone functionality was found. This reaction shows promise for analysis of ketones. However, time did not permit its full development.

Bis (tri-n-butyltin) oxide for derivatization of asphalt (21) The reaction shown in Scheme VIII was performed on asphalt AAG-1 and the product analyzed by ^{119}Sn -NMR spectroscopy (21). A resonance about 102 ppm, in the ^{119}Sn chemical shift range for a phenolic derivative, was found. No resonance was detected between 70 and 80 ppm, the approximate range for thiol derivatives. This should be a good reagent for detection of thiols because the chemical shift range of the products does not overlap with other Sn derivatives. Because the reaction is also not very efficient for hindered phenols, it was not seen to have any particular advantages for this research.

Formation of trimethyl silyl derivatives (19, 31) Silyl derivatives shown in Scheme IX can be analyzed by ^1H -, ^{13}C - and ^{29}Si -NMR. Although nitrogen derivatives can be obtained, they usually require more stringent conditions than do hydroxyl derivatives. Therefore, this methodology is best suited to analysis of hydroxyl groups (19, 31). In this laboratory evidence for the presence of phenols and alcohols was found. However, the reaction was not found to confer special benefits and was not further studied.

Derivatization of sulfides The reaction between sulfide groups and ^{13}C -methyl iodide in dimethylformamide (DMF) (Scheme X) proceeded well but provided no selectivity and had no ready means for quantitation. Therefore, it was not pursued further.

Summary of work on heteroatom-containing functional groups

Several derivatization reactions were explored by which the content of various -OH containing groups could be assessed. Phase-transfer methylation, which permits quantitation of hindered and unhindered phenols, aliphatic alcohols and carboxylic acids was most seriously studied. From products of this reaction, quantifiable ^{13}C -NMR spectra were obtained which provided reasonably reproducible concentrations of phenols and aliphatic alcohols. Concentrations of carboxylic acids were more problematic because of the possibility of unwanted side-reactions under the reaction conditions.

Carboxylic acid concentrations were quantified by use of a reaction with diazomethane which specifically derivatizes carboxylic acids (not phenols or alcohols) and causes no hydrolysis of native esters.

Means of quantifying ketone concentrations were explored in two reaction sequences. Optimizing these analyses required more time than was available during this project but the reactions have some potential for discriminating this important but elusive functional group.

Although several derivatization reactions were potentially useful for analysis of nitrogen and sulfur-containing functional groups, only one showed sufficient promise to warrant development. The derivatization of primary amines with a reagent called "CDMPOPS" revealed very low concentrations of this group. Thiol groups should have been exposed by at least one procedure, but no evidence was found for their existence.

The core asphalts may be ranked with respect to some of the functional group parameters. In these rankings, the asphalt with the highest value is listed first, by its identifying letter. Enclosure in parenthesis indicates that, although there may be trends among the asphalts, the differences are probably not statistically significant.

Concentration of all phenol, alcohol and carboxylic acids (by short- term PTM reaction):

$G > > F > B > A \approx M > D > K \approx C$

Carboxylic acid concentration (by diazomethane reaction)

$G > > D > > K > > A > M \approx C \approx B \approx F$

Concentration of primary amines (from "CDMPOPS" reaction)

$G > M > B = A > D > K$ (asphalts C and F not analyzed)

Average molecular structures of core asphalts

Derivation of average structures

The molecular structures of asphalt components no doubt vary extensively from those which might be entirely aromatic to those with no conjugated entities at all. Differences in the range of molecular weight, the content of functional groups containing heteroatoms, the extent of substitution and branching of chains will also be found. Indeed, the degree of variability may itself be important to asphalt characteristics. It is necessary to keep these points in mind even while discussing the concept of an "average molecule" of an asphalt cement.

An "average molecule" is a construct derived from average molecular weight, elemental analysis and NMR data. It may not represent an existent molecule but provides a valuable visual means of describing the overall characteristics of an asphalt. Average structures have been derived only for the eight core asphalts, but with some additional data, could be derived for fractions such as those from ion exchange chromatography. Models for the latter, for example for strong acids and neutrals, could be very useful in understanding asphalt behavior.

Data required for construction of average molecular structures has been discussed and tabulated earlier in this report. These references are listed for the reader's convenience.

Table 8 contains the numbers of aromatic and aliphatic carbon and hydrogen atoms, the aromatic-substitution indices (ASI) and double bond equivalents for each core asphalt.

Table 5 lists the types of carbon atoms to which peaks in the aliphatic region of the ^{13}C -NMR spectrum have been assigned; the number of carbon atoms represented by each peak may be found in Table 6. Carbon atoms not specifically assigned were found in the broad resonance envelope below the sharp peaks of the aliphatic region. These carbons could be methyl, methylene or methine types. It is not possible to assign these definitively because of overlapping resonance regions for different carbon types (see Table 5, bottom). Based on a visual inspection of the shape of this envelope in an effort to estimate the relative areas most likely to be attributed to each of these carbon types, it appears that the "extra" carbons should be assigned to no more than one methyl group with the remainder divided about equally between methylene and methine groups in each of the asphalts. To some extent the developing structural model dictated the assignments of these "extra" carbon atoms.

Aliphatic quaternary carbon atoms (no hydrogens attached) caused some concern because they can not be identified uniquely by techniques available to us. However, the carbon/hydrogen ratios and the very small proportion of terminal methyl groups found in the ^{13}C -NMR spectra indicate that aliphatic quaternary carbons are rare at best.

Heteroatoms posed a special problem in constructing average molecular structures because they are present in very low concentrations. As a matter of convention, if the molecular formula indicated the presence of > 0.5 atoms of a heteroelement, an appropriate functional group was included in the structure.

Nitrogen was included as a substituent usually in an aliphatic chain or a saturated ring, although it could certainly be present in an aromatic system.

Sulfur was included in an aromatic ring in most cases. If the possibility of a second sulfur was indicated, it was placed as an aliphatic sulfide.

There are a number of considerations in constructing an average molecule and it must be stressed that the structures shown (Scheme XI) are in no way unique. A number of ways could be found to draw other structures based on the same data.

In each case, the model was begun by drawing the aromatic core to accommodate the required number of aromatic carbon atoms plus sulfur and aromatic hydrogen. Fractional parts of atoms were rounded to the nearest whole. (The aromatic substitution index of the model as drawn may differ slightly from the ASI calculated because of the unavoidable use of fractional atoms in the molecular formulae.) The ratio of aromatic H to aromatic C and the number of double bond equivalents (DBE) available require that the aromatic core be highly condensed. Ultraviolet spectra support this concept.

Next, remaining DBE's were consumed by drawing naphthenic and alicyclic rings condensed and fused to the aromatic system. This reflects the relatively small number of methylene groups not in long, unbranched chains and the small number of terminal methyl groups, either or both of which would be required for isolated alicyclic rings.

Then the number of aliphatic chains was determined from the number of remaining open sites on the aromatic system (i.e., not occupied by hydrogen or alicyclic fragment), the number of terminal methyl groups (peak 11), the number of methylene groups adjacent (α) to methyl groups (peak 9), and the number of CH_2 groups β to CH_3 (peak 5). Ideally, these latter three numbers should be identical since they form the last three units of an aliphatic chain of more than three carbons. The values are remarkably close considering the difficulties involved in integrating coalesced peaks in the NMR spectrum, the overlapping of carbon types and the problems inherent in working with an average structure for so complex a system. Finally, the remaining aliphatic chains were constructed considering the number of methylene units in long chains (which must be isolated from all other groups by at least two methylenes), the number of branching CH groups, branched methyls, other heteroatoms, etc. It is this process which would permit most variation in the structure.

Before discussing the average structures, the limitations of the concept must be stressed. The variability in molecular structures in an asphalt is very wide. An average structure of necessity features only the most common traits. Other characteristics, a carboxylic acid group, for example, do not appear in an average structure because their concentrations are not large enough to make them "average." However, that is not to say that such groups may not be important to the behavior of the asphalt. One further caution relates to the fact that aliphatic and aromatic characteristics are combined in the average molecule when in fact they may be more widely separated.

Discussion of the average structures

The average structure for asphalt AAM-1 (Scheme XI.1) is clearly different from that of the other core asphalts. Its aromatic core contains five condensed aromatic rings to which are fused two naphthenic and an alicyclic ring. To this are attached three long aliphatic chains. There are a few branches on these chains but only one for every 14 carbons in the chain backbone. There is only one heteroatom, that is a nitrogen which has been placed as a secondary amine in one of the chains (it could have been fit into the aromatic system). There is only 0.4 of a sulfur atom per average molecule, 1.1% by weight in the asphalt. It is noteworthy that asphalt AAM-1 contains one of the lowest percentages of aromatic carbon atoms but its aromatic units are the largest of the core asphalts.

Asphalt AAD-1 (Scheme XI.2) is also unique among the core asphalts with a very small aromatic core including only 12 carbon atoms and a sulfur atom. It requires two alicyclic

rings and two chains as well as one nitrogen and an additional sulfur atom. There are several short branches on the chains, about one for every eight backbone carbons.

Asphalts AAA-1 (Scheme XI.3) and AAK-1 (Scheme XI.4) have nearly identical average structures. There are 16 aromatic carbon atoms, three alicyclic rings, nitrogen and sulfur. Asphalt AAK-1 requires a second sulfur atom and three more aliphatic carbon atoms than AAA-1. These asphalts have nine or ten backbone aliphatic carbon atoms for each branch.

Asphalt AAF-1 (Scheme XI.5) has a somewhat larger aromatic core (20 carbon atoms). It alone of the core asphalts requires an oxygen atom which has been placed in one of the two naphthenic rings. Like asphalt AAK-1, it has about ten backbone carbon atoms per branch.

Asphalts AAB-1 (Scheme XI.6) and AAC-1 (Scheme XI.7) have both been drawn with 18-carbon aromatic systems and three alicyclic rings. However, the ring structures are not represented identically because the aromatic rings are more substituted in AAC-1 than in AAB-1. Both require a nitrogen atom, but only AAB-1 includes sulfur as well. There are five more aliphatic carbon atoms in AAC-1 than in AAB-1; AAC-1 is somewhat less highly branched.

Finally, asphalt AAG-1 has a small aromatic system, on average, only one heteroatom, a nitrogen, and fewer aliphatic carbon atoms than the other core asphalts. The aliphatic chains have only five backbone carbons for each branch.

Summary and ramifications of average structures

While reminding the reader that these structures represent "average molecules," the possible ramifications of the structure will be on the mode of intermolecular interaction. Three kinds of interactions are possible: pi-pi interactions (between flat, aromatic rings), hydrogen bonds (involving heteroatomic groups, one with a hydrogen atom), and van der Waals interactions (among straight chain hydrocarbons).

Pi-pi interactions, which result in stacking of aromatic rings, are more efficient for larger rings and less sterically hindered systems. Steric hindrance can result from substituents on the aromatic ring such as aliphatic chains or large saturated rings with restricted movement. Pi-pi interactions could involve several molecules with appropriate configurations.

Hydrogen bonding interactions may also contribute to self-assembly in asphalt. Although the concentration of functional groups capable of hydrogen bonding is very low, the energy of such bonds is on the order of 5 kcal. (Hydrogen bonding energy is highest for oxygen-containing functional groups and is much lower for nitrogen and sulfur.) They would be encouraged by the generally non-polar environment and could conceivably link

two molecules or even two pi-bound "stacks" described above. However, their low concentration reduces the likelihood of hydrogen bonding.

Van der Waals interactions are encouraged by the presence of long, straight-chain hydrocarbons, and hindered by branching along the chains.

Considering *only* the average structures one might expect pi-pi interactions to be important in asphalt AAM-1 because of its large, flat systems with few substituents. Van der Waals interactions may also be important because of the length of aliphatic chains and sparsity of branching. Polar interactions are less prominent, however, because of the low concentration of heteroatoms.

Because asphalt AAD-1 has small aromatic structures, the potential strength of pi-pi interactions is comparatively less. The branching of its aliphatic chains reduces the effectiveness of van der Waals forces, but it is quite highly polar, thus increasing the potential of polar interactions in this asphalt.

Intermolecular interactions should be quite similar in asphalts AAA-1 and AAK-1 and should include all three types. Asphalt AAK-1 is the more polar of the two, however.

Although asphalt AAF-1 has more aromatic carbon atoms in its average structure than AAA-1 and AAK-1, the aromatic core in AAF-1 is more hindered, indicating that pi-pi interactions are likely to be less influential. Similarly, the aromatic system in asphalt AAC-1 is more hindered than that in AAB-1.

Asphalt AAG-1, because of its small and hindered aromatic core, its low polarity and short, branched aliphatic chains may exhibit few interactions of any kind.

Again, based only on average structures, the influence of interactive forces would be expected to decrease in the orders listed below.

pi-pi interactions: $M > K = A > B > D > F > C > G$
polar interactions: $(D = K) > (A = B) > (M = G = F) > C$
van der Waals interactions: $M > (K > F > A > C = D) > (B = G)$

Effects of oxidation on asphalt chemical characteristics

Because of the perceived importance of oxidation to asphalt behavior, considerable effort is being expended in the study of this process. Researchers at WRI have devised laboratory procedures to simulate the effects of long-term pavement aging by treatment in a pressure oxygen vessel (POV). The added effect of short-term (mix plant) aging is being simulated by thin film oven (TFO) aging. Samples of each of the core asphalts which have been subjected to either POV or TFO plus POV aging were submitted for

NMR analyses. Two effects were observed: changes in the percentage of aromatic carbon and changes in the oxygen-containing functional groups.

Effects on percentage of aromatic carbon

The percentage of aromatic carbon was measured for all oxidized samples as previously described for core asphalts. Following POV treatment, a decrease in the percentage of aromatic carbon was found for all core asphalts except AAG-1, AAK-1 and AAM-1 (Table 14). However, when POV oxidation was preceded by TFO aging, decreases in percent aromatic carbon were found only in asphalts AAF-1, AAG-1 and AAD-1. Figure 14 contains a comparison of the percentages of aromatic carbon by ^{13}C -NMR between untreated core asphalts and their oxidized counterparts. The percentage changes in aromatic carbon content as a result of POV or TFO/POV processes are shown graphically in Figures 15 and 16, respectively. Changes of $\leq 5\%$ are not likely to be significant, however. (Please note that the order of the core asphalts is the same in both Figures 15 and 16.)

Oxidation of aromatic moieties to quinones (Scheme XII-A) could account for a loss of aromatic carbon resonances (115-130 ppm) as the ^{13}C -NMR signals for the resulting carbonyl carbons shift downfield of 180 ppm. Ring opening could also account for loss of aromatic carbon content, as could losses due to volatility.

Increase in the percentage of aromatic carbon may be attributable to the aromatization of naphthenic rings adjacent to aromatic systems. The differences in results from POV treatment as compared to POV with prior TFO processing are somewhat surprising. One might have expected the trends seen with POV oxidation alone to be extended with the addition of TFO treatment. However, the results in Figure 15 and 16 show that not to be the case. Reactions leading to loss of aromatic carbon content predominate in POV treatment of asphalts AAA-1, AAB-1, AAC-1, AAD-1, and AAF-1. However, prior TFO oxidation either inhibits that reaction and/or causes sufficient aromatization to counter-balance that effect to varying degrees in all of those asphalts except AAF-1. In asphalt AAK-1, the increase in aromatic carbon content is dampened by TFO treatment; that is, aromatization appears to be more likely with POV treatment alone. Nevertheless, it seems clear that POV and POV preceded by TFO result in different types of chemical change. To sort this out, the TFO process should be carried out alone and the products analyzed. Further, the volatility of components under POV conditions should be determined. Some changes in aromatic hydrogen content were also observed (Table 15). Those in asphalts AAA-1, AAB-1, AAD-1 and AAK-1 are probably not significant. In asphalt AAM-1, there appears to be a sharp increase in aromatic hydrogen content with POV treatment, but very little if any change with the addition of TFO processing. There are small increases in aromatic hydrogen content (about 1%) in asphalts AAC-1, AAG-1 and AAF-1.

Earlier in this report (page 12) an effort to estimate benzylic protons in the core asphalts was described. Although it was not possible to obtain an accurate count because of coalescence of ^1H -NMR resonances and overlapping of resonances, it was possible to estimate a maximum possible ratio of benzylic protons to all aliphatic protons. These protons are of interest because they represent potential sites for oxidation. In comparing ^1H -NMR spectra of untreated with those of oxidized asphalts, no significant change in the ratio of benzylic plus overlapping protons to all aliphatic protons was noted in any asphalt except AAK-1 (Table 16). In that case, the ratio of the spectral areas decreased from about 0.20 to 0.14 after TFO/POV oxidation. This does not constitute proof that benzylic protons are involved in the oxidation of asphalt AAK-1, but does appear to indicate that the mechanism of oxidation of AAK-1 differs from that of the other core asphalts.

Effects on some oxygen-containing functional groups

Using derivatization reactions described earlier, the effects of the two oxidation procedures on the content of carboxylic acids, alcohols and phenols have been investigated.

The core asphalts vary considerably in their susceptibility to oxidation as measured by increases in the oxygen in the functional groups just mentioned (Figure 17, Table 17). Asphalt AAM-1 shows only a nine percent increase in oxygen content after POV and no further increase with the addition of TFO treatment. Little susceptibility to POV oxidation is shown by asphalt AAB-1 but the extent of oxidation is increased somewhat by TFO/POV treatment. Similar, relatively small increases in oxygen content are exhibited by asphalts AAF-1 and AAG-1 following POV oxidation but larger changes are induced by TFO/POV. The amount of oxygen in OH and COOH groups in AAA-1 is increased by about 63 percent by POV; not much additional change is induced by TFO treatment, however. The remaining asphalts, AAD-1, AAC-1 and AAK-1, show very large percentage changes after POV treatment and continued oxidization in the TFO/POV procedure. In Asphalt AAC-1, the oxygen content is increased nearly 350 percent by TFO/POV. *Nevertheless, the concentration of OH + COOH remains very low with a maximum of about 31×10^{-5} moles/gram of asphalt in AAG-1 after TFO/POV treatment* (Figure 17, Table 17).

Summary data in Table 17 is broken down into individual functional groups in Table 18. It can be seen that more aliphatic alcohols form in AAC-1 than in any other asphalt, but the concentration remains very low (C, Table 18). Asphalts AAC-1 and AAK-1 outstrip the other asphalts in formation of phenols upon oxidation but the final concentrations remain lower than those for AAF-1 and AAG-1 (B and D, Table 18).

Asphalt AAC-1 has the largest increase in COOH concentration after oxidation (A, Table 18). Asphalt AAG-1 increases COOH concentration less than one-fourth as much

but still has the highest concentration of COOH of all the asphalts (see *POV* and *TFO/POV*, A, Table 18).

It appears that, in terms of oxygen uptake, as in change in aromatic carbon, *POV* oxidation is not the same as *TFO/POV* treatment. However, the effect of the processes on oxygen uptake is, in general, additive.

Summary of oxidation effects

From the foregoing discussion, it may be concluded that asphalt oxidation is a complex process that is dependent not only on reaction conditions, but also on the nature of the asphalt itself. Several effects have been observed in different asphalts: a decrease in percentage of aromatic carbon; an increase in percentage of aromatic carbon; an increase in carboxylic acids content; an increase in aliphatic alcohol concentration; an increase in the amount of phenol. The reactions outlined in Scheme XII are possible mechanisms by which the observed effects could be explained. However, some of these reactions (C, F, H, and I) take place under certain specific conditions and it is not obvious how they might be initiated in asphalt. They should be considered hypothetical, but can, nevertheless, be used as a point of departure.

In Table 19 are listed the possible reactions with a broad indication of the importance of the reaction (i.e. *-minor, **-moderate, ***-major) for each core asphalt. The last four columns in the table rank the asphalts by content of aromatic carbon and total COOH plus OH both before and after *POV/TFO* aging (1 = lowest concentration → 8 = highest concentration).

Most of the asphalts are relatively inactive in terms of change in aromatic carbon percentage (Table 14). Asphalts AAA-1, AAB-1 and AAC-1 change in concentration of measured functional groups very little (Table 17, column 4). In fact, these three asphalts have the lowest concentrations of oxygen groups after *TFO/POV* (Table 17, column 3).

Asphalt AAK-1 oxidizes strongly to form carboxylic acids and phenols (Table 18). The tendency to oxidize could be explained in part by the very high concentration of vanadium complexes present in this asphalt.

The most highly reactive asphalt is AAC-1. Its concentration of COOH plus OH groups increases by almost 290 percent (Table 17). Its rank in terms of oxygen-containing functional groups rises from 1 to 7 (Table 19).

Asphalt AAG-1 is only moderately reactive but, even after *TFO/POV* treatment, it still has the highest carboxylic acid concentration of the core asphalts (Table 18).

Four asphalts appear to form aliphatic alcohols--AAF-1 to a very minor degree, AAB-1 and AAM-1 to a somewhat greater degree, and AAC-1 more than any other (Table 18).

Several questions remain to be answered:

1. Does the TFO procedure mimic, chemically, the mixing of asphalt with aggregate; does POV accurately predict long-term field aging? If so, then the procedures must be considered in tandem, since field aging will never occur without prior mixing with aggregate.
2. Are the carboxylic acids, phenols and alcohols significant to asphalt performance; in what ways?
3. Is the oxidizability more important than the final result? For example, although AAC-1 is highly susceptible to oxidation, AAG-1 still has a higher concentration of OH and COOH in the end. This consideration includes, for example, the question of whether native functional groups migrate to the surface of the aggregate or whether newly-formed groups influence this bonding.

Fractions from Ion Exchange Chromatography

The SHRP core asphalts were separated into five fractions based on their acid-base character by ion exchange chromatography (IEC) at Western Research Institute. These fractions differ in a variety of ways, but the result of these differences is most important, i.e., each of the fractions makes a characteristic contribution to the physical properties of the asphalt. Therefore, it was desired to have the same kind of chemical information as had been collected for the whole asphalts. Unfortunately, because of time constraints under this contract, a full battery of NMR analyses could not be accomplished on the resulting 40 samples. However, percentage of aromatic hydrogen and carbon were determined for all neutral, strong acid and strong base fractions.

In general, the percentage of aromatic carbon in neutrals fractions is less than 20 (Table 20). Neutrals from AAF-1 are exceptional, containing more than 24 percent aromatic carbon. (The whole asphalt AAF-1 has the highest aromatic carbon content of the core asphalts.) However, it must be noted that, because the neutrals fractions comprise at least 50 percent of the whole asphalt, they account for a significant portion of the aromatic carbon in the whole asphalt (Table 21).

Strong acids and strong bases are, with one exception, *much* more aromatic than the whole asphalts from which they are derived (Table 20). The exception is strong bases from AAG-1: there is no difference between the aromatic carbon contents of the whole asphalt and the strong bases. The strong acids fraction accounts for between seven and 26 percent of the asphalt, but it supplies a larger proportion of the aromatic carbon. The percentage of aromatic carbon in the whole asphalt accounted for by each of the fractions is given in Table 21. Inasmuch as aromatic structure and functional group characteristics may contribute to self-assembly in asphalts, this information may contribute to understanding asphalt behavior.

Summary and Conclusions

The goal of this research effort has been to use solution-state NMR spectroscopy to elucidate key chemical characteristics of the SHRP core asphalts. A number of different techniques were explored. Those which appeared to hold most promise were optimized and are fully described in this report.

It was determined that the aromatic carbon contents of the core asphalts range between about 23 and 33 percent while aromatic proton contents range between 6.5 and 8.7 percent. This indicates that, on average, the aromatic structures are highly condensed and somewhat substituted.

A convention has been adopted for general comparisons among asphalts. For each parameter, the identifying letter of the asphalt with the highest value is listed first. Use of parenthesis indicates that, although there may be trends within a group of asphalts, the differences may not be statistically significant. Using this convention for percent aromatic hydrogen:

$$F > (B > A = G > D = K) > (M > C)$$

and for percent aromatic carbon:

$$(F > B) > (G > A = C > K > M) > D$$

Aromatic substitution index (the number of aromatic carbon atoms per aromatic hydrogen) indicates how many aliphatic substituents there are on an average aromatic unit:

$$(C > B = G > F > A = K = M) > D$$

Pi-pi interactions (between flat, aromatic rings) may be very important to asphalt properties so the size, substitution and configuration of aromatic units must be considered in assessing the importance of pi-pi interactions.

The asphalts were found to be remarkably similar in the *kinds* of aliphatic carbons contained and to differ only slightly in the numbers of carbon atoms representing most types. The major difference was found to be in the number of carbon atoms found in long methylene chains:

$$M > > C > (F > B > K > A) > (D > G)$$

Because long, unbranched aliphatic chains can contribute to van der Waals interactions, this parameter may be important to asphalt behavior.

Using data from NMR analyses, molecular weights and elemental analyses, an average structure was defined for each asphalt (Scheme XI). Although these structures are not unique and can be misleading if their average nature is not kept firmly in mind, they do serve to show some characteristics which may influence the asphalt's behavior.

Derivatization procedures were adapted in order to analyze some functional groups by NMR spectroscopy. For example, phenol content ranged from 1.5 to 5.5×10^{-5} moles/gram of asphalt:

$G > (F=B) > (A \approx M > D) > (C > K)$

Carboxylic acid content ranged from 2.8 to 9.1×10^{-5} moles/gram:

$G > B > A > (M > D > F) > (K > C)$

These functional groups may be important to the properties of asphalt but they are present in very low concentrations.

Asphalts which had been oxidized in the laboratory by a pressure oxygen vessel technique (POV) and by POV preceded by thin film oven treatment (TFO/POV) were obtained from SHRP-A-002A contractors at Western Research Institute. It was found that not only do the procedures have different effects but also those effects differ from asphalt to asphalt. The aromatic carbon content of most asphalts changed very little (less than 10%) although there were small decreases as well as increases within that group. POV oxidation appeared to induce aromatization in some asphalts that was reduced if the higher temperature TFO treatment was used first. From this standpoint, oxidation is very complex and not clearly understood, although possible mechanisms for reactions have been proposed.

In terms of increases in the oxygen-containing functional groups, the asphalts were found to differ greatly and the effects of POV and TFO were observed to be additive. After TFO/POV, the increase in concentrations of phenols, alcohols and carboxylic acids, i.e., the susceptibility to oxidation were in the order:

$C > K > D > (F > G > A) > B > M$

From these and other data, the asphalts will be described in the following paragraphs. *These descriptions will not explain all asphalt properties and should be regarded as speculative.* They should be used together with chemical data being generated elsewhere within SHRP.

Asphalt AAM-1 is clearly unique among the SHRP core asphalts. With the highest average molecular weight, it has the largest aromatic core in its average structure and a low substitution index. Thus, pi-pi interactions are likely to be strong. However, its percent aromatic carbon is quite low and its aliphatic carbons are arranged in very long chains with only one branch for 14 backbone carbon atoms. Therefore, van der Waals interactions are also likely to be very strong. It has the lowest concentration of heteroatoms, thus making polar interactions unlikely. Asphalt AAM-1 is quite inert to oxidation and so may be tender when placed. Its average structure (Scheme XI.1) shows relatively few sites at which oxidation or aromatization would be possible. However, it seems unlikely to be subject to oxidative aging.

Another unique asphalt is AAD-1. Like AAM-1, it has a low concentration of aromatic carbons, but these carbons are arranged, on average, in very small condensed ring systems which are not highly substituted. One would expect that pi-pi interactions would be likely, but their strength would not be very great. Its aliphatic chains are relatively short and have one branch for every eight chain backbone carbon atoms, thus interfering with van der Waals interactions. However, it has more heteroatoms per average molecule than any other core asphalt, therefore, polar interactions are probably strong contributors. Its aromatic structure is not particularly affected by oxidation but it undergoes large increases in OH and COOH concentrations upon oxidation and is therefore likely to be susceptible to aging. The average structure (Scheme XI.2) shows more oxidizable sites for average molecular weight than AAM-1.

Asphalt AAG-1 is also unlike any other core asphalt. Its aromatic content is "average" and the aromatic structure, although best described as linear, is not highly unusual. However, it is more highly substituted than either AAM-1 or AAD-1 and these substituents are, we believe, likely to be alicyclic. These may interfere with pi-pi interactions. Its aliphatic chains are relatively short and more highly branched (1/5) so van der Waals interactions are less likely. Although its overall heteroatom content is very low it has the highest concentrations of phenols and carboxylic acids of the core asphalts. However, because of the refinery process, these are present as salts and are therefore prevented from hydrogen bonding. The authors would expect AAG-1 to form so-called "tender" mixes. It is not susceptible to oxidation although it showed some loss of aromatic carbon after TFO/POV treatment. Its average structure (Scheme XI.8) contains an aromatic ring that could be susceptible to quinone formation.

Asphalt AAC-1 stands out not so much in its average structure as in its tendency to oxidize. Its aromatic structure is similar to that of AAG-1 although it is slightly more substituted and so even less able to form pi-pi bonds. The aliphatic chains are longer than those of AAG-1 (but not so long as AAM-1) and have just one branch for eight backbone carbons, thus somewhat favoring van der Waals interactions. In its original state, it has few heteroatoms and the lowest concentration of OH and COOH groups. However, this concentration increases by 133% after POV and 288% after TFO/POV treatment. (Note several oxidizable sites in the average structure, Scheme XI.7.) If this phenomenon also occurs in the field, the authors expect poor performance because of the predominance of van der Waals interactions and the increasing influence of polar forces but little balance from pi-pi interactions.

The aromatic/alicyclic ring structure of asphalt AAA-1 differs from that of AAC-1 in that it is less substituted and, therefore, more likely to form pi-pi bonds. Its aliphatic chains are somewhat shorter but less branched (1/9). Its content of heteroatoms is quite high, so one would expect a greater contribution from polar interactions to self-assembly. Unlike AAC-1, however, it is much less susceptible to oxidation. This asphalt seems to have a better balance of interactive forces and should perform reasonably well, except for moderate aging.

In asphalt AAB-1, the aromatic system does not differ greatly from others described so far (except AAM-1). Substitution is low but the substitution pattern discourages pi-pi interactions to some degree. Aliphatic chains are of "average" length but are highly branched (1/5) so van der Waals interactions would not predominate. The original heteroatom content is "average" and changes very little on oxidation. The aromatic portion also remains relatively unchanged. This asphalt seems to have a reasonable balance of interactive forces and should also perform acceptably.

The ring system of asphalt AAF-1 is fairly large but the number of substitutions including alicyclic rings reduces the ability to form pi-pi bonds. The aliphatic chains are shorter but not highly branched (1/10) favoring van der Waals interactions to some degree. Heteroatom content is quite high at first but changes only slightly upon oxidation. However, it appears to lose aromatic carbon during that process.

Finally, asphalt AAK-1 has an aromatic system like that of AAA-1 with substituents arranged to favor pi-pi interactions. It has two aliphatic chains of average length with only one branch for each 11 straight chain carbon atoms, thus favoring van der Waals interactions somewhat. Its heteroatom content is very similar to that of AAA-1. This appears to be a good balance of interactive forces in the untreated asphalt. However, it apparently gains OH and COOH functionality upon oxidation (144% after POV, 225% after TFO/POV). Its average structure provides opportunity for these phenomena. This may be due to the presence of high concentrations of vanadium (although that explanation would not account for the high oxidation of AAC-1). Nonetheless, AAK-1 is likely to age unacceptably.

References

1. D.A. Netzel, F.P. Miknis, "N.m.r. study of US Eastern and Western shale oils produced by pyrolysis and hydropyrolysis", *Fuel*, 1982, 61, 1101.
2. T. Suzuki, et. al., "Chemical structure of tar-sand bitumens by ^{13}C and ^1H -NMR spectroscopic methods", *Fuel*, 1982, 61, 402.
3. P.L. Gupta, et. al., "Estimation of average structural parameters of petroleum crudes and coal-derived liquids by ^{13}C and ^1H -NMR", *Fuel*, 1986, 65, 515.
4. M.U. Hasan, et. al., "Structural Characterization of Saudi Arabian medium crude oil by NMR spectroscopy", *Fuel*, 1985, 64, 839.
5. S. Gillet, et. al., "Optimum conditions for crude oil and petroleum product analysis by carbon-13 nuclear magnetic resonance spectrometry", *Anal. Chem.*, 1980, 52, 813.
6. M. Araujo, et. al., "Nuclear magnetic relaxation of protons in Venezuelan crude oil", *Fuel*, 1989, 68, 1079.

7. T. Yoshida, et. al., "Derivation of structural parameters for coal-derived oil by carbon-13 nuclear magnetic resonance spectrometry", *Anal. Chem.*, 1980, 52, 817.
8. V. Sklenar, et. al., "Analysis of coal asphaltenes by carbon-13 Fourier transform nuclear magnetic resonance spectrometry", *Anal. Chem.*, 1980, 52, 1794.
9. D.M. Cantor, "Nuclear magnetic resonance spectrometric determination of average molecular structure parameters for coal-derived liquids", *Anal. Chem.*, 1978, 50, 1185.
10. E. Hirsch and K.H. Altgelt, "Integrated structural analysis. A method for the determination of average structural parameters of petroleum heavy ends", *Anal. Chem.*, 1970, 42, 1330.
11. L.P. Blanchard, et. al., "Structure parameter analysis of asphalt fractions by a modified mathematical approach", *Anal. Chem.*, 1978, 50, 1212.
12. G.A. Haley, "Molecular and unit sheet weights of asphalt fractions separated by gel permeation chromatography", *Anal. Chem.*, 1971, 43, 371.
13. K.H. Altgelt and E. Hirsch, "GPC separation and integrated structural analysis of petroleum heavy ends", *Sep. Sci.*, 1970, 5, 855.
14. C.E. Snape, "Analysis of fossil fuels" in *Analytical NMR*, L.D. Field and S. Sternhell, eds., John Wiley and Sons, 1989, 65.
15. A.P. Hagen, et. al., "¹³C NMR studies on roadway asphalts", *Fuel Science and Technology Int'l.*, 1989, 7, 1289.
16. K.D. Rose and M.A. Francisco, "NMR characterization of acidic heteroatoms in heavy petroleum fractions", *Symposium on Magnetic Resonance of Heavy Ends*, Division of Petroleum Chemistry, Inc., American Chemical Society Miami Beach Meeting, April, 1985, page 262.
17. K.D. Rose and M.A. Francisco, "A two-step chemistry for highlighting heteroatom species in petroleum materials using ¹³C-NMR spectroscopy", *J. Am. Chem. Soc.*, 1988, 110, 637.
18. K.D. Rose and M.A. Francisco, "Characterization of acidic heteroatoms in heavy petroleum fractions by phase-transfer methylation and NMR spectroscopy", *Energy and Fuels*, 1987, 1, 233.
19. C.E. Snape, et. al., "Estimation of oxygen group concentrations in coal extracts by nuclear magnetic resonance", *Anal. Chem.*, 1982, 54, 20.

20. A.E. Wroblewski, et. al., "Phosphorus-31 NMR spectroscopic analysis of coal pyrolysis condensates and extracts for heteroatom functionalities possessing labile hydrogen", *Energy Fuels*, 1988, 2, 765.
21. E. Rafii, et. al., "Characterization of phenols from coal liquefaction products by ^{119}Sn nuclear magnetic resonance spectrometry", *Anal. Chem.*, 1985, 57, 2854.
22. B.A. Stoochnoff, et. al., "The methylation of some phenols with sodium hydride/methyl iodide in tetrahydrofuran at room temperature", *Tetrahedron Letters*, 1973, 21.
23. C.A. Brown and D. Barton, "Rapid stereospecific methylation of alcohols and glycols with sodium hydride/methyl iodide", *Synthesis*, 1974, 434.
24. M.P. Spratt, et. al., "Carbon-13 and fluorine-19 nuclear magnetic resonance chemical shift studies of carbon-13 enriched p-fluorobenzoyl derivatives", *Anal. Chem.*, 1985, 57, 359.
25. R. Nayaran, et. al., "Chemical structural units in a subbituminous (Wyodak) coal", in *1987 International Conference on Coal Science*, Elsevier Science Publishers B.V., Amsterdam, 1987, p. 61.
26. J.G. Speight and S.E. Moschopedis, "On the molecular nature of petroleum asphaltenes", in *Chemistry of Asphaltenes*, J.W. Bunger and N.C.Li, eds., *Advances in Chemistry Series*, American Chemical Society, 1981, 195.
27. L.B. Ebert, et. al., "Reductive alkylation of petroleum residua using potassium metal and tetrahydrofuran at room temperature", *Fuel*, 1989, 68, 935.
28. A.F. Cockerill, et. al., "Lanthanide shift reagents for nuclear magnetic resonance spectroscopy", *Chem. Reviews*, 1973, 73, 553.
29. B.C. Mayo, "Lanthanide shift reagents in nuclear magnetic resonance spectroscopy", *Rev. Chem. Soc.*, 1973, 2, 49.
30. T.H. Black, "The preparation and reactions of diazomethane" for Aldrich Chemical Company; "Diazald, MNNG and diazomethane generators", technical information bulletin, Aldrich.
31. F.K. Schweighardt, et. al., "Trimethylsilyl ether formation to quantitate hydroxyls by nuclear magnetic resonance spectroscopy", *Anal. Chem.*, 1978, 50, 368.
32. J.R. Murphy, "Procedures for grouping a set of observed means," Ph.D. Dissertation, Oklahoma State University, 1973.

33. R. Gopalan, "A simulation study of procedures for classifying a set of observed means into distinct groups," M.S. Dissertation, Oklahoma State University, 1986.

Figures

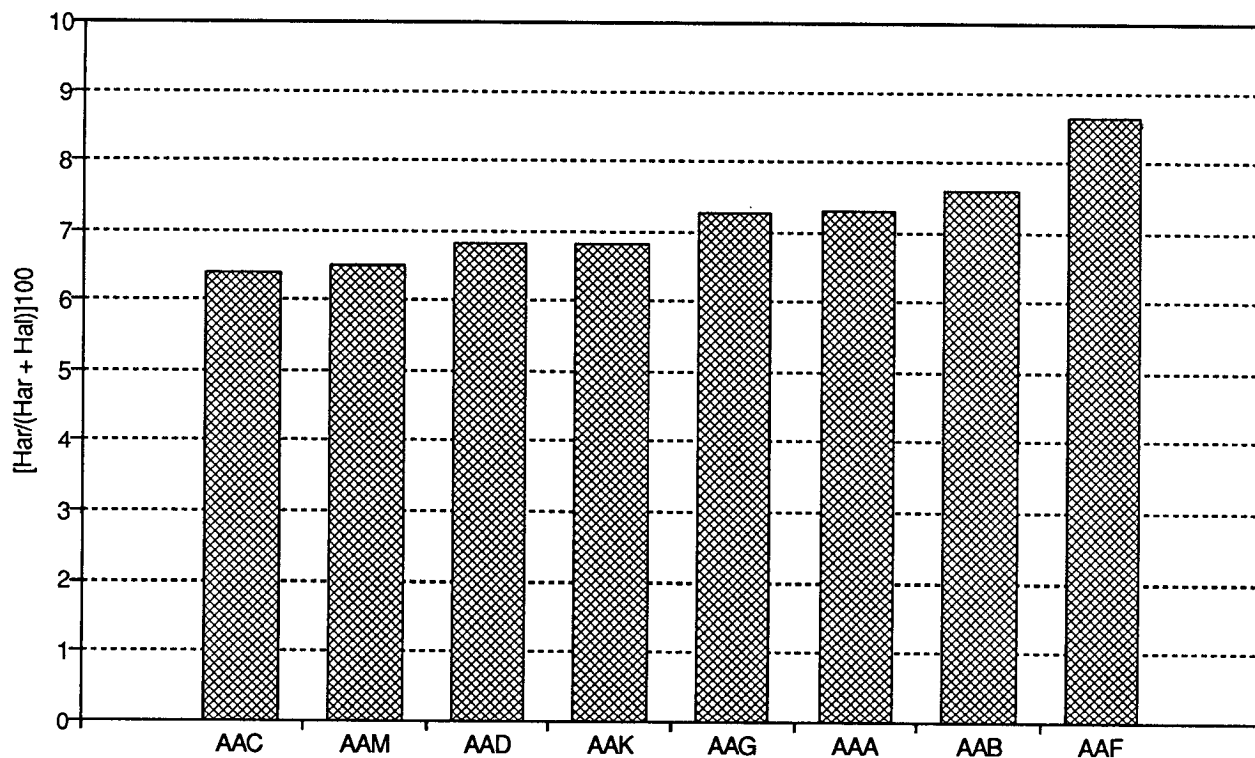


Figure 1. Percentage of aromatic hydrogen in core asphalts. Bars represent the average of three replications.

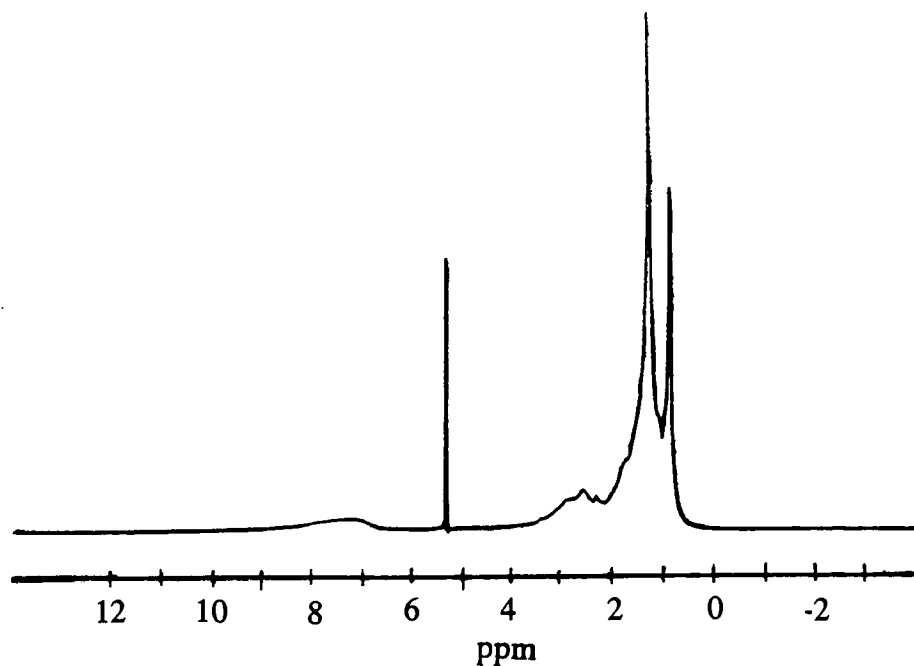


Figure 2. Example of ¹H-NMR spectrum of asphalt

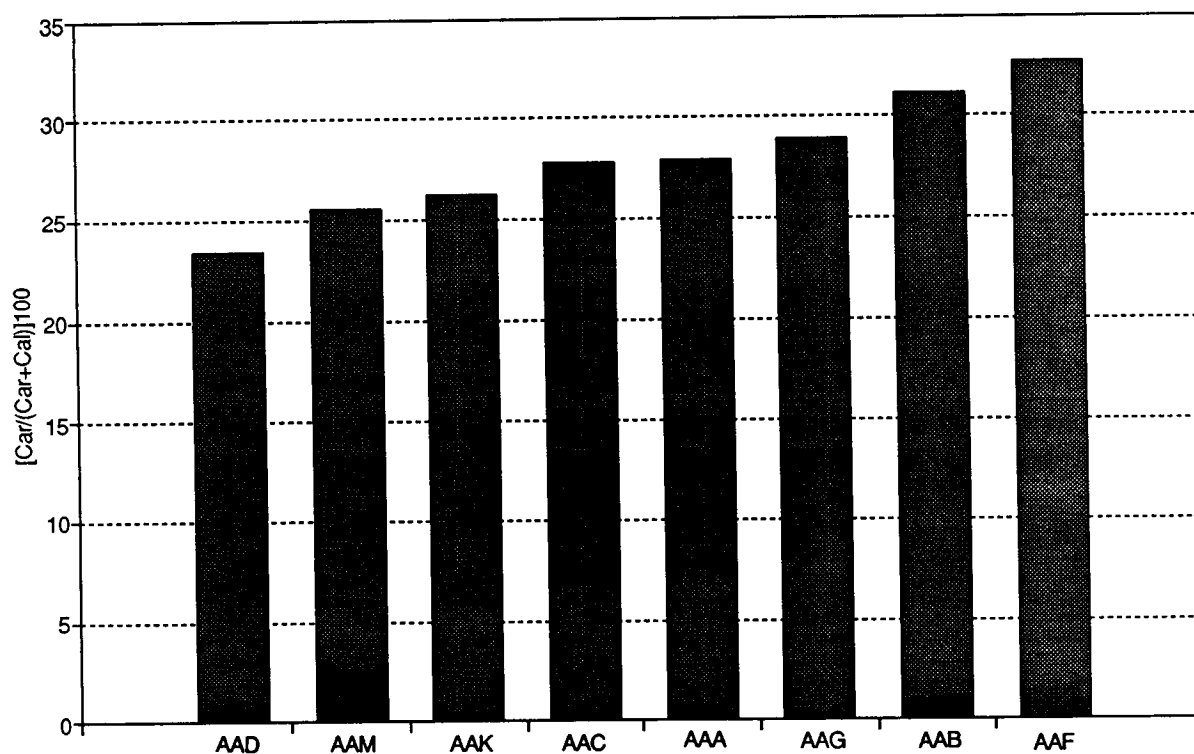


Figure 3. Percentage of aromatic carbon in core asphalts. Bars represent the average of replicated measurements.

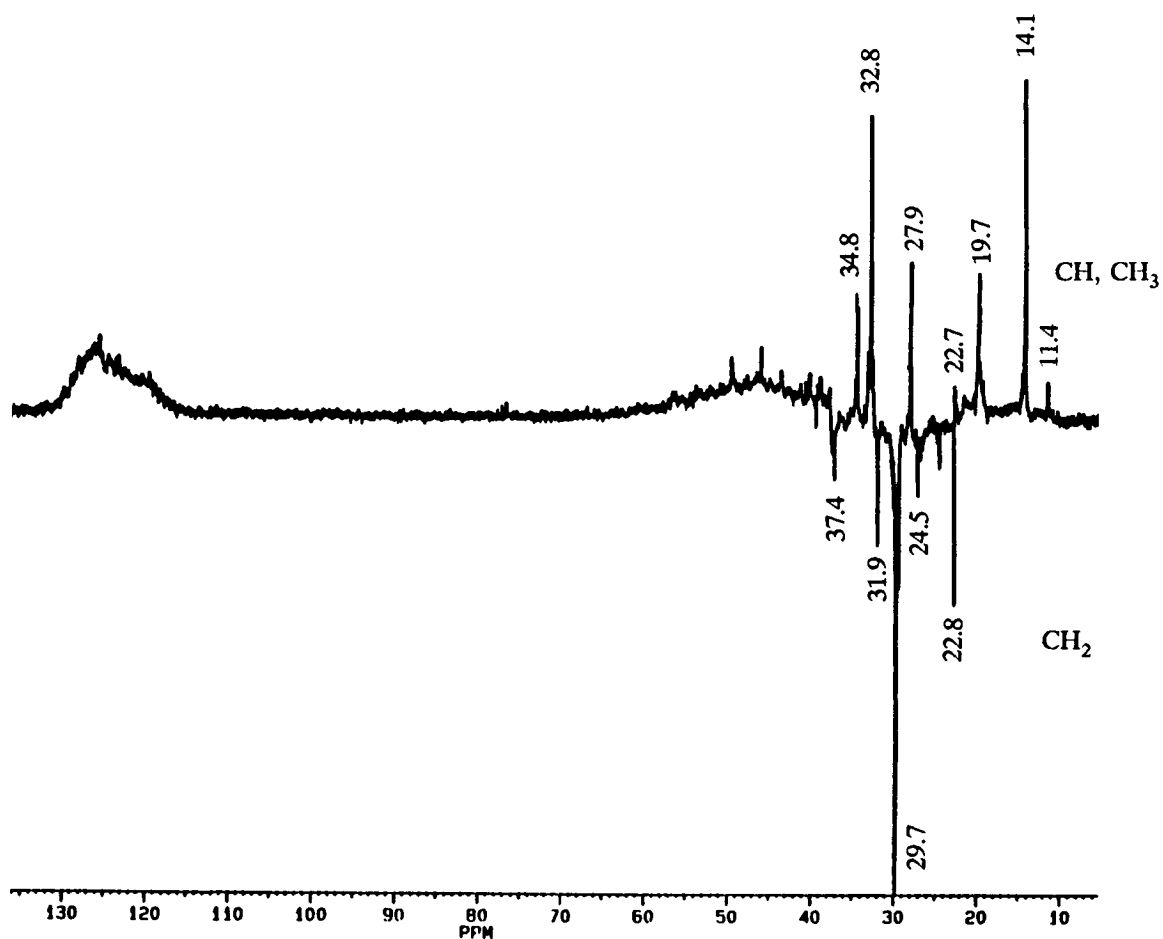


Figure 4. Typical spectrum from DEPT 135 experiment

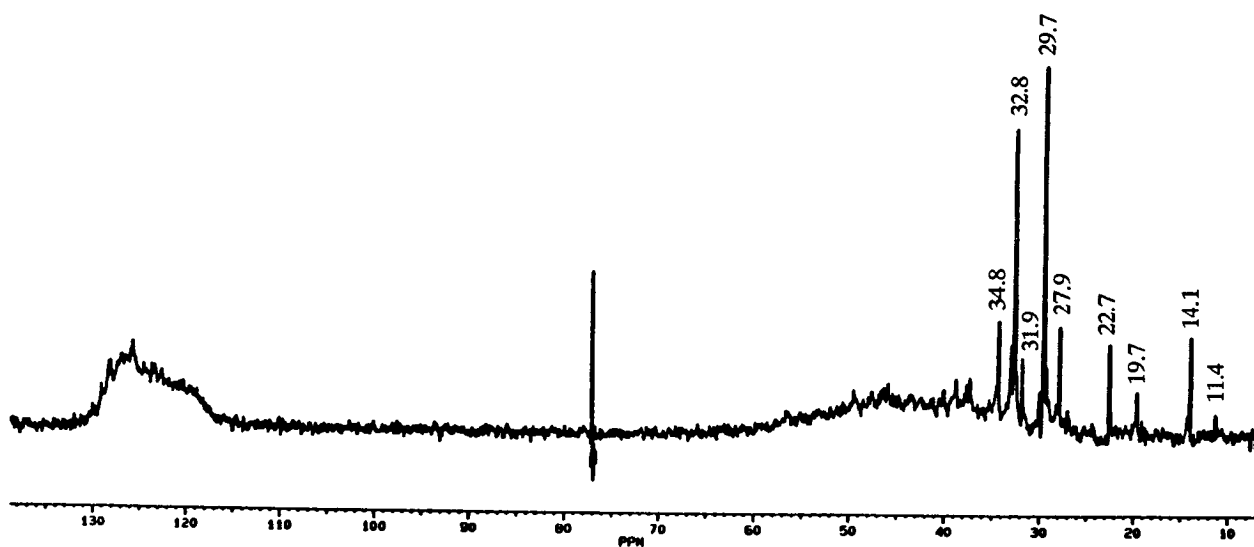


Figure 5. Typical spectrum from DEPT 90 experiment

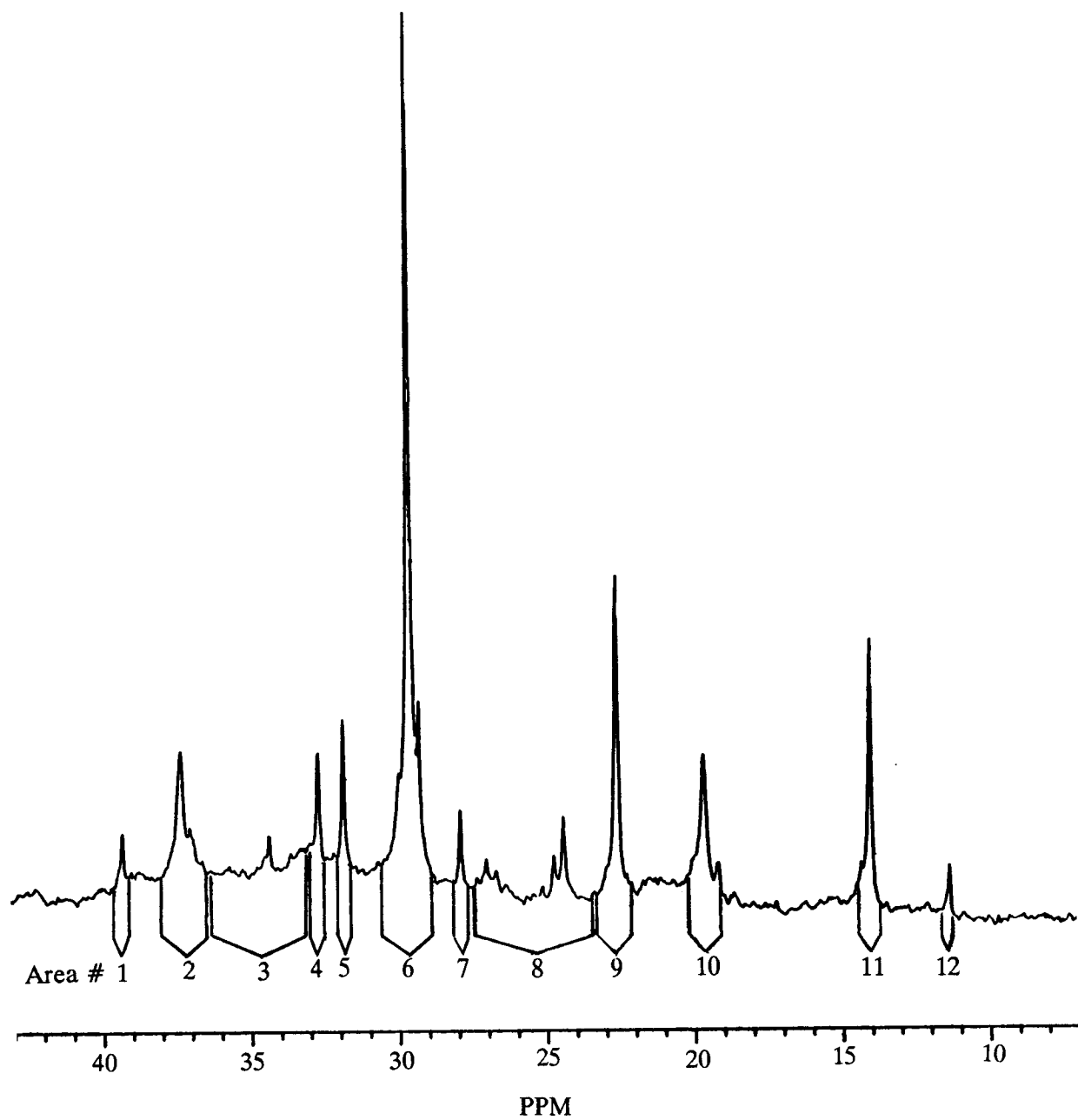


Figure 6. ^{13}C -NMR spectrum of aliphatic region, showing integration limits for peaks identified by number in Tables 5 and 6

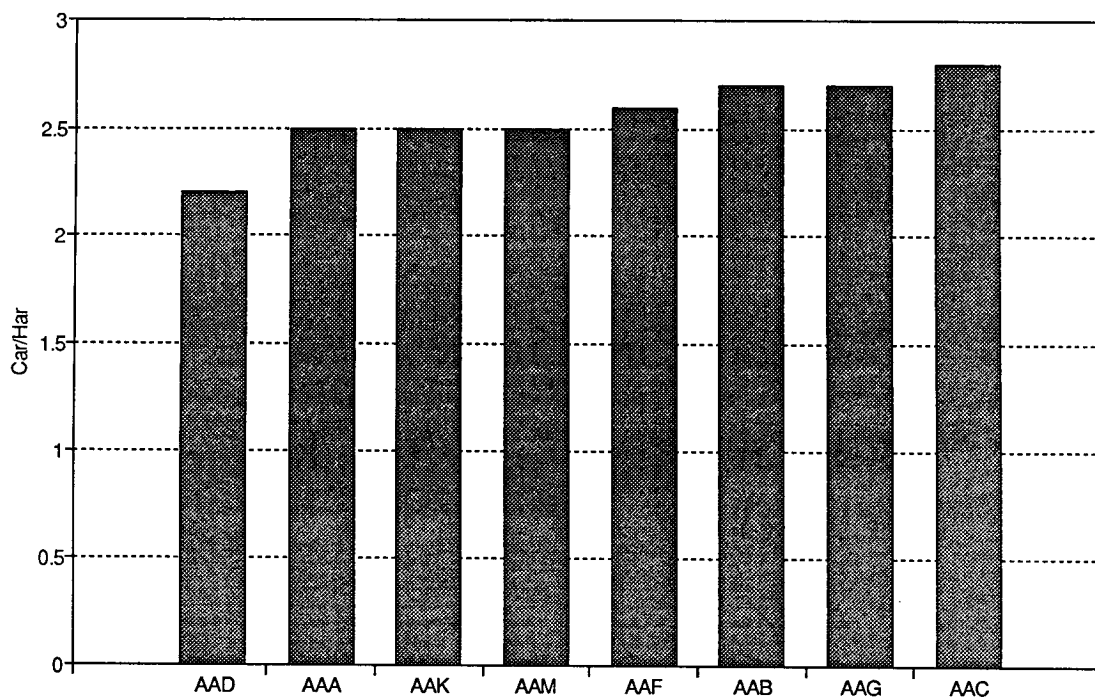


Figure 7. Aromatic Substitution Index (ASI) for eight core asphalts

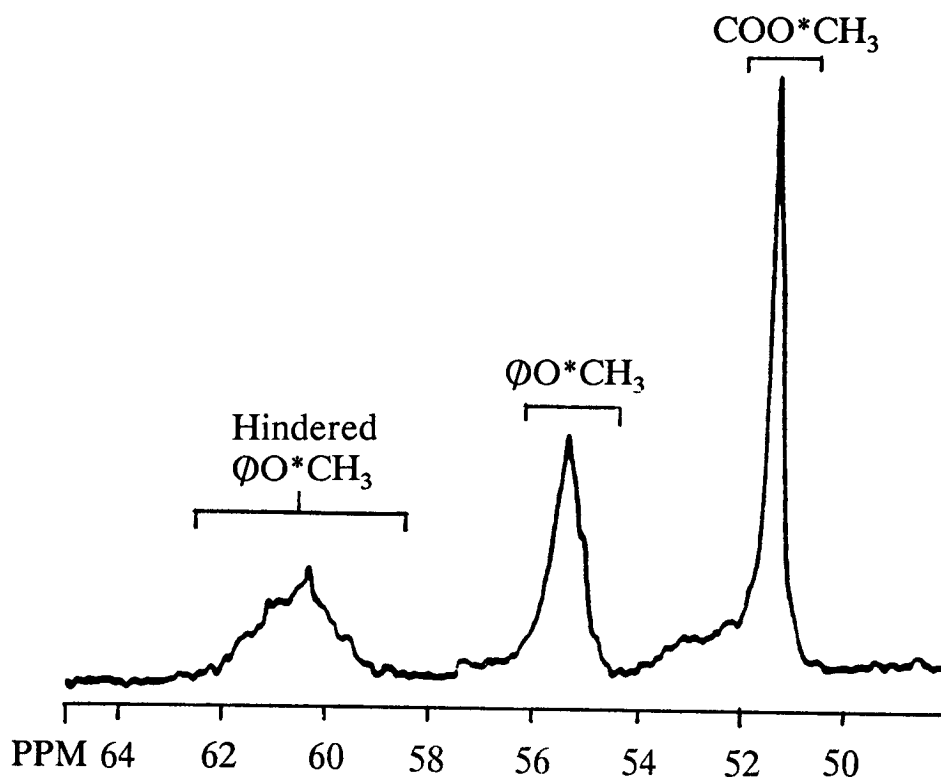


Figure 8. Methoxy region of ^{13}C -NMR spectrum of asphalt after phase-transfer methylation (PTM) treatment

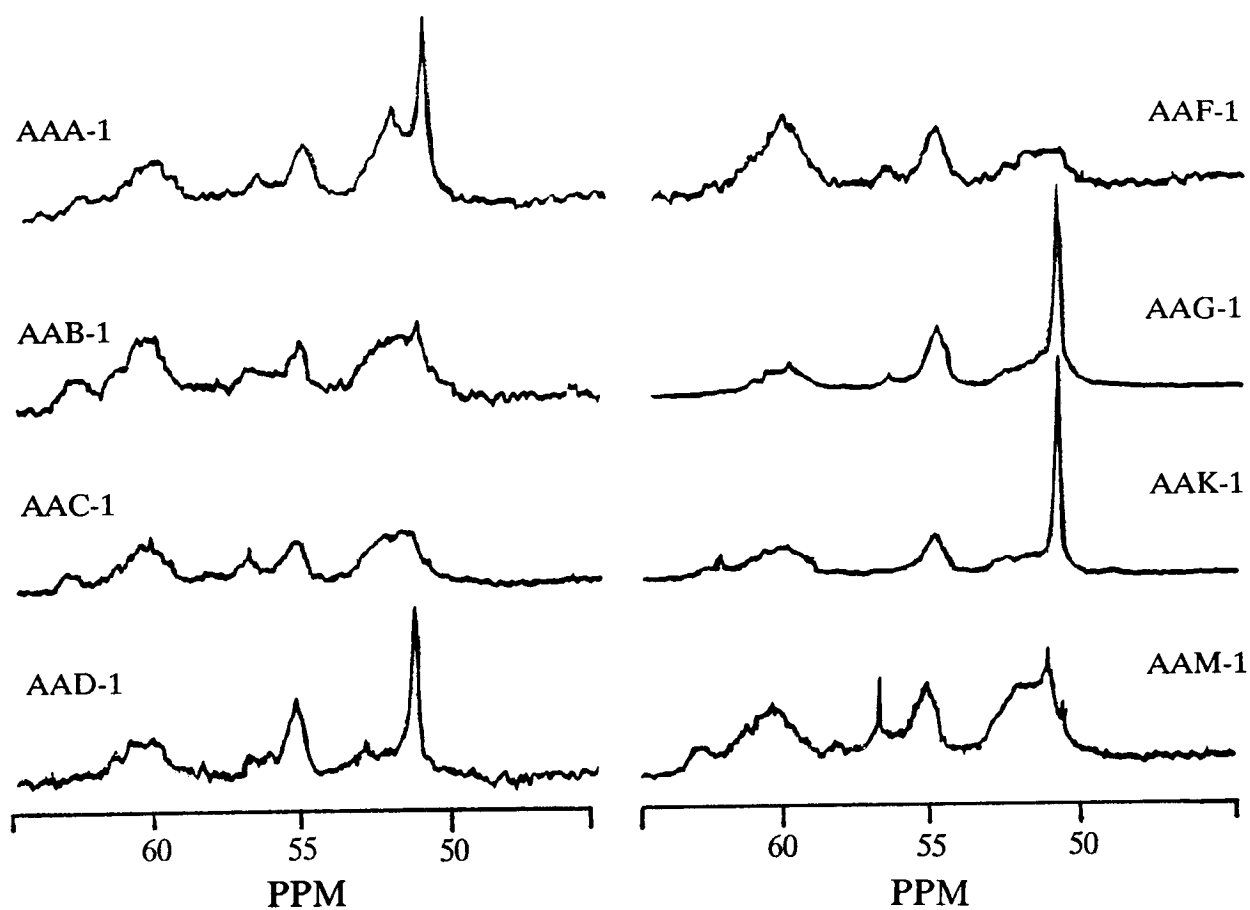


Figure 9. Methoxy regions of ^{13}C -NMR spectra after short-term PTM

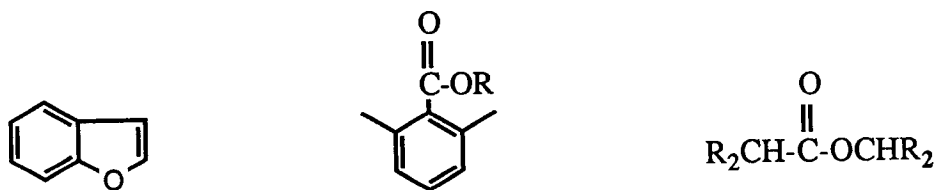


Figure 10. Example of aromatic and hydrolysis-resistant oxygen functionalities

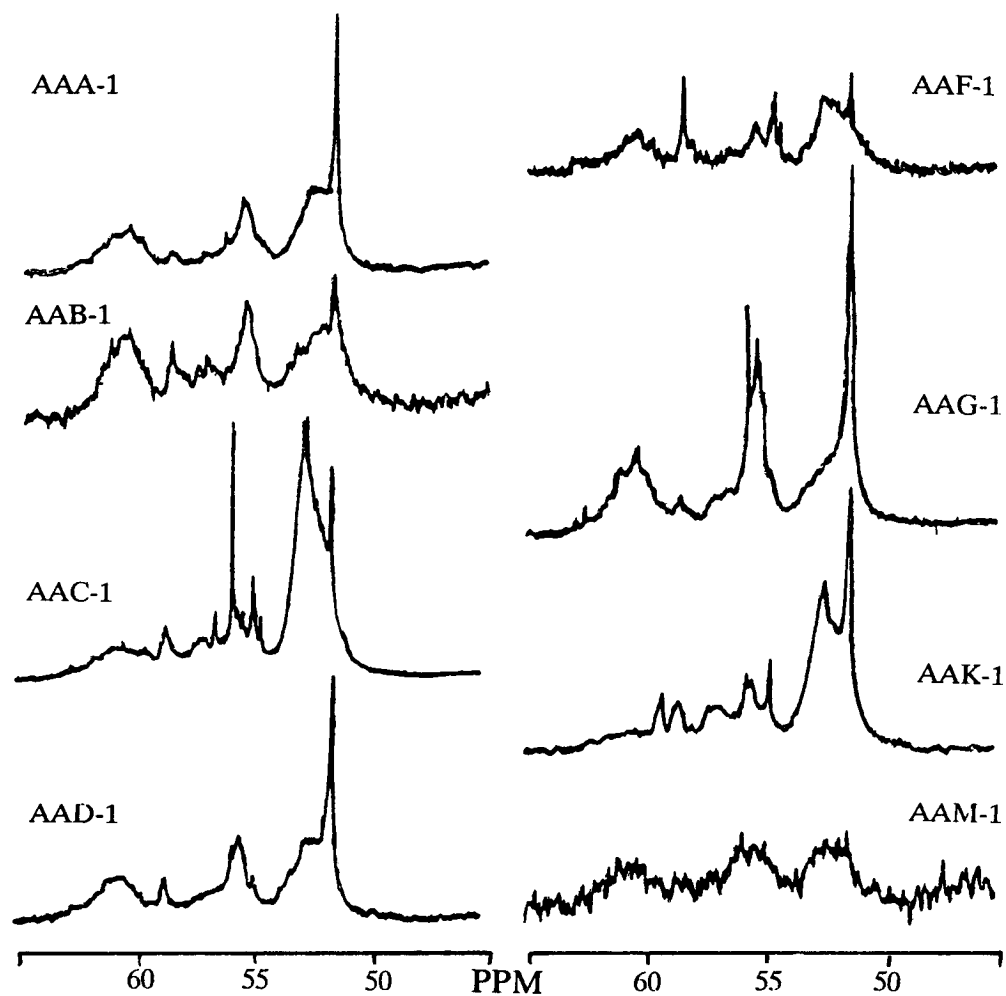


Figure 11. Methoxy regions of ^{13}C -NMR spectra after long-term PTM

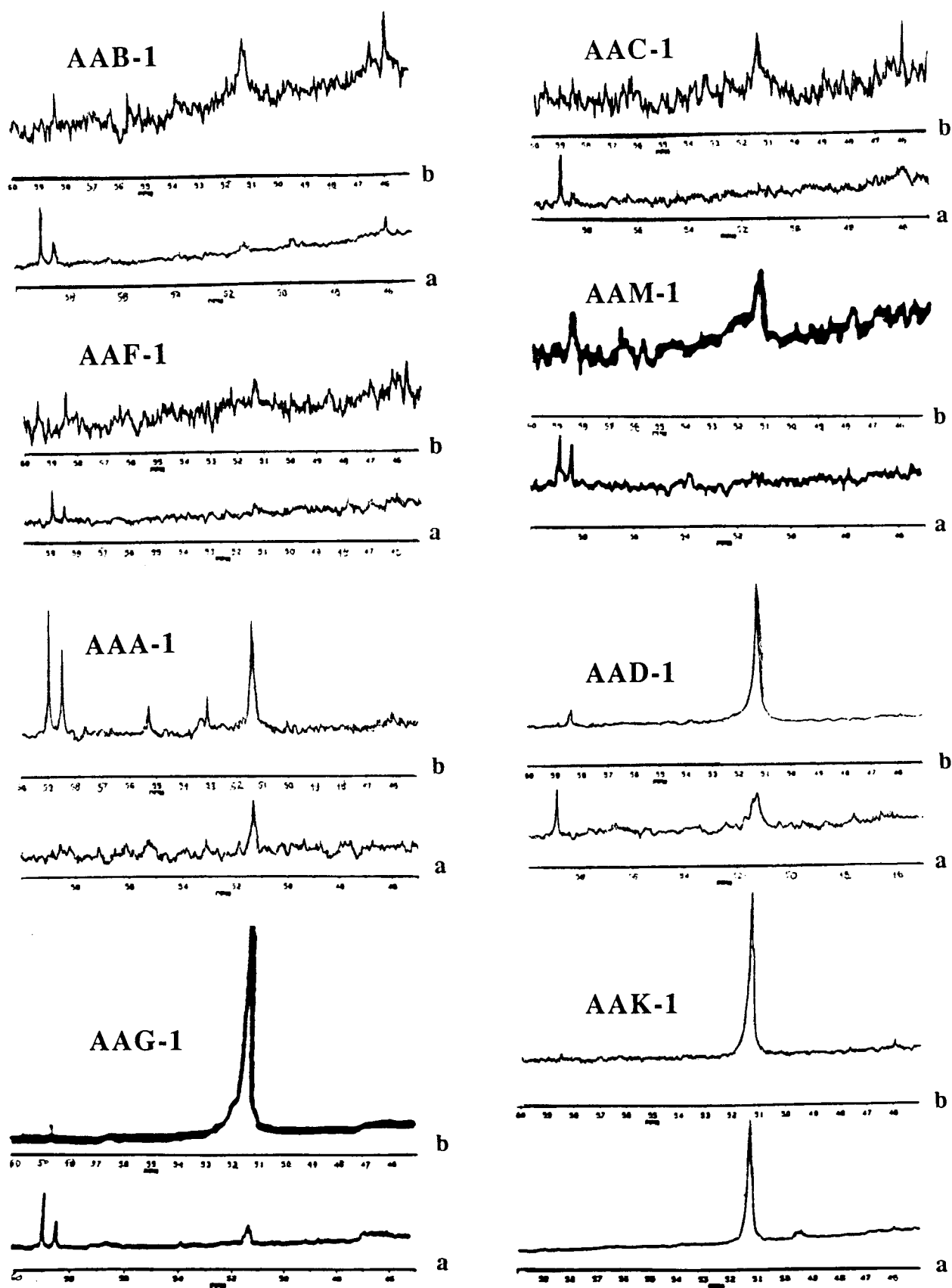


Figure 12. Comparisons of ^{13}C -NMR spectra of methoxy regions of core asphalts after one reaction with diaxomethane (spectrum a of each pair) and after second reaction (spectrum b)

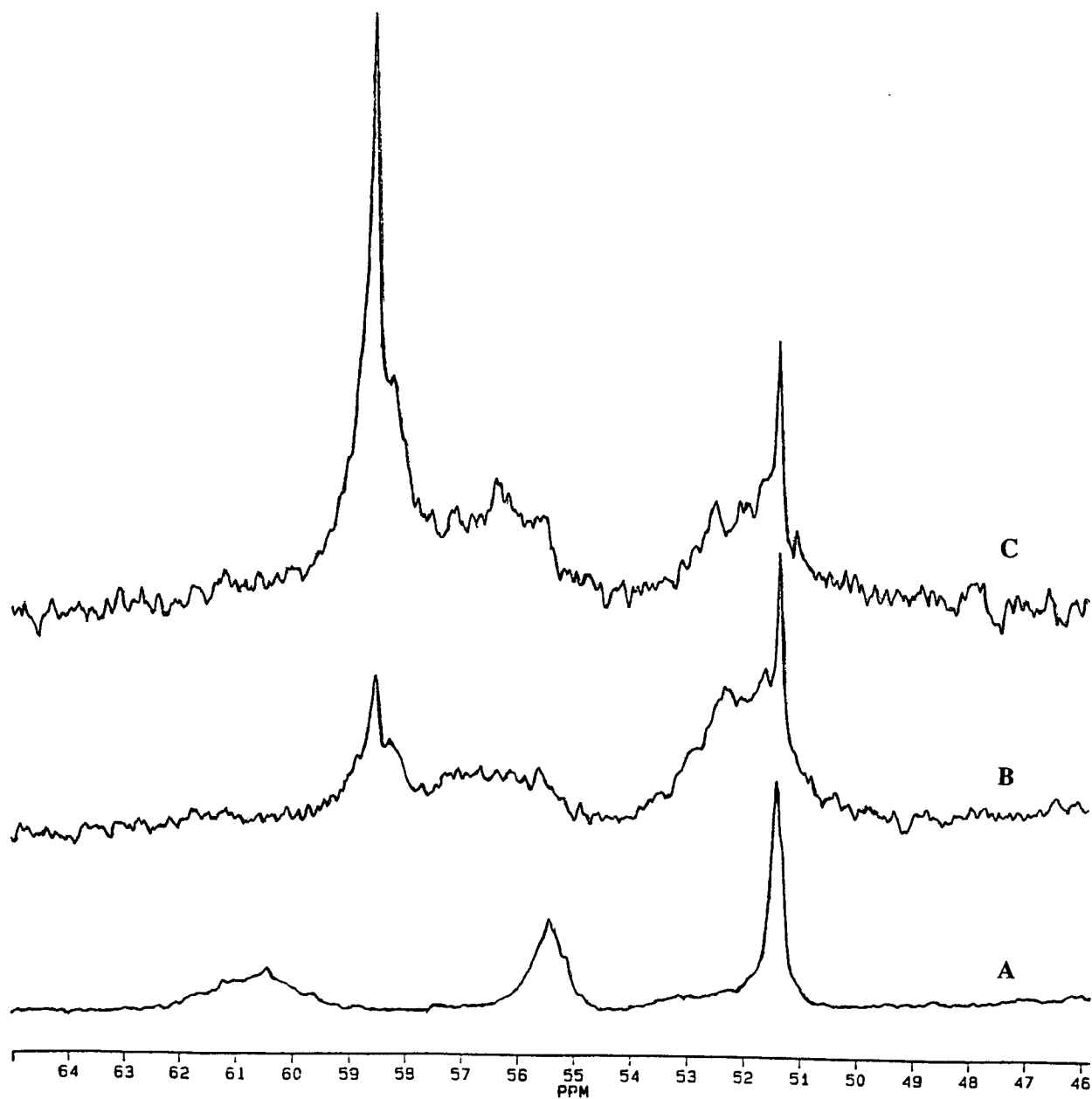


Figure 13. ^{13}C -NMR spectra resulting from LAH reduction and subsequent methylation of esters and ketones

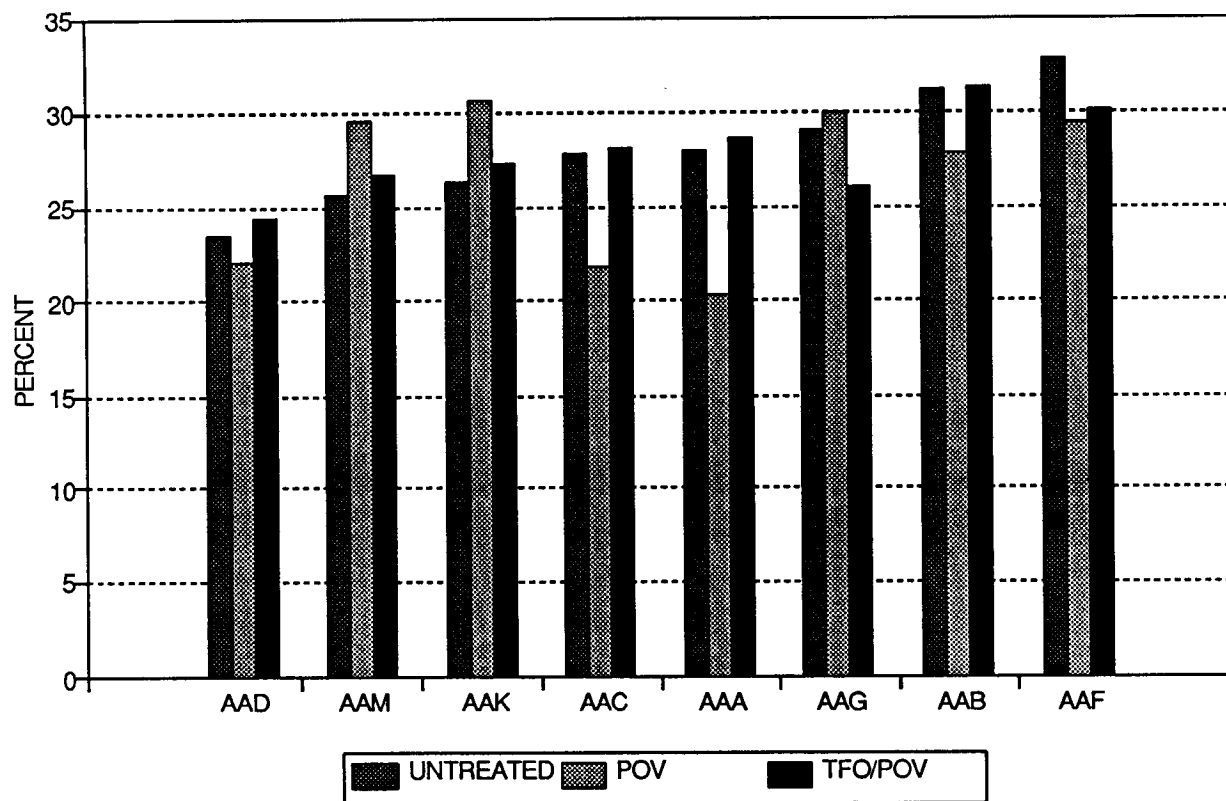


Figure 14. Comparison of aromatic carbon content before and after POV and TFO/POV oxidation

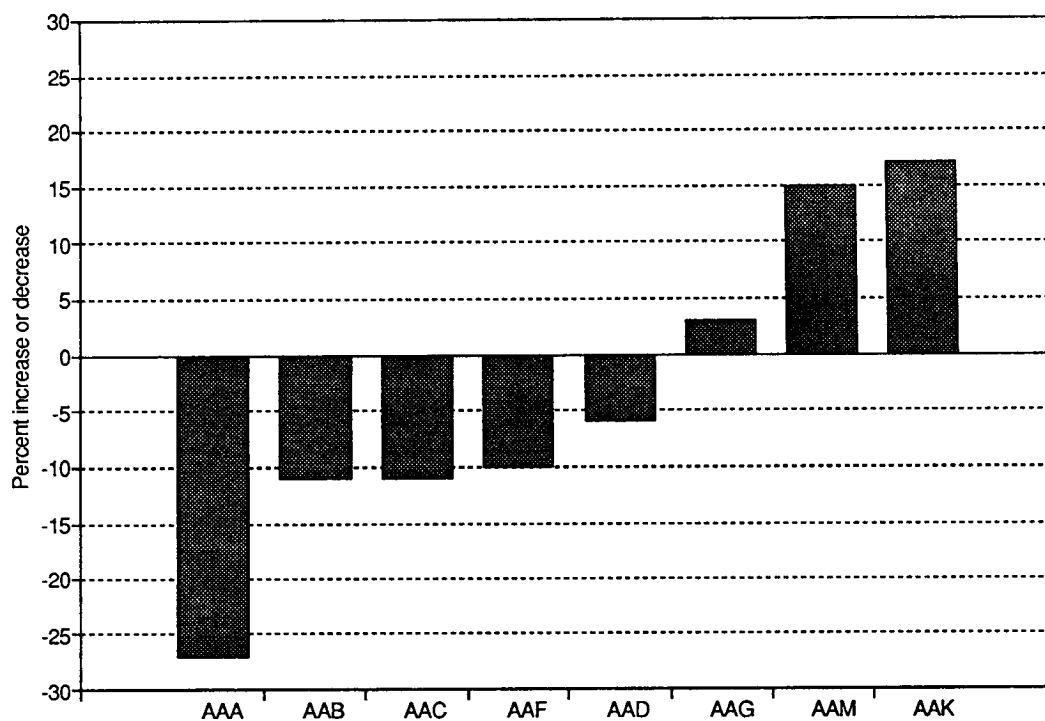


Figure 15. Change in aromatic carbon percentage after POV oxidation

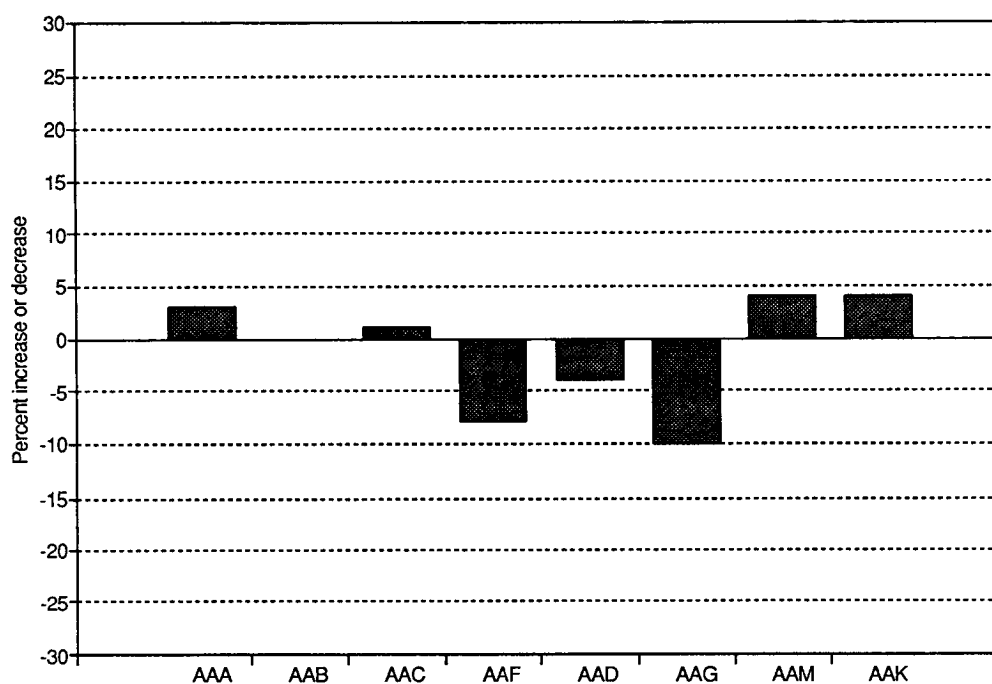


Figure 16. Change in aromatic percentage after TFO/POV oxidation

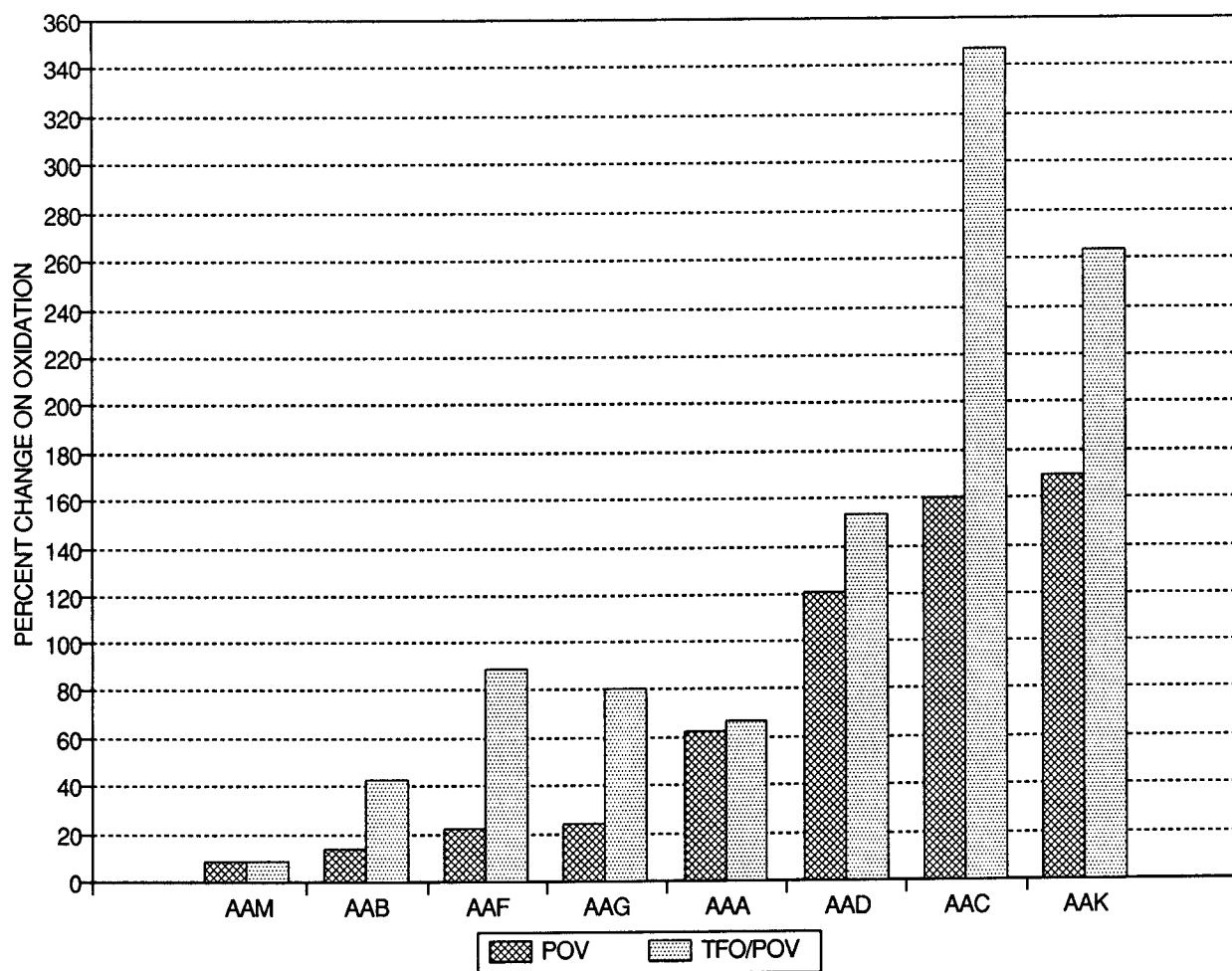


Figure 17. Susceptibility to POV and TFO/POV oxidation: change in Wt% O as COOH plus OH

Tables

Table 1. Outline of SHRP A-002C workplans

Subtask 1a. Solution NMR Characterization of Core Asphalts

Work Element 1a.1	Determine the aromatic/aliphatic ratios of core asphalts
Work Element 1a.2	Investigate the use of shift reagents as general tools for resolution enhancement
Work Element 1a.3	Functional group analysis
Work Element 1a.4	Investigate Aliphatic Structure
Work Element 1a.5	Investigate Aromatic Structure
Work Element 1a.6	Elaborate Oxidation Sites

Subtask 1b. Solid State NMR Characterization of Core Asphalts

Table 2. Percent aromatic carbon and hydrogen from ^{13}C - and ^1H -NMR spectroscopy.

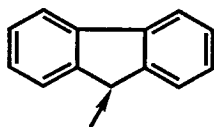
Core Asphalt	% Aromatic Carbon ^a			Aromatic Hydrogen ^a	
	Replicated Analyses		Average		
AAA-1	28.1	(± 0.3)	27.9	7.3	(± 0.6)
	27.7	(± 0.2)			
AAB-1	31.9	(± 0.2)	31.2	7.6	(± 0.2)
	30.6	(± 0.2)			
AAC-1	27.0	(± 0.3)	27.8	<u>6.4</u>	(± 0.1)
	28.5	(± 0.1)			
AAD-1	23.7	(± 0.2)	<u>23.4</u>	6.8	(± 0.2)
	23.8	(± 0.2)			
AAF-1	32.8	(± 0.2)	<u>32.8</u>	<u>8.7</u>	(± 0.4)
	32.8	(± 0.6)			
AAG-1	28.3	(± 0.3)	29.0	7.3	(± 0.3)
	29.1	(± 0.2)			
	29.5	(± 0.2)			
AAK-1	26.7	(± 0.2)	26.2	6.8	(± 0.1)
	25.1	(± 0.2)			
	26.8	(± 0.0)			
AAM-1	24.7	(± 0.3)	25.6	6.5	(± 0.1)
	26.4	(± 0.2)			

^a average

Highest and lowest values are underlined

Table 3. Resonance assignments for ^1H -NMR spectra

Description	range, ppm
Any CH_3 except α or β to aromatic; some CH_2 in cycloalkanes and naphthenic substituents	0-1
CH_2 in long chains	1.25
CH_2 , CH not α to aromatic; CH_3 β to aromatic	1-2
CH_2 β to aromatic; CH in hydroaromatics (e.g., tetralin)	1.5-2.0
Division between H α to aromatic (benzylic H) and other aliphatic H	~ 2
H α to aromatic	~ 2-5
H α to two aromatics, e.g.	3.4-4.5
Olefins	4.5-6
Aromatic H; OH	~ 5-10
SCH_n ; $(\text{CH})_n\text{COOH}$ ($n = 1$ or 2)	1.8-3.0
OCH_n	3.5-4.2

**Table 4. Approximate ratio of protons between 2 and 5 ppm (including benzylic protons) to all aliphatic protons in core asphalts**

Asphalt	Ratio	Asphalt	Ratio
AAA-1	0.19	AAF-1	0.19
AAB-1	0.20	AAG-1	0.19
AAC-1	0.16	AAK-1	0.20
AAD-1	0.21	AAM-1	0.15

Table 5. Peak assignments for aliphatic region of ^{13}C spectra of asphalts (14, 15)

resonance	peak number			resonance	peak number
39.4	1			26.9	8
37.4	2			24.9	8
37.1	2		$-\text{CH}_2-$	24.5	8
34.8	3			22.7	9
32.8	4			19.7	10
31.9	5			14.0	11
30.0	6			11.4	12
29.7	6				
27.9	7		in general: CH_3 CH_2 CH	10 - 24 21 - 45 25 - 60	

Table 6. Number of aliphatic carbon atoms per average molecule in each ¹³C-NMR peak area.

Area# ^a	AAA-1	AAB-1	AAC-1	AAD-1	AAF-1	AAG-1	AAK-1	AAM-1
1	0.4	0.4	0.5	0.5	0.4	0.5	0.5	0.8
2	3.1	3.1	3.6	3.3	<u>2.7</u>	3.1	3.3	<u>3.7</u>
3	4.7	4.3	4.9	4.2	4.2	4.2	4.9	<u>7.2</u>
4	1.0	1.0	1.2	1.2	0.9	1.0	1.2	1.1
5	1.5	1.6	2.0	1.3	1.6	<u>1.0</u>	1.6	<u>2.9</u>
6	9.4	11.8	15.2	7.8	12.2	<u>6.7</u>	10.6	<u>27.5</u>
7	0.6	0.6	0.8	0.6	0.6	0.5	0.6	0.8
8	4.4	4.1	5.7	3.9	4.2	<u>3.8</u>	4.5	<u>8.6</u>
9	2.1	2.4	2.8	2.0	2.3	1.7	2.1	2.8
10	2.6	2.6	3.2	2.5	2.3	2.5	2.7	2.1
11	1.7	2.1	<u>2.3</u>	1.4	2.2	<u>1.0</u>	1.7	2.2
12	0.3	0.3	0.4	0.3	0.3	0.2	0.3	0.1
Other	7.9	5.6	3.0	7.8	5.7	9.9	8.8	10.1

^a See Figure 6 and Table 5 for definition of areas and resonance assignments.
Highest and lowest values for each area are underlined

Table 7. Molecular weights and formulae for SHRP core asphalts

Asphalt	M.W. ^a	Elemental Analysis ^a					Average Molecular Formula					H/C Ratio M.F.
		C	H	N	O	S						
AAA-1	790	84.2	10.5	1.2	0.6	5.3	C ₅₅	H ₈₂	N _{0.7}	<u>O</u> _{0.3}	S _{1.3}	1.49
AAB-1	840	82.3	10.6	1.2	0.8	4.7	C ₅₈	H ₈₈	N _{0.7}	O _{0.4}	S _{1.2}	1.52
AAC-1	870	86.5	11.3	0.67	0.9	1.9	C ₆₃	H ₉₈	N _{0.4}	O _{0.5}	S _{0.5}	1.56
AAD-1	700	81.6	10.8	1.5	0.9	6.9	<u>C</u> ₄₈	H ₇₅	N _{0.7}	O _{0.4}	S _{1.5}	1.56
AAF-1	840	84.5	10.4	0.55	1.1	3.5	C ₅₉	H ₈₇	<u>N</u> _{0.3}	<u>O</u> _{0.6}	S _{0.9}	1.47
AAG-1	710	85.6	10.5	2.0	1.1	1.2	C ₅₁	<u>H</u> ₇₄	N _{1.0}	O _{0.5}	<u>S</u> _{0.3}	1.45
AAK-1	860	80.7	10.2	1.6	0.8	6.4	C ₅₈	H ₈₇	N _{1.0}	O _{0.4}	<u>S</u> _{1.7}	1.50
AAM-1	1300	86.7	11.4	1.2	0.5	1.1	<u>C</u> ₉₄	<u>H</u> ₁₄₇	<u>N</u> _{1.1}	O _{0.4}	S _{0.4}	1.56

^a Average molecular weight by VPO in toluene, Western Research Institute and SHRP Materials Reference Library
High and low values are underlined

Table 8. Data for average structures of core asphalts

Core asphalt	Atoms of aromatic carbon ^a	Atoms of aromatic hydrogen ^a	ASI ^b	DBE ^c
AAA-1	15.3	6.1	2.5	15
AAB-1	18.1	6.8	2.7	15
AAC-1	17.5	6.3	2.8	15
AAD-1	<u>11.2</u>	<u>5.2</u>	<u>2.2</u>	<u>11</u>
AAF-1	19.4	7.5	2.6	17
AAG-1	14.8	5.5	2.7	15
AAK-1	15.2	6.0	2.5	15
AAM-1	24.1	9.6	2.5	21

^a Calculated from data in Tables 2 and 7

^b Aromatic Substitution Index - the number of aromatic carbon atoms per aromatic hydrogen atom

^c Double Bond Equivalents = $1 + (\text{total number of carbons} - \frac{1}{2} \text{total number of hydrogens})$

Highest and lowest values are underlined

Table 9. Concentrations of phenols and carboxylic acids from short-term phase transfer methylation

Asphalt	mol/g.(x10 ⁵) φOH ^a	φOH ^b	COOH ^c	% of OH+COOH ^d	Total
AAA-1	2.5	3.5	4.4	10.3	~ 40
AAB-1	3.1	4.2	5.0	12.7	35
AAC-1	1.7	<u>1.8</u>	<u>2.8</u>	<u>6.6</u>	<u>17</u>
AAD-1	2.2	2.2	3.7	8.2	21
AAF-1	3.2	<u>6.3</u>	3.6	13.5	24
AAG-1	5.5	4.2	<u>9.1</u>	<u>18.8</u>	41
AAK-1	<u>1.5</u>	2.5	3.1	7.0	20
AAM-1	2.8	3.5	3.9	10.2	<u>50</u>

^a methyl ethers of unhindered phenols

^b methyl ethers of hindered phenols

^c carboxylic acid esters

^d total OH + COOH represented by resonances between 50 and 65 ppm

^e percent of oxygen in elemental analysis accounted for by these resonances
Highest and lowest values underlined

Table 10. Concentrations of phenols and carboxylic acids from long-term phase transfer methylation

Asphalt	mol/g (X 10 ⁻⁵)					
	ϕ OH ^a	ϕ' OH ^b	ROH ^c	COOH ^d	(OH+COOH) ^e	% of total ^f
AAA-1	6.8	4.4	1.3	18.0	30.5	130
AAB-1	9.8	6.2	2.0	22.0	40.5	125
AAC-1	19.2	7.5	4.2	31.7	62.6	168
AAD-1	13.2	5.5	2.3	32.7	53.7	153
AAF-1	5.9	5.1	1.4	9.1	21.5	45
AAG-1	9.9	5.6	1.6	10.3	27.4	55
AAK-1	5.9	4.0	1.3	11.8	23.0	70
AAM-1	5.0	3.3	1.1	7.9	17.3	80

^a methyl ethers of unhindered phenols

^b methyl ethers of hindered phenols

^c methyl ethers of aliphatic alcohols

^d carboxylic acid esters

^e total OH + COOH represented by resonances between 50 and 65 ppm

^f percent of oxygen in elemental analysis accounted for by these resonances

Highest and lowest values underlined

Table 11. Concentrations of aliphatic carboxylic acids from methylation of asphalt using diazomethane

Asphalt	mol(COOH)/gr. asphalt (X 10 ⁻⁶)		% of O ^a
AAA-1	5.2	(\pm 0.7)	2.8
AAB-1	0.92	(\pm 0.1)	0.4
AAC-1	1.0	(\pm 0.5)	0.3
AAD-1	23.0	(\pm 1.0)	8.2
AAF-1	0.56	(\pm 0.12)	0.2
AAG-1	30.0	(\pm 2.0)	8.7
AAK-1	14.0	(\pm 0.1)	5.6
AAM-1	1.7	(\pm 0.4)	1.0

^a percent of oxygen in elemental analysis accounted for by this resonance.

Table 12. Concentrations of phenols and carboxylic acids from recommended procedures.

Asphalt	ϕOH^a	$\frac{\text{mol}}{\text{g.}}(\times 10^{-5})$ $\phi'\text{OH}^b$	COOH^c	$\text{OH} + \text{COOH}$	% of Total O ^d
AAA-1	2.5	3.5	0.52	6.52	18
AAB-1	3.1	4.2	0.09	7.39	15
AAC-1	1.7	1.8	0.10	3.60	7
AAD-1	2.2	2.2	2.30	6.70	16
AAF-1	3.2	6.3	0.06	9.56	14
AAG-1	5.5	4.2	3.00	12.70	23
AAK-1	1.5	2.5	1.40	5.40	14
AAM-1	2.8	3.5	0.17	6.47	21

^a methyl ethers of unhindered phenols from short-term PTM

^b methyl ethers of hindered phenols from short-term PTM

^c methyl esters of free carboxylic acids from diazomethane methylation

^d percent of oxygen in elemental analysis account for
Highest and lowest values underlined

Table 13. Concentrations of primary alkylamines from ³¹P-NMR spectra of asphalts phosphorylated with CDMPOPS

Asphalt	Mole NH ₂ per gram asphalt	wt. % N ^b
AAA-1	0.15 x 10 ⁻⁶	0.0002
AAB-1	0.16 x 10 ⁻⁶	0.0002
AAC-1	2.1 x 10 ⁻⁶	0.003
AAD-1	0.049 x 10 ⁻⁶	0.00007
AAG-1	1.9 x 10 ⁻⁶	0.003
	3.4 x 10 ⁻⁶ ^a	0.005
AAF-1	5.4 x 10 ⁻⁶	0.008
AAK-1	0	
AAM-1	1.1 x 10 ⁻⁶	0.002

^a from calculated Lorentzian curve

^b Wt. % nitrogen per gram of asphalt as primary alkylamine

Table 14. Changes in percent aromatic carbon during oxidation

Asphalt	% arom. carbon		TFO/POV
	untreated ¹	POV	
AAA-1	27.9	20.3	28.6
AAB-1	31.2	27.8	31.3
AAC-1	27.8	21.8	28.1
AAD-1	23.4	22.1	24.4
AAF-1	32.8	29.4	30.1
AAG-1	29.0	30.0	26.0
AAK-1	26.2	30.6	27.2
AAM-1	25.6	29.5	26.7

¹ Average value

Table 15. Changes in percent aromatic hydrogen during oxidation

Asphalt	% arom. hydrogen		TFO/POV
	untreated	POV	
AAA-1	7.3	6.9	7.4
AAB-1	7.6	8.1	7.7
AAC-1	6.4	7.3	7.8
AAD-1	6.8	6.5	6.6
AAF-1	8.7	9.4	9.6
AAG-1	7.3	8.5	8.3
AAK-1	6.8	7.2	7.0
AAM-1	6.5	8.0	6.9

Table 16. Change in maximum possible ratio of benzylic to all aliphatic protons with oxidation

Asphalt	untreated	POV	TFO/POV
AAA-1	0.187	---	0.188
AAB-1	0.200	0.188	0.191
AAC-1	0.163	0.172	0.168
AAD-1	0.207	0.203	0.201
AAF-1	0.195	0.197	0.184
AAG-1	0.193	0.194	0.204
AAK-1	0.203	0.192	0.141
AAM-1	0.151	0.154	0.155

Table 17. Changes in measured OH + COOH after POV and TFO/POV oxidation

A. Total OH plus COOH ^a					B. Wt. % O (as OH + COOH)		
Asphalt	Core ^b	POV	TFO/POV	Approx. % incr. ^c	Core ^b	POV	TFO/POV
AAA-1	10.4	16.2	16.7	61	0.24	0.39	0.40
AAB-1	12.8	13.7	17.3	35	0.28	0.32	0.40
AAC-1	6.7	15.6	26.0	288	0.15	0.39	0.67
AAD-1	8.1	17.1	19.6	142	0.19	0.42	0.48
AAF-1	13.5	14.5	23.2	72	0.27	0.33	0.51
AAG-1	18.8	21.6	31.3	66	0.45	0.56	0.81
AAK-1	7.1	17.3	23.1	225	0.16	0.43	0.58
AAM-1	9.9	10.0	10.2	3	0.22	0.24	0.24

^a in moles/gm X 10⁻⁵

^b untreated asphalt

^c TFO/POV

Table 18. Changes in concentrations of oxygen-containing functional groups after POV and TFO/POV oxidation, from short-term PTM.^a

A. COOH														
B. ϕOH^d										Total				
Asphalt	Core ^b	POV	TFO/POV	ΔPOV	ΔTFO	ΔTOTAL	% incr.	Core ^b	POV	TFO/POV	ΔPOV	ΔTFO	ΔTOTAL	Total % incr.
AAA-1	4.4	8.3	8.3	3.9	0.0	3.9	89	2.5	4.4	4.4	1.9	0.0	1.9	76
AAB-1	5.0	6.6	7.7	1.6	1.1	2.7	54	3.1	3.4	4.5	0.3	1.1	1.4	45
AAC-1	2.8	9.0	15.6	6.2	6.6	12.8	457	1.7	3.2	5.2	1.5	2.0	3.5	206
AAD-1	3.7	9.1	10.7	5.4	1.6	7.0	189	2.2	4.5	5.1	2.3	0.6	2.9	132
AAF-1	3.6	6.0	8.8	2.4	2.8	5.2	144	3.2	3.5	6.3	0.3	2.8	3.1	97
AAG-1	9.1	13.4	19.1	4.3	5.7	10.0	110	5.5	4.5	6.9	-1.0	2.4	1.4	25
AAK-1	3.1	9.4	12.9	6.3	3.5	9.8	316	1.5	3.8	5.3	2.3	1.5	3.8	253
AAM-1 ^c	3.9	4.9	4.8	1.0	-0.1	0.9	23	2.4	2.1	2.2	-0.3	0.1	-0.2	-8
C. ROH ^e														
D. $\phi'\text{OH}^f$										Total				
Asphalt	Core ^b	POV	TFO/POV	ΔPOV	ΔTFO	ΔTOTAL	% incr.	Core ^b	POV	TFO/POV	ΔPOV	ΔTFO	ΔTOTAL	Total % incr.
AAA-1	0.0	0.32	0.53	0.32	0.21	0.53	~	3.5	3.2	3.5	-0.3	0.3	0.0	0
AAB-1	0.49	0.52	1.21	0.03	0.69	0.72	147	4.2	3.2	3.9	-1.0	0.7	-0.3	-7
AAC-1	0.36	0.81	2.60	0.45	1.79	2.24	622	1.8	2.6	2.6	0.8	0.0	0.8	44
AAD-1	0.0	0.41	1.02	0.41	0.61	1.02	~	2.2	3.1	2.8	0.9	-0.3	0.6	27
AAF-1	0.36	0.35	0.70	-0.01	0.35	0.34	94	6.3	4.6	7.4	-1.7	2.8	1.1	17
AAG-1	0.0	0.56	0.53	0.56	-0.03	0.53	~	4.2	3.1	4.8	-1.1	1.7	0.6	14
AAK-1	0.0	0.96	1.32	0.96	0.36	1.32	~	2.5	3.1	3.6	0.6	0.5	1.1	44
AAM-1 ^c	0.10	0.16	0.0	0.06	-0.16	-0.10	-100	3.5	2.8	3.2	-0.7	0.4	-0.3	-9

^a in moles/gm X 10⁻⁵

^b untreated asphalt

^c average values

^d unhindered phenols

^e aliphatic alcohols

^f hindered phenols

^a in moles/gm X 10⁻⁵

^b untreated asphalt

^c average values

^d unhindered phenols

^e aliphatic alcohols

^f hindered phenols

Table 19. Possible reactions in TFO/POV for core asphalts

Asphalt	1	2	3	4	5	6	7	8	9
	Reaction from Scheme XII C, D, H,I E,F G					RANK - % AROM Ca RANK - [OH + COOH] ^{a,b} UNTR. ^c TFO/POV UNTR. ^c TFO/POV			
AAA-1		*	*	O	*	5	6	5	2
AAB-1	*		*	**	*	7	8	6	3
AAC-1		***	***+	***	***	4	5	1	7
AAD-1		*	**	O	**	1	1	3	4
AAF-1	**		**	*	**	<u>8</u>	7	7	5
AAG-1	**		**	O	*	6	2	<u>8</u>	<u>8</u>
AAK-1	***		***	O	***	3	4	2	5
AAM-1		**	*-	**	O	2	3	4	1

* Minor importance--relative to other asphalts

** Moderate importance--relative to other asphalts

*** Major importance--relative to other asphalts

+/- Emphasizes ranking

0 No apparent contribution

^a Rank 1-8, 1 being lowest concentration. Rankings ignore statistical significance for sake of discussion.

^b From short-term PTM

^c Untreated asphalt

Table 20. Percent aromatic carbon in some fractions from ion exchange chromatography (IEC)

Asphalt	Whole Asphalt	Neutrals		Strong Acids		Strong Bases	
	% Arom C ^a	Percent of Asphalt ^b	% Arom C	Percent of Asphalt ^a	% Arom C	Percent of Asphalt ^a	% Arom C
AAA-1	27.9	59.6	19.8 (±0.1)	17.4	38.1 (±0.2)	6.4	32.2 (±0.3)
AAB-1	31.2	56.9	16.8 (±0.4)	15.0	46.7 (±0.4)	9.1	38.3 (±0.2)
AAC-1	27.8	68.2	18.3 (±0.2)	7.5	44.7 (±0.2)	7.4	34.6 (±0.3)
AAD-1	23.4	51.6	19.7 (±0.2)	26.0	32.2 (±0.5)	7.8	34.1 (±0.2)
AAF-1	32.8	56.7	24.5 (±0.2)	15.4	37.4 (±0.3)	6.1	39.9 (±0.2)
AAG-1	29.0	50.3	16.6 (±0.2)	18.0	37.0 (±0.4)	12.0	29.0 (±0.5)
AAK-1	26.2	52.2	18.4 (±0.3)	18.7	33.5 (±0.3)	8.0	34.8 (±0.9)
AAM-1	25.6	53.4	14.7 (±0.3)	13.7	35.1 (±0.8)	10.4	32.3 (±0.5)

^a Average values

^b Percent of fraction present in whole asphalt. From Western Research Institute and SHRP Materials Reference Library, Nov., 1990.

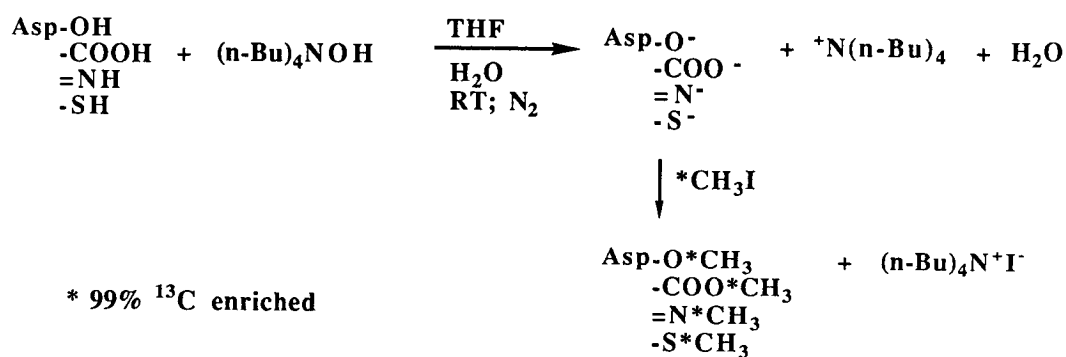
Table 21. Percentage of total aromatic carbon supplied by IEC fractions.

Asphalt	Neutrals	% in Asphalt	Strong Acids	% in Asphalt	Strong Bases	% in Asphalt	Weak Acids and Bases ^b	% in Asphalt
AAA-1	42.3	(59.6)	23.8	(17.4)	7.4	(6.4)	26.5	(16.6)
AAB-1	30.6	(56.9)	22.5	(15.0)	11.2	(9.1)	35.7	(19.0)
AAC-1	44.9	(68.2)	12.1	(7.5)	9.2	(7.4)	33.8	(16.9)
AAD-1	43.4	(51.6)	35.8	(26.0)	11.4	(7.8)	9.4	(14.6)
AAF-1	42.3	(56.7)	17.6	(15.4)	7.4	(6.1)	32.7	(21.8)
AAG-1	28.8	(50.3)	23.0	(18.0)	12.0	(12.0)	36.2	(19.7)
AAK-1	36.7	(52.2)	23.9	(18.7)	10.6	(8.0)	28.8	(21.1)
AAM-1	30.7	(53.4)	18.8	(13.7)	13.1	(10.4)	37.4	(22.5)

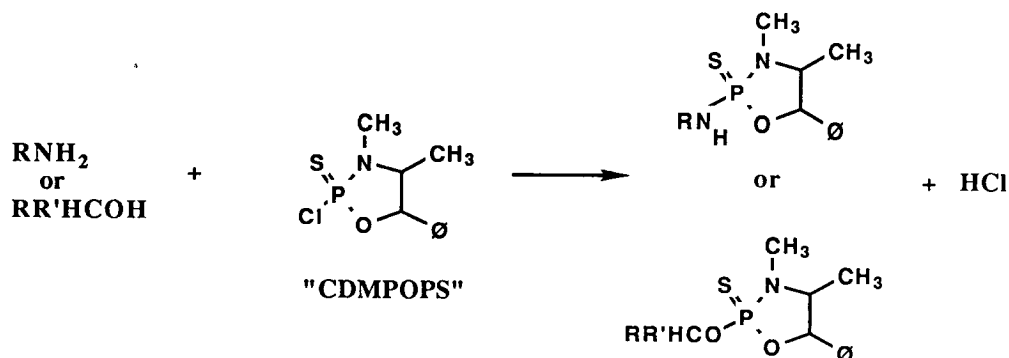
^a Percent of fraction in whole asphalt

^b By difference

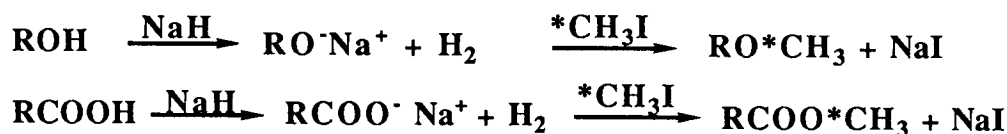
Schemes



Scheme I. Phase-transfer methylation reaction

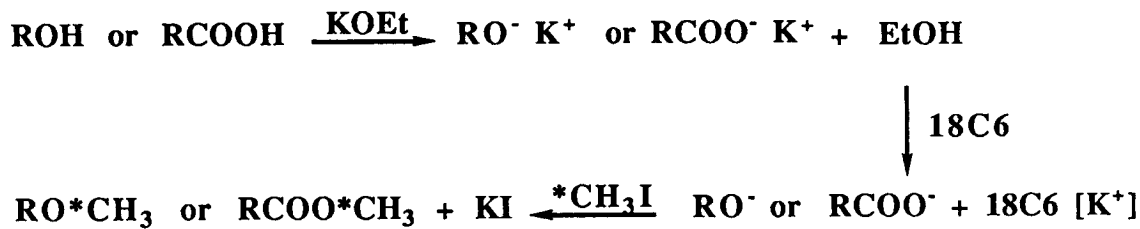


Scheme II. Derivatization of primary amines



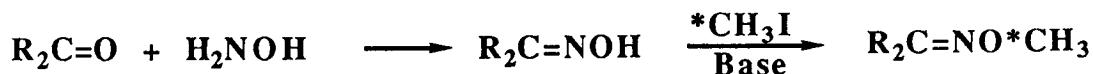
where R = alkyl or aromatic groups

Scheme III. Sodium hydride for deprotonation prior to methylation of -OH and -COOH groups

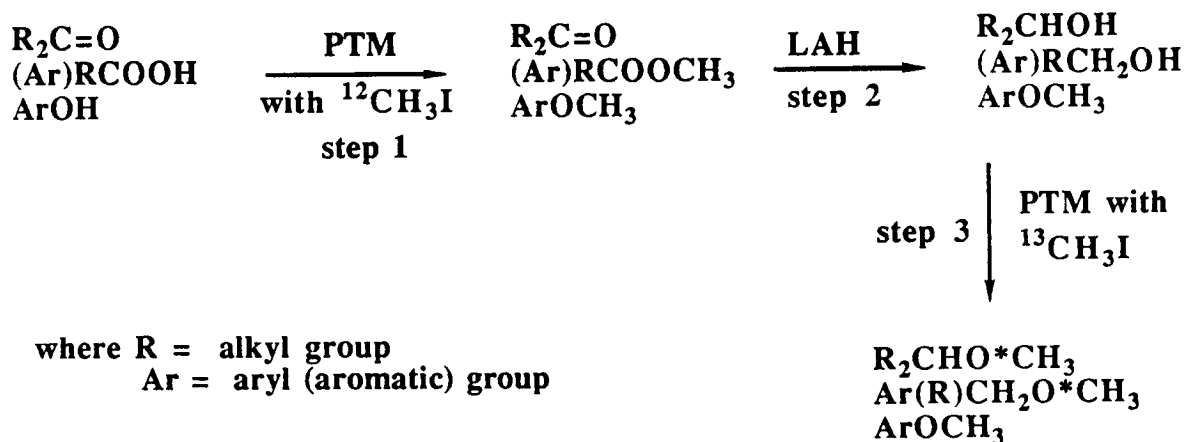


where R = alkyl or aromatic group

Scheme IV. Potassium ethoxide and 18-crown-6 ethers for deprotonation



Scheme V. Methoximation reaction for analysis of ketones



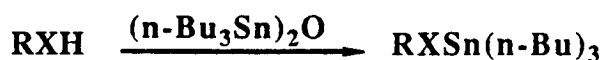
where R = alkyl group
Ar = aryl (aromatic) group

Scheme VI. Lithium aluminum hydride reduction



where R = alkyl or aryl group

Scheme VII. Sodium borohydride in analysis of ketones



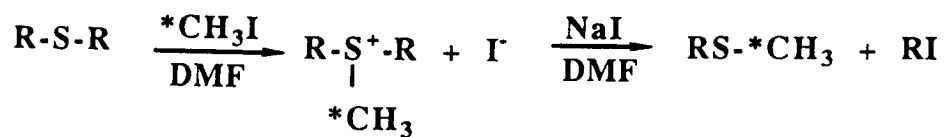
where X is O or S

Scheme VIII. Bis (tri-n-butyltin) oxide derivatization



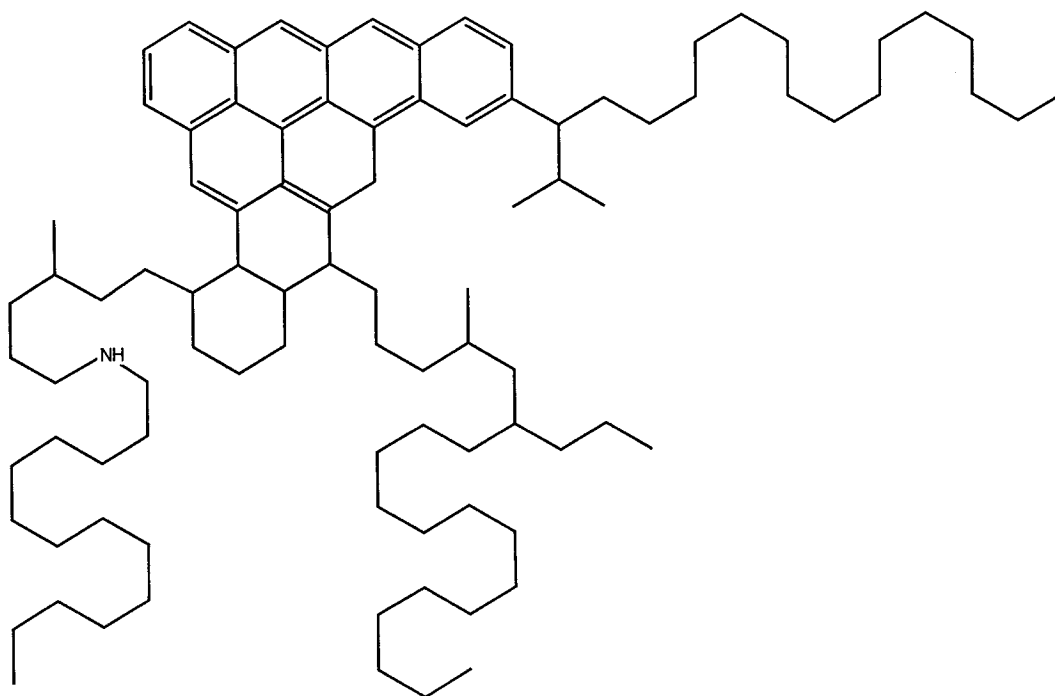
where R is alkyl or aryl and X is O, COO, S, N, or NH

Scheme IX. Formation of trimethylsilyl derivative

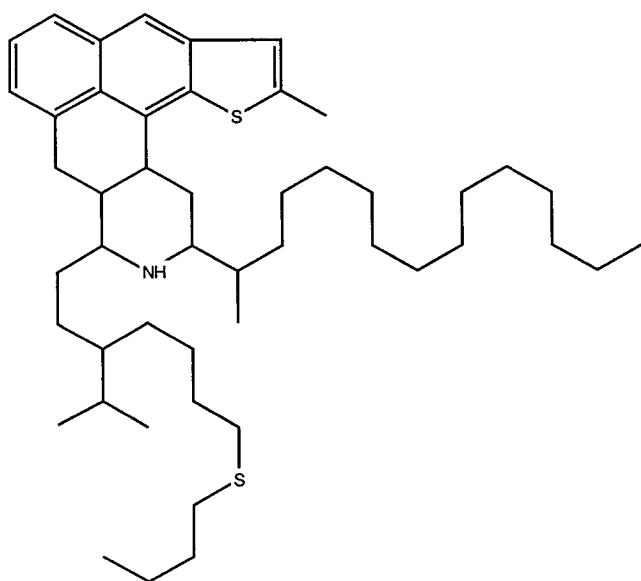


Scheme X. Derivatization of sulfides

Scheme XI. Average molecular structures of core asphalts

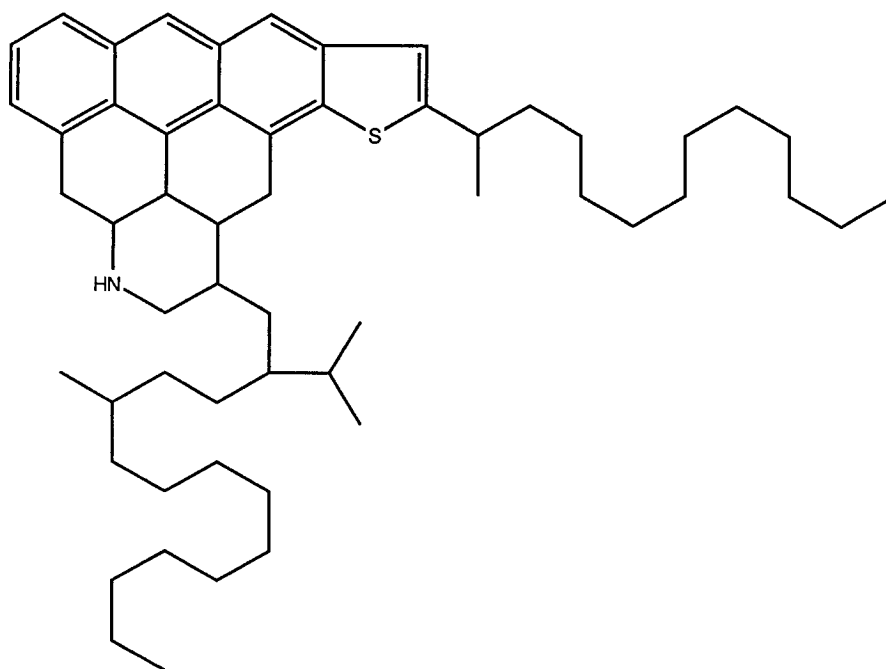


Scheme XI.1 AAM-1

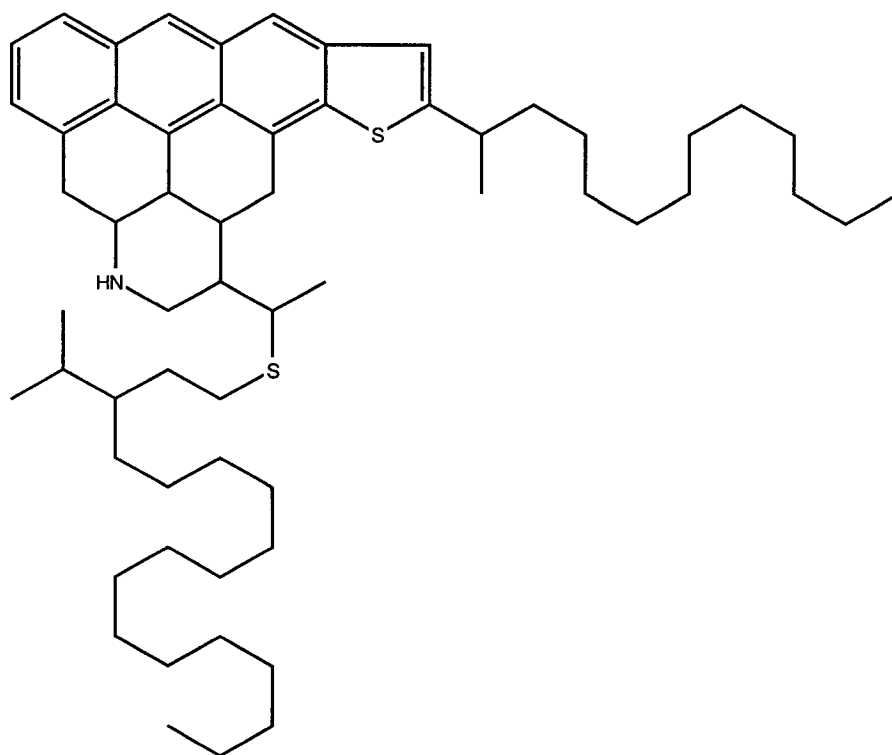


Scheme XI.2 AAD-1

Scheme XI. Average molecular structures of core asphalts (continued from p. 69)

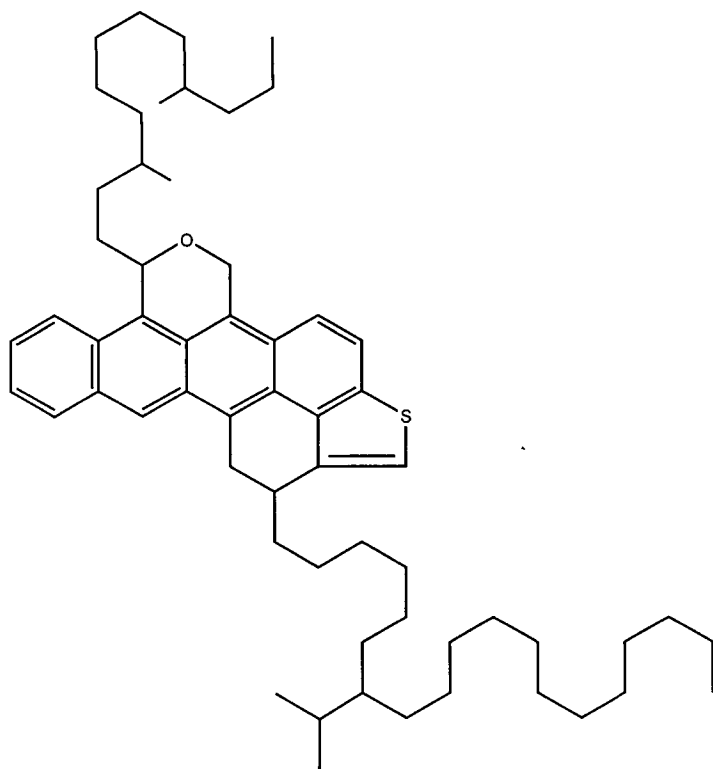


Scheme XI.3 AAA-1

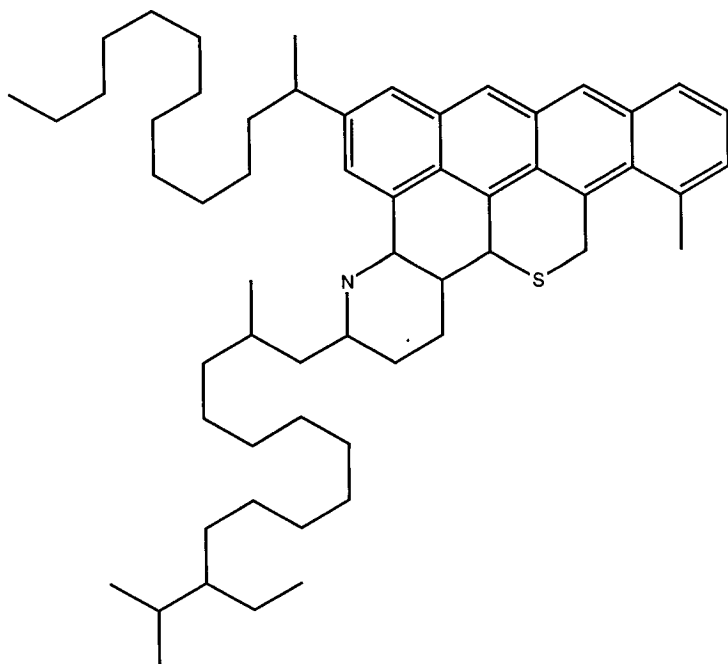


Scheme XI.4 AAK-1

Scheme XI. Average molecular structures of core asphalts (continued from p. 69)

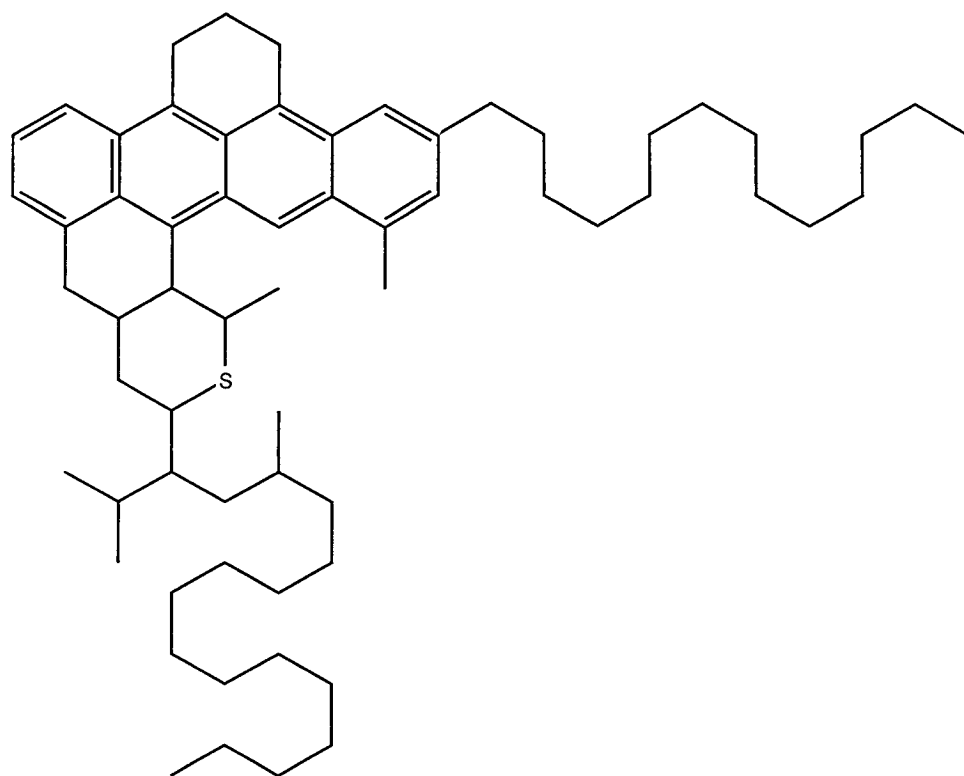


Scheme XI.5 AAF-1

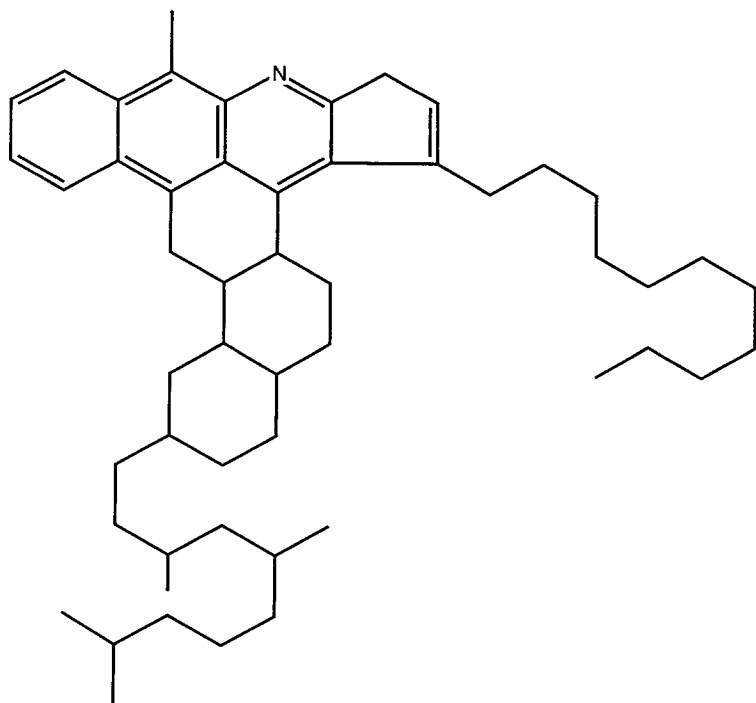


Scheme XI.6 AAB-1

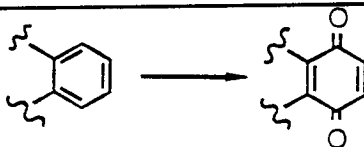





Scheme XI. Average molecular structures of core asphalts (continued from p. 69)



Scheme XI.7 AAC-1



Scheme XI.8 AAG-1

	Reaction	Consequence
A		loss of aromatic carbon
B		increase of aromatic carbon
C		loss of aromatic carbon and increase in carboxylic acid
D		increase in carboxylic acid
E	$R_3CH \longrightarrow R_3C-OH$	increase in alcohol content
F		increase in alcohol content
G		increase in phenol content
H	$\begin{array}{c} O \\ \\ -CCH_3 \end{array} \longrightarrow -COOH$	increase in carboxylic acid
I	$-CH_2-OH \longrightarrow -COOH$	increase in carboxylic acid

Scheme XII. Possible reactions under oxidizing conditions in asphalt

Solid State NMR Characterization of SHRP Core Asphalts

Introduction

General comments

The solid-state nuclear magnetic resonance (NMR) investigation of SHRP core asphalts was carried out by W.F. Manders and D.L. VanderHart at the National Institute of Standards and Technology. This study had strong components of a) basic research probing the molecular properties and organization of asphaltic cements and b) exploration of a new characterization technique. At the outset we were led by expectations that asphalt cements (hereafter referred to simply as asphalts) are characterized by some tendencies towards molecular self-association or 'structuring.' These tendencies would presumably lead to the production of heterogeneities of mobility and composition (e.g. micelles) on some typical size scale. An important goal of this study was to verify, if possible, the existence of structural heterogeneity, its size scale, and its dependence, if any, on temporal aging, thermal history or the presence of aggregate surfaces. It was our hope that any difference in such structuring could be attributed to variations in the chemical make-up of the different asphalt constituents, thereby giving some insight into the correlation of chemical structure and performance. We looked to Western Research Institute (WRI) for component fractions and to Wyn Jennings, our principal investigator at Montana State University, for solution-state NMR data on these fractions.

Brief review of the kinds of experiments and the nature of the corresponding information

For the convenience of the reader, an appendix describing several terms and concepts relating to solid state NMR and the interpretation of the NMR data have been included. For those not so familiar with solid state NMR, it is strongly recommended that the appendix be read first.

The vast majority of the experimental data collected on the asphalts employed proton NMR rather than ^{13}C NMR techniques since the latter were found to be unreliable from a quantitative point of view because of the rather unique molecular mobility characteristic of asphalts. The proton spectra which were collected fell into two categories, namely, FID spectra and multiple pulse (MP) spectra. The principal distinction between these kinds of spectra is as follows: the FID spectra are sensitive to molecular motion when correlation times for rotational and translational motion are shorter than 10^{-4} s. The most evident lineshape changes occur when the correlation times are in the 10^{-4} to 10^{-6} s range. The MP spectra stand in contrast to the FID spectra. The MP spectra are sensitive to chemical composition particularly distinctions between aromatic and aliphatic protons.

A great deal of time was spent probing the *length scale* for heterogeneities in either mobility or chemical composition (aromatic/aliphatic ratios). These experiments give one *upper limits of minimum domain dimensions* (ULMDD's), i.e. distances across domains for spherical domains and distances across the thinnest dimension for non-spherical domains. These experiments are classified as spin diffusion experiments and are based on the fact that dipolar-coupled spins exchange polarization with one another. These experiments are analogous to microscale heat conduction experiments in which one has the ability to change the temperature of some domains relative to others and subsequently to watch the process of temperature reequilibration. Assuming that the conductivity is known, the time taken for reequilibration gives one information about the length scale for the shortest pathway between domains. The optimum range of lengths appropriate to this spin diffusion technique is 2.5 - 30 nm.

Importance of the micellar model as a theory to be tested

It seemed to us crucial to see if we could get insight into the molecular structure of asphalts, particularly as it pertains to viscosity and the latter's very strong temperature dependence. One of the theories of asphalt structure is the micellar theory.¹ The micellar theory postulates a segregation of cores of strongly associating molecules (based on favorable polar or aromatic interactions). These cores are separated from each other and are 'peptized' or stabilized by a much more fluid, oily phase which is presumed to have low polarity and/or aromaticity. A spherical shape is generally associated with the concept of micelles. The size of these micelles is probably an open question, but I will offer my biased view that if the dimensions of the 'micelles' are comparable to a few molecular diameters, then the micellar model becomes less compelling. Why? Because a wide range of chemical species is present in asphalts and mere statistics could create a distribution in space of mobility and aromatic/aliphatic proton ratio on a comparable spatial scale.

Results and Discussion

Perspective on the use of ^{13}C versus ^1H NMR Techniques

In view of the inherently better resolution of ^{13}C versus ^1H spectra, we say a word about the application of solid-state ^{13}C methods to asphalts and why we chose to emphasize strongly ^1H rather than ^{13}C NMR in this report. There are three considerations, namely, quantitative aspects of the data obtained, sensitivity and the influence of magic angle spinning (MAS). First, the most informative, i.e. highest resolution, experiments are those taken with MAS and CP (see the appendix). Because of very short and non-exponential $T_{1\rho}$ behavior for the protons in the various asphalts, the CP signals, while obtainable, were very far from being reliably quantitative. Moreover, those signals obtained directly from Boltzmann populations typically indicated that some carbon resonances were strongly broadened. The existence of unpaired electrons, e.g. substantial vanadium and iron contents, also complicated our understanding of the uniformity of relaxation in the asphalt matrix. (By the way, the paramagnetic content also kept us from focussing on relaxation characteristics as a means of probing aging.) The fact that asphalt exhibits linebroadening in the proton spectra (to be discussed) over the whole range of road service temperatures also implies that there are no road service temperatures where CP spectra will be quantitative.

Second, sensitivity is a factor. Protons are much more numerous than ^{13}C carbons (1.1% natural isotopic abundance) and their signals are correspondingly stronger. Thus, signals can be collected much more rapidly for proton spectra.

Third, MAS at the usual spinning rates for ^{13}C spectroscopy at a magnetic field of 4.7 T are usually 3.5 - 4 kHz in a 6 mm ID rotor. The rotational stresses and the corresponding flow which accompanies those stresses may disrupt the asphalt 'structure' which may spontaneously form and which we hope to study. Therefore, one of the principal methods for enhancing ^{13}C resolution was considered a potential threat to the stabilization of that which we wished to study.

The result was that we tried a few non-spinning ^{13}C experiments where one can distinguish, to a very reasonable extent, aromatic versus aliphatic carbon intensities. In Figure 1 we show spectra at 300 K for asphalt AAK-1 and the ranges over which the aromatic and aliphatic signals extend. These spectra illustrate problems of quantitation. Bear in mind that high resolution results indicate that the aromatic carbons are 28.9% of the total carbons in this sample. The so-called FID spectrum in Figure 1 should give quantitative results since it is not a CP spectrum. However, the apparent aromatic fraction is 46%, implying that there are some aliphatic resonances which are very broad because molecular motion in the 10^{-4} to 10^{-7} s correlation time range causes excess linebroadening and this tends to be more serious for methylene rather than methine carbons. The CP spectrum, on the other hand, has an aromatic content within a few percent of the theoretical using a CP time of 0.2 ms. However, at this short CP time, a sizeable fraction of unprotonated aromatic carbons is only about halfway towards full

intensity. If the CP time is lengthened much more, the total CP intensity falls off rapidly because of the very short $T_{1\rho}$ and the aromatic fraction of the line grows to be significantly larger than 28.9%. So there is no CP time that one can choose where one can expect quantitative intensities. As a result of the foregoing considerations, the ^{13}C spectra were abandoned because the proton spectra offered quantitatively reliable spectra, even though resolution was significantly poorer relative to ^{13}C spectra. It should be noted that we will make reference to a couple of other ^{13}C spectra where we have either used strong acid fractions or low-temperature CP; in all the latter cases, the molecular motion is slow enough to provide more quantitative CP results.

Proton FID lineshapes

Temperature dependence

In Figure 2 four spectra, taken at different temperatures, are shown. These spectra are designated FID (free induction decay) lineshapes because they result from Fourier Transformations of the FID signals. These lineshapes are dominated by dipolar couplings and the narrowing with temperature is a result of averaging by molecular motion (see appendix and Figures 23 and 24). At 260 K, the lattice looks quite rigid on the timescale of 10^{-4} s. At 300 K, substantial motional averaging appears and the fullwidth at half height (FWHH) falls to about 8 kHz. At the same time, however, the lineshape maintains a very broad base, implying that many spins are yet rigid on this timescale. The motion could be, but need not necessarily be, associated with extensive trans-gauche conformational interconversion in aliphatic chains (see the NC peak in Figure 23A). By 330 K, the linewidth has fallen to about 1.4 kHz, implying that rapid reorientation and at least limited translation is happening for many protons on this timescale. Again, however, one can discern a broad base to the resonance, indicating that not all protons enjoy this motional freedom. In fact, one can very crudely estimate that 30% of the protons are still rigid at 330 K, i.e. have their full rigid-lattice linewidth. While it is true that heterogeneity of molecular motion is expected if micellar structure exists in asphalts, significant heterogeneity of molecular motion (associated with different sites) is also seen in homopolymers such as poly(carbonate).²

In Figure 3 the FID spectra at 300 K and 340 K are plotted for all of the core asphalts. Each group of spectra is normalized to the same total intensity. One sees considerable differences in the peak intensities indicating that local molecular motion varies considerably in these asphalts. In particular AAG-1 is the least mobile at both temperatures.

In Figure 4 we attempt to quantify these differences by plotting the FWHH of all of the core asphalts as a function of temperature. If we rank the asphalts according to the temperature where the halfwidth has reached 20 kHz, then AAA-1, AAB-1 and AAD-1 are most mobile, AAC-1, AAK-1 and AAM-1 are the next group, AAF-1 is next and in a group by itself while AAG-1 is least mobile, a position it maintains over the whole

temperature interval. AAF, on the other hand, exhibits the largest slope and, to the extent that the motion of a given asphalt bears some relation to its viscosity profile, would be predicted to have the largest temperature susceptibility. In Table 1 we collect viscosity data for comparison with the NMR linewidth rankings. As can be seen from Table 1, the ranking of the asphalts based on NMR linewidths is very similar to that obtained from viscosities at 298 K with the exception of asphalt AAB-1, which is slightly out of place. Incidentally, rankings based on the Fraass brittle-point temperature are also highly correlated with both viscosity and NMR linewidths. The ranking comparison using the 333 K viscosities is not as well correlated. In particular, asphalt AAK-1 emerges at 333 K with the highest viscosity. From Figure 4 we would also infer that asphalt AAF-1 has the highest temperature susceptibility, since it has the largest linewidth change with temperature. Table 1 supports the idea that the temperature susceptibility of AAF-1 is one of the highest, but its susceptibility is comparable to that of AAG-1 and AAC-1. Table 1 also shows that the temperature susceptibility of AAK-1 is the smallest; nevertheless, the NMR linewidth change with temperature for AAK-1 is not uniquely small. NMR linewidths and viscosities do have a reasonable correlation, but this correlation of viscosity with very local motions, which NMR linewidths sense, is not highly reliable.

The data of Figure 4 were taken by starting from room temperature and proceeding downward and then upward to 340 K. About 15 minutes separated consecutive points, 10 of these minutes used for temperature equilibration. It was usual to see hysteresis in these curves as is shown in Figure 5, where FWHHs are plotted for both the decreasing and increasing cycles of temperature. The points chosen for Figure 4 are averages at a given temperature. The hysteresis is indicative of low-temperature aging, such as was seen in flexural creep stiffness measurements.³

The probable origin of this effect is a volume change that develops slowly below the glass transition temperature, T_g . While this hysteresis is seen at temperatures that are thought to be above T_g for asphalts (typical range of T_g is about 238 to 253 K), the establishment of T_g should not be regarded as anything but a sample-average T_g in view of the wide distribution of molecular mobilities indicated by the proton lineshape. In fact, different regions of the asphalt will most likely have different T_g s. Conventionally measured T_g s probably correspond to the *onset* temperature for strong NMR linewidth narrowing.

One very important point regarding the interpretation of Figure 4 is that the motion of the *most mobile protons* is featured. The protons in the broad portion of the line are strongly discriminated against as the line narrows since the peak height, and hence the halfwidth, is so dominated by the narrower components. It is therefore of interest to obtain some relative measure of the intensity in the broad base of the line. We have taken ratios, R_b , of the intensity in the broad base (i.e., in regions greater than 12.5 kHz from the resonance center) of the various asphalt spectra with respect to the base

intensity of the AAG-1 spectrum. We have done this for non-spinning samples at two temperatures, namely, 300 K and 340 K. Results are summarized in Table 2.

A crude idea based on the data of Table 2 is that viscosity ought to be correlated with the amount of the most rigid material in the asphalts at, say, 340 K where many of the molecules have achieved some fluidity, judging by the NMR linewidths. If this is the case, then the ranking of viscosities at 333 K, which is close to 340 K should be, in increasing order of viscosity: AA(BAMDCFKG)-1 but according to Table 1 the experimental order (column 3) is AA(CABDMFGK)-1. While these rankings have some degree of correlation, there are notable exceptions e.g. AAC-1 and AAG-1. There would be even less correlation if we sought to make the viscosity directly proportional to the amount of rigid material. Thus, the amount of material which is 'rigid' on the NMR timescale of 10^{-4} s at 340 K is not a consistent measure of the viscosity of different asphalts, nor is the viscosity linear in the amount of this material for a given asphalt as will be seen (see ahead to point d.) for the oxidized samples where an increase of about 10% in the broad fraction is accompanied by a 7 - 40-fold increase in viscosity (see Table 1). *The notion that some molecules are rigid on a particular NMR timescale does not imply a uniformity in the strength of association with other molecules*; rather, similar mass fractions of 'solid-like' domains in two different asphalts could contribute differently to, say, shear viscosity if the strength of association between molecules in these regions differed. It is indeed a critical point in our understanding of asphalt structure whether the more rigid material forms a *continuous* network in the asphalt matrix or whether isolated regions of immobilized material are distributed in a more fluid phase. Perhaps, the temperature dependent viscosities observed reflect, among other things, a slow transformation from a continuous network at low temperatures to more isolated regions at higher temperatures.

While we are addressing the problem of the molecular origins of viscosity, it is good to bear in mind what is known about the dependence of viscosity on molecular weight in melts of linear polymers. At weights below the critical entanglement molecular weight, M_c , viscosity is proportional to the molecular weight.⁴ M_c values usually range from 4000 to 35000. The molecular weights (in toluene) of the core asphalts are at least a few times smaller than critical entanglement molecular weights. The variation in molecular weight for the core asphalts, therefore, is much too small to account for the differences in viscosity. It is thus concluded that one will have to invoke other factors such as molecular shape and molecular associations in order to understand the viscoelastic properties of asphalts.

In this context we might speculate on possible differences between asphalts AAG-1 and AAK-1. Asphalt AAG-1 differs from AAK-1 in the gel permeation chromatogram in that the latter has a significant large-molecular-size (LMS) fraction while the former shows no LMS peak.⁵ The intriguing thing is that if the LMS peaks (using THF as a solvent) are indicating a tendency of molecules to aggregate in the whole asphalt, the experimental fact remains that molecules in the 'non-aggregating' AAG-1 asphalts have lower mobility, on average. Therefore, one might speculate that the chemical structures

present in the AAG-1 are more uniform in shape and/or mix of chemical functionalities and hence can pack together more efficiently even though there are very few especially strong interactions between molecules. A support for this line of thinking is the very small amount of asphaltenes found in AAG-1 (5.8%) relative to AAK-1 (21.1%).⁶

Another possible source of the uniqueness of AAG-1, relative, say, to AAK-1, is that AAG-1 has been treated with lime. Hence there is the possibility that the calcium ions are acting as bridges between polar groups on two molecules, thereby rendering the matrix more rigid. We have recently compared lineshapes at 297 K for AAK-1, AAG-1 and ABD where the latter asphalt is the AAG-1 asphalt prior to lime treatment. In Figure 6 these normalized lineshapes are compared and it is seen that the relative rigidity of the AAG-1 asphalt molecules is *not* the result of lime treatment. In fact the ABD lineshape, while very close to that of AAG-1, is very slightly broader suggesting a slightly greater rigidity compared to the AAG-1 asphalt.

There is another observation⁷ from the NMR literature where motions in the midkilohertz range (which motions are present in asphalts based on the observed ¹H spectral linewidth narrowing) are correlated with impact strength in polymers. The fact that AAG-1 is, relatively speaking, deficient in motion in this range at the lower road service temperatures implies that it will have a reduced impact strength and be prone to low-temperature cracking. The fact that the average molecular weight for AAG-1 is also low exacerbates cracking.

Spectra of components versus the spectrum of a whole asphalt: an illustration

In one case, namely for asphalt AAD-1 we ran spectra of the heptane asphaltenes and the heptane maltenes (obtained from WRI) in order to test whether the lineshape of the whole asphalt mimicked the lineshape of the weighted sum of the constituents. From the mass fraction of asphaltenes in the original asphalt and from the known proton mass fractions in both the asphaltenes and the whole asphalt, the proper weighting can be calculated. In AAD-1, the asphaltene protons comprised 17.5% of the total proton intensity. In Figure 7A-7E, the spectra, respectively, represent the maltenes, the asphaltenes, the weighted sum, the original asphalt and the difference between the latter two spectra. The difference spectrum, 7E (=7C - 7D), shows that in the synthesized spectrum, 7C, there is an excess of narrow-line intensity and a depletion of broader intensity. The interpretation is obvious and important, but it is not very specific: it is that in the whole asphalt at least some of the maltenes interact with asphaltenes with the net effect that there is, on average, a slowing down of molecular mobility within the maltenes. A corresponding increase in the average mobility of the asphaltene fraction is not so obvious from Figure 7E, but this effect must be present also. We conclude that *it is a poor approximation to say that the asphaltenes form a separate phase in AAD-1*. This general comment is still consistent with the micellar picture since the asphaltenes in the

hard cores must be ‘peptized’ by the maltenes, i.e. some interaction between these molecules is required.

Influence of temporal aging on the ^1H lineshapes

In the vicinity of room temperature, the lineshapes of all of the asphalts were changing in such a way that a difference in mobility accompanying a 1 K change in temperature could be detected as a change in the lineshape. We decided on a protocol where we sealed asphalts under a partial pressure of nitrogen, initialized them at 413 K for one hour, and then tested them by obtaining spectra at 304 K at various times from the time of initialization. Five separate thermal histories were also adopted, namely: a) 253 K-fixed temperature, b) 298 K-fixed, c) 333 K-fixed, d) 253 K to 298 K and back to 253 K over a 24 h period with a 1 h soaking period at both extremes, i.e. each linear temperature ramping took 11 h and e) as in d) except the temperatures ranged between 302 K and 333 K. The different diurnal cycles were adopted in case the formation of phase structure was enhanced by some combination of temperature-dependent molecular mobilities and temperature-dependent phase structure.

The results of the aging studies were that, using the proton lineshapes at 304 K, no effects of aging were detected which were outside of the range of lineshape change corresponding to a 1 K temperature change. Aging of certain samples like AAG-1 and AAK-1 covered periods of 15 minutes to 6 months. All asphalts were tested for aging but, in the absence of positive results on the AAG-1 and AAK-1 asphalts, others were tested for times ranging from 3 months (AAD-1) to 1 week (AAA-1). These findings, it turns out, are in reasonable agreement with at least one paper in the literature⁸ where changes in viscosity measured at 298 K were found to be of the order of 20% over 1 week and roughly logarithmic in time. It also agrees quite well with changes in viscosity for asphalt AAK-1 at 298 K reported by WRI⁹. Considering that there is approximately a decade of viscosity change over a 10 K interval in a typical asphalt, changes associated with aging would be comparable to a 1 K temperature decrease over any timescale of one to several weeks. So, after getting the impression as we began this work that steric hardening was an important concern, we now conclude that, at least at ambient temperatures, it has virtually no importance. At temperatures at or below the nominal glass transition temperature; however, changes in mechanical properties with time are expected in analogy with well-known glass transition phenomena¹⁰ in both polymers and other glass-forming molecular systems. In other words, one need not invoke growth of domains to explain time dependent effects.

Lineshape changes accompanying oxidation

In Figure 8 we illustrate the spectral differences at 300 K observed upon aging using samples obtained from WRI. Spectra 8A -8E are normalized to the same intensity. The POV samples have been exposed to 300 psig oxygen for 300 h and the TFO-POV

samples have experienced prior thin film aging before identical POV treatment. The spectra on the left show that there is very little difference between the spectra of the oxidized versus the original asphalt. In fact, a counterintuitive result obtains. From Table 1 we see that there has been a 40-fold increase in the viscosity measured at 333 K for POV oxidation. This probably means a comparable increase in viscosity at 300 K. A similar viscosity increase of about 20-fold accompanies a temperature decrease of 10 K near room temperature.¹¹ Decreasing the temperature slows down all of the molecules as can be seen on the right side of Figure 8 where we compare lineshape changes which accompany a lowering of temperature by 10 K to 290 K. The difference spectrum shows that as the temperature is lowered, some portion of the narrower intensity is converted to intensity in the broad base of the resonance. In contrast, the difference spectra on the left side of Figure 8 which result from comparisons with the oxidized samples, have similar shapes to the difference spectrum on the right, but the differences are much smaller. More importantly, the differences have a *sense opposite to that expected*. Oxidation apparently has increased the intensity in the narrowed portion of the line, even though the sample viscosity has risen! This increase in the intensity of the narrowed portion of the line was common to all of the oxidized asphalt samples with the exception of sample AAK-1 where a slight decrease was noted. The interpretation of this result is that oxidation, with its accompanying viscosity increase, does not appreciably alter the mobility of the most mobile molecules in the system. In fact, mobility is slightly enhanced for these molecules.

The apparent contradiction that resonances narrow as viscosity increases can be resolved in part by comparing lineshapes at a higher temperature. At 300 K (Figure 8), a minority of the protons have large-amplitude, fast motions on the timescale of 10^{-4} s. In fact a good share of the motional narrowing may arise from local motion of sidechains or flexible naphthenic rings, i.e. molecular fragments as opposed to whole molecules. Oxidation may have decreased the mobility of some molecules but those and many others have not yet, at 300 K, achieved sufficient mobility to enter the linewidth narrowing region (see ahead to Figure 24). If the temperature is raised, more molecules will participate in the motional narrowing of the resonance line with the consequence that there will be a better opportunity to evaluate whether the more rigid fraction of the proton lineshape has increased upon oxidation. Figure 9 shows that the broad base of sample AAF-1 has increased about 10% in intensity for a POV-oxidized sample relative to the unoxidized AAF-1. The difference spectrum, greatly reduced in vertical scale, indicates that upon oxidation, a medium-narrow component (negative-going signal) has been redistributed both to an increase in the broad base as well as a very small increase in the most narrow signal (positive going). This may be evidence, albeit weak, for *oxidation reducing the compatibility of asphaltic components*. In any case, the general message is that the viscosity increase upon oxidation is accomplished with only minor modifications to the lineshape, indicating that the mobility of a small percentage of the molecules is altered. This stands in contrast to a viscosity increase upon a lowering of temperature where all molecules slow down. The increase of viscosity upon oxidation and the concurrent lack of influence on the more mobile molecules reinforces the notion of a spatial separation of mobile and more rigid molecules (as the micellar theory suggests).

Measurement of changes in molecular mobility upon mixing asphalt and aggregate

The objective of these experiments is to test whether the mobility of the asphalt molecules is influenced by the introduction of the solid aggregate surfaces during the formation of the asphalt concrete. Also, if possible, we wish to probe the question whether any interaction with the aggregate surface induces a phase separation into components which have a special surface affinity.

Experimental evidence¹² has appeared in the literature indicating that prolonged exposure to surfaces at temperatures like 150 °C causes a buildup of an oriented layer up to 70 microns thick after a few weeks. Measurements also suggest that this layer possesses a polarization, judging by its preferential alignment in a strong electric field. Moreover, hot asphalt flowing over aggregate particles tends to produce an asphaltic layer which progressively restricts further flow. This coating, however, as judged by IR, bears a strong resemblance to the original asphalt, i.e. this layer does not seem to be built up of material with a very unique chemical structure compared to the average asphalt molecules.¹³ The mechanism postulated for the growth of the oriented layer involves polar, highly aromatic rings. By necessity, these molecules are a very small subset of all of the possible molecules in the asphalts, judging by the dominance of the aliphatic protons and carbons in the average asphalt molecules. On the other hand, if this subset of molecules is also responsible for the coating of the aggregate particles in the flow experiments, then the mechanism is called into question since the IR spectrum of an aromatic-rich layer ought to be apparent. The experiments we report on here are intended to address the question whether any structuring from the aggregate surface results in an overall change in the mobility of the average asphalt molecule.

Sample preparation The asphalt samples were mixed with the solids at 120 °C for 20 minutes. The weight ratio of asphalt to aggregate was 1:4.

Two of the four aggregates were examined, namely the RC and the RJ. These samples were sieved so that the material used fell into the 270 - 325 mesh range (78 - 94 micron diameter). The RL material, as received, did not have any particles of this size in it. Small particles were deemed essential so that the surface to volume ratio would be increased.

In order to reduce the influence of magnetic particles, the sieved aggregates were suspended in water and stirred in contact with a submerged cylindrical pole piece of a strong portable magnet. Magnetic particles stuck to the edges of the pole piece. Iterative, tedious procedures involving 30 - 50 such cleaning cycles finally resulted in the removal of most of the magnetic particles. However, at no point did one reach the condition that no more material stuck to the pole piece. The non-spinning linewidth of a small amount of water in contact with this cleaned aggregate was about 2 kHz, full width at half height. There were no discernible wide tails to this resonance which would indicate a few remaining ferromagnetic particles.

Pure samples of SiO_2 and CaCO_3 , which are the major constituents of the RJ and RC aggregates, were ordered from commercial sources and sieved to the 270 - 325 mesh in order to compare their behavior with that of the aggregates.

NMR method In the presence of the aggregate, there is a linebroadening due to the discontinuities in the magnetic susceptibility as one moves from the aggregate into the asphalt phase. This generates a spread in the resonance line so that one can no longer compare linewidths directly in order to tell whether molecular motion is affected. Therefore, we went to an experiment involving a spin echo¹⁴. This is simply a 90° pulse, followed by a delay time, τ , followed by a 180° (with a 90° rf phase shift) refocussing pulse, another period, τ , and then observation of the echo amplitude, $I(2\tau)$, at the end of this second τ period. The importance of the echo method is that inhomogeneities in the magnetic field can be separated from the dipolar interactions as contributions to the linewidth. The 180° pulse is transparent to the dipolar interactions but the contributions from magnetic field inhomogeneities are eliminated. In a crude sense, the rate of decay of the echo will be related to the inverse of the linewidth, but this relationship is not precise. Therefore, the decay will be used as a relative measure of change in the dipolar couplings which result from a change in the molecular mobilities of a given asphalt cement when solid particles are added. The data is taken as a function of τ . The functional form of this decay will not be any recognizable function since there is a wide range of mobilities present in the asphalt at ambient temperatures.

Summary of asphalt/aggregate results In Figure 10 we show a comparison of the echo decay profile for the asphalt cements AAD-1 and AAG-1. The faster decay of the AAG-1 sample correlates with its broader proton lineshape.

In order to test for the sensitivity of this echo decay to changes in molecular motion, we illustrate in Figure 11 that the echo decay profile is sensitive to a temperature change of 2°C because of changes in mobility causing small changes in average dipolar couplings.

In Figures 12 and 13 we compare the echo decay profiles of the asphalts AAG-1 and AAD-1, respectively, with and without the presence of the various solids, including the magnetically cleaned aggregates, RJ and RC. As can be seen from these plots, there is no evidence for any significant deviation in the average molecular mobility of the asphalts in the presence of the aggregate versus that in the absence of the aggregate. There is some scatter from these curves but the scatter is not consistently above or below the line for the parent asphalt. *Thus, within the precision and signal to noise of our current measurements, we conclude that motions in the asphalt cements are not, on average, modified by the presence of the aggregates investigated more than would correspond to a 2°C temperature change.*

Multiple-pulse proton spectra: The partial resolution of aromatic and aliphatic protons

Multiple pulse (MP) techniques were developed¹⁵ about 1968 and are intended to be linewidth narrowing strategies in solids based on eliminating the dipolar interaction while leaving chemical shift information behind (see appendix). This multiple pulse technique, when combined with magic angle sample spinning at nominal rates (1.5 - 2 kHz), results in spectra where, generally, aliphatic and aromatic protons may be distinguished. In Figure 14 MP spectra of asphalts AAD-1 and AAG-1 are shown. In the AAD-1 spectrum the aromatic protons appear as a shoulder near 7 ppm, while for AAG-1 they are a separate but incompletely resolved peak. This lower resolution with AAD-1 is expected given that more protons, compared to the AAG-1 sample, have correlation times of the order of 10^{-5} s, judging by the stronger linewidth narrowing in the FID spectra. Motion at this frequency interferes with the averaging of the dipolar interaction to zero over times characteristic of the multiple pulse cycle times.

This MP technique has the following advantages: a) spectra are quantitative, b) proton spectra have superior signal-to-noise over ^{13}C spectra, c) one can tailor polarization gradients with much greater versatility for the spin diffusion experiments (described in the next section) and d) one need not go to low temperatures to examine domain structure based on aromatic-rich and aromatic-poor phases. The major disadvantages are that the experiments are difficult and require a very precisely tuned spectrometer; moreover, sample spinning is required so that the phase structure which one is searching for must be stable under the spinning conditions. This latter point should not present a great obstacle since spinning speeds (1.5 - 2 kHz) are nominal and the rotor has only a 4 mm ID so that centrifugal forces are not high.

It is also possible to observe relaxation in the presence of MP irradiation. In that case signals disappear at a rate characterized by $T_{1\text{KZ}}$. This type of relaxation is sometimes useful to follow since, to a first approximation, the relaxation is the superposition of the individual relaxation times for each proton, and, since relaxation times are dictated by molecular mobility, one can often select signals from the least mobile protons this way. Motions with correlation times in the range of 10^{-4} to 10^{-6} s tend to restore a measure of dipolar coupling so that the relaxations of neighboring spins become coupled again.

Spin diffusion measurements and estimates of domain size for motional and compositional heterogeneities

The following experiments are designed to expose regions of varying composition (aromatic/aliphatic proton ratio) or varying mobility and to estimate the minimum domain dimension (MDD) across such regions in the event that the MDD's fall into the range of about 4 - 20 nm. If the MDD's are larger than 20 nm, then only the existence of the domains and not their dimensions will be determined. If the MDD is smaller than 4 nm, then dimensions are comparable to only two or three molecular diameters and the

meaning of 'domain' becomes more fuzzy because the random distribution of molecules would result in variations in composition over very similar dimensions.

The idea behind spin diffusion experiments has been described in the appendix. The experiments consist of four steps: 1) Produce a non-equilibrium polarization gradient, ideally in the absence of spin diffusion, 2) Let spin diffusion proceed for a varying amount of time, t , 3) Monitor the signal shape as a function of t , and 4) Wait until thermal equilibrium polarization (i.e. Boltzmann population) is reestablished in the spin system. From a practical point of view, the equilibrium NMR lineshape, designated M_0 , is that one which reflects the Boltzmann polarization where all spins, on average, have the same polarization per spin. When a non-equilibrium polarization is produced in step 1, we expect that the lineshape, immediately after the production of the non-equilibrium polarization, will have a shape different from M_0 . However, if all domains are sufficiently small, spin exchange between spins will cause all spins to equilibrate to the same level of polarization per spin because of spin diffusion. At this point the lineshape of the NMR signal will be the M_0 shape even though the polarization per spin may still be much smaller than the Boltzmann value. It is important to recognize that the signature of a good spin diffusion experiment, which takes place in a time short compared to T_1 (the time constant for recovery of the Boltzmann populations), is that the total integral of the lineshape is constant while the lineshape is changing.

In designing the spin diffusion experiments we were guided by ideas that asphalt has a micellar structure in which the more rigid molecules, which are strongly associating because of polar interactions and/or aromatic $\pi - \pi$ overlap, are surrounded or 'peptized' by more weakly interacting, less aromatic and less polar molecules which form a more fluid medium. Thus, we expected gradients of both aromaticity and mobility over distance scales of about one-half the center-to-center distance separating micelles. The size (MDD) of these regions may be limited in view of the fact that even in the most aromatic molecule in the asphalt about 50% of the carbons are aliphatic. Therefore, every molecule brings along flexible portions which have no strong intermolecular interactions. In any region of rigidity, these flexible fragments become structure disrupting since they have to be accommodated also. So this may eventually limit the MDD's to dimensions of only a few molecular diameters unless something like a mesogenic (liquid crystalline) structure can develop. The latter structure would probably require a uniformity of molecular structure beyond that found in the asphalts...but we do not know this in advance.

Spin diffusion measurements based on mobility gradients

The concept of this experiment was to enrich the initial polarization for those protons which have the highest mobility, i.e. the longest T_2 relaxation times. Then, one would monitor the changes in the lineshape until the M_0 lineshape returned. In monitoring the return of the lineshape towards equilibrium, both FID lineshapes and MP lineshapes were employed. The selection of enriched polarization in the narrow portion of the

lineshape was accomplished by applying a Carr-Purcell¹⁴ sequence using a fixed τ where storage of the polarization along the static field occurred at the fifth echo. The sequence is $[90^\circ-(\tau-180^\circ-\tau)_5-\pm 90^\circ]$. The choice of τ was sample-dependent and was chosen to satisfy the condition that 8 - 10% of the M_0 polarization was stored. This pulse preparation resulted in a preferential selection of the narrower-line protons, i.e. the most mobile protons.

In Figure 15 three spectra are shown pertaining to the FID-readout version of this experiment for asphalt AAG-1 at 304 K. At the earliest time, one sees that the lineshape is indeed narrower than in the M_0 spectrum. By 7 ms, it is indistinguishable in shape from the M_0 spectrum, which, in this display, is scaled down in intensity. It was a typical result that the FID lineshapes returned to their equilibrium shape after 7 ms of spin diffusion. Results of the times required to achieve equilibrium for the various core asphalts are tabulated in Table 3 in the first data column. It should be recognized that the choice of spin diffusion times in these experiments was fixed at 2, 4, 7, 15, 30, 60, 120 and 240 ms. So when an entry appears in this table it simply means that the time for equilibration lies between the given time and the next shorter time.

When the MP spectrum was used to monitor the recovery of the magnetization, then slightly longer times (15 ms) were obtained for several of the asphalts (see columns 2 - 4 of Table 3). This increase in the time is probably due to the more detailed shape of the MP lineshape relative to the FID lineshape with the result that smaller deviations from internal spin equilibrium could be detected more easily. In general, however, agreement by the two methods is quite reasonable. Moreover, for the oxidized samples, monitored via the MP lineshapes, similar results were obtained relative to the unoxidized samples. In AAK-1, there was a slight indication of an increase in domain size upon oxidation. The maximum MDD's ($= 2x$ where x is given in Equation 2 and $D = 5.5 \times 10^{-12} \text{ cm}^2/\text{s}$) implied by this data are 4 nm (7 ms data) and 6 nm (15 ms data). We shall return to a more detailed discussion of the interpretation of this data following the presentation of the spin diffusion data based on chemical shifts.

Two other pieces of data will be mentioned in connection with the mobility-based spin diffusion experiments. First, in Figure 16 spin diffusion spectra taken at both short spin diffusion times (0.1 ms) and long times (7 ms) are compared to a scaled M_0 spectrum. At the shorter time we already know that the polarization is predominantly associated with the most mobile protons. In the MP lineshape at 0.1 ms in Figure 16, one can see that these more mobile protons have fewer aromatic protons (the region near 7 ppm) compared with the sample-average aromatic protons in the M_0 spectrum. Moreover, the large aliphatic wing is slightly shifted in the upfield direction relative to M_0 . This shift of the aliphatic resonance is consistent with a depleted signal strength for benzylic protons (on aliphatic carbons bound to aromatic rings), whose resonances generally appear in the 2 - 4 ppm region, and an enrichment of signal strength for the aliphatic protons which are concentrated in the 0 - 2 ppm band. This correlation held for all of the asphalts. Therefore, *we can confidently associate the most mobile protons with more aliphatic*

protons. This is consistent with expectations based on the micellar theory of asphalts but it is no sufficient proof of the micellar theory.

The second point of note is found in the results of Table 4. As will be discussed later, it is possible to get the experimental results which were obtained in the mobility-based spin diffusion experiment and still fail to detect existing domains larger than 4 - 6 nm. This happens if, given a two phase system, there is not sufficient contrast in the fraction of mobile (or rigid) protons in the two phases. Thus, if at 300 K we suppose that the most mobile fraction originates primarily in the aliphatic *portions* of molecules as opposed to originating in the most aliphatic molecules *as whole molecules*, then all phases will have mobile protons since all molecules have some aliphatic portions; moreover, the contrast in their numbers would likely not be large enough to detect the existence of separate phases. Therefore, guided by the micellar ideas we argued that as the temperature was raised, some whole molecules should gain fluidity with the result that if these molecules resided in domains very large with respect to, say, 50 nm, then the contrast in the fraction of rigid protons would become sufficiently great to see the two phases in a spin diffusion experiment (via an inability to observe spin equilibration at long spin diffusion times). Simultaneously, there is another important trend which develops as molecules gain fluidity, namely, that the dipolar interactions between molecules weaken and eventually disappear. In other words, the mechanism for spin diffusion (spin exchange) weakens and finally disappears. Thus, if we carry out the mobility-based spin diffusion experiment at successively higher temperatures, if no large phases exist, then the time required for spin equilibration ought to *steadily* increase with temperature as the spin exchange process becomes less efficient. On the other hand, if large domains exist, then when the molecules of one phase become sufficiently fluid to provide the needed contrast, one ought *suddenly* to find that one fails to recover spin equilibrium, i.e. the undistorted equilibrium lineshape. Table 4 shows that increasing temperature between 300 and 340 K results in reasonably steadily increasing spin diffusion times for equilibration, *consistent with the idea that domains are small and the spin diffusion times given are determined by spin exchange efficiency*. This interpretation is also supported by Figure 3 where AAD-1 is shown to have the highest mobility (hence the longest spin diffusion time in Table 4) and AAG-1 the lowest at 340 K in the group of three asphalts considered in Table 4. The times indicated at 340 K in Table 4 reflect this ordering. As will be discussed presently, these mobility-based experiments are the most convincing for the viewpoint that if micelles exist, they have dimensions of the order of only 2 -3 molecular diameters, i.e. they are *small*!

Spin diffusion measurements based on chemical aromatic/aliphatic composition

Spin diffusion measurements were carried out using the differences in chemical shift between aromatic and aliphatic protons as a basis for generating the polarization gradients.¹⁶ Both MP and MAS were employed. In our version of the experiment MP irradiation was applied for a fixed time (equal to an integral number of MAS rotor

periods), then this magnetization was stored along the magnetic field direction. A variable spin diffusion period followed before signal observation under MP commenced. Figure 17 illustrates the changes of lineshape as a function of spin diffusion time, τ_{SD} , along with the scaled M_0 spectrum. In Figure 17, the spin diffusion spectra each have a total integral which is 2% of M_0 . Therefore, total polarization is small compared to the Boltzmann polarization. These conditions were chosen carefully to maximize the sensitivity to phase structure under the presumption that the phase structure presents a significant variation of the aromatic/aliphatic proton ratio. As can be seen at the earliest time in Figure 17, one can generate a very large relative polarization gradient between the aromatic and the aliphatic protons. Over the first millisecond much of this initial gradient is washed out. This is expected because aromatic protons, wherever they are, are surrounded by more numerous aliphatic protons on the same molecule. By the time intramolecular spin reequilibration is complete (after about 2 ms of spin diffusion), most of the initial gradient has disappeared. The remaining small changes which occur are those which can possibly be interpreted in terms of phase structure. It is because of the dominance of the intramolecular spin-equilibration process for creating lineshape changes, that the detection of phase separation depends critically on the initial magnetization gradient. It turns out that the smaller the integral of the spin diffusion spectrum, relative to M_0 , the more sensitively will the spin diffusion lineshapes indicate the presence of phase structure. Thus, the sensitivity of this experiment to the existence of phase structure is very dependent on the choice of initial integral in the spin diffusion experiment. In Table 3 we collected the spin diffusion times required to restore fully spin equilibrium for experiments in which the spin diffusion spectra had intensities of 1.5% of M_0 . The spin diffusion times listed in Table 3 are those times at which the relative amplitudes of the aromatic and aliphatic peaks agreed to within 3% of their M_0 values. The values given are for the original asphalts and most of the oxidized asphalts. The fact that these times are, in general, longer than those determined in the mobility experiments most likely reflects the fact that this experiment is exceedingly sensitive to small deviations from spin equilibrium, much more so than in the mobility-based experiments. The latter experiments did not allow such a fine tuning of the initial conditions. In the chemical-shift-based experiments the initially imposed polarization gradient can be followed to about 0.2% of its initial value. In contrast, in the mobility-based experiments, lineshapes become indistinguishable from the M_0 shape after gradients diminish to about 2 - 3% of their initial values, so equilibrium will be perceived at earlier times, as was found.

We come to two preliminary conclusions, based on the data of Table 4. First, there is little difference between asphalts. Second, oxidized and unoxidized samples look the same in this experiment. Both conclusions imply that chemical heterogeneity within all asphalts, whether oxidized or unoxidized, occurs on about the same length scale. Normally a 60 ms spin diffusion time would correspond to MDD's of about 11 nm, but these results must be put in perspective, and that is what is attempted in the next section.

Comments on the interpretation of spin diffusion data

The spin diffusion experiments have a fundamental ambiguity which arises from the fact that for the mobility-based experiments we do not have a prior knowledge of the fractions of mobile protons in the different regions we are trying to identify. Likewise, in the chemical-shift based experiments, we do not have a prior knowledge of the variation in aromatic/aliphatic ratios in these phases. There is an underlying assumption in these experiments that if the phases are distinct, then they differ from one another in one of these two ways, either in mobility or aromatic/aliphatic composition. While such differences are certainly expected based on models such as the micelle theory of asphalts, it is also true that we may not presume to know that which we set out to prove. Thus, we are forced to leave open the question of 'how different' these phases are in these two respects.

In order to distinguish different phases (assume there are only two phases) in these experiments, there must be a sufficient difference in the ratios of mobile to immobile protons (R_{mi}) or immobile to mobile protons (R_{im}) or aromatic to aliphatic protons (R_{ra}). If these ratios are too similar to one another then two things happen in the spin diffusion experiments. First, the signals associated with each region will look more similar so one's ability to distinguish different polarizations in different regions diminishes. Second, it becomes more difficult to generate polarization differences between regions. The net result of these two considerations is that the concept of thresholds for detection becomes appropriate. Perhaps a perspective can be more easily generated using an example from polymers where we have a similar problem to the asphalt problem, but with slightly more manageable numbers.

The system is a 50/50 blend of two highly aromatic polymers, poly(etherimide) or PEI and poly(benzimidazole) or PBI. This blend has a lopsided distribution of aromatic and aliphatic spins, just like asphalt, except that the aliphatic spins are in the minority in the blend. PEI has 25% of its protons in an aliphatic band while PBI has only 8% of its protons resonating in this region. Therefore, aromatic protons outnumber the aliphatic protons by a ratio of about 5:1 (1:13 in the asphalt case). We consider two samples of 50/50 PEI/PBI, one is an untreated blend which is an intimate mixture of the two polymers on a molecular level, the other sample has been heat treated at 643 K for 1 h which has induced some phase separation. Figure 18 displays data, shown in two plots, from a spin diffusion experiment analogous to that in Figure 17. In Figure 18 the polarization of the aliphatic peak is followed as a function of spin diffusion time. This is the solid line. Starting from a polarization far from internal equilibrium at very short spin diffusion times the equilibrium polarization is rapidly approached. The dashed (or dotted) horizontal line in the plot represents the aliphatic polarization level past which spin diffusion *between* different polymers is required. Above that line, changes in polarization can be attributed simply to spin equilibration within each kind of polymer. So information about the mixing of the two polymer chains is associated with the behavior of the polarization as it falls below this line. We can draw this line because we know the composition of the homopolymers and the overall stoichiometry of the blend.

In the lower portion of Figure 18, we repeat the data in the upper plot using a vertically amplified scale and a horizontally compressed scale. We have also added the data from the same experiment on the heat treated blend sample. Since the heat treatment produced phase separation, we now notice that the spin diffusion curve for this sample changes curvature just below the phase separation line and a new slope develops. This is the point at which polarization changes are no longer dominated by spin diffusion within the same molecule but by spin diffusion between domains, which, in this case have compositions close to pure PEI or pure PBI. From the slope of this latter portion of the curve, one can obtain an estimate of domain size. If the domain size were very large, i.e. greater than about 50 nm, the spin diffusion curve would become more horizontal and spin equilibration would be slow and very incomplete on this timescale.

In Figure 18 we have also included the rate of change of the aromatic intensity (labelled AAC-1 in the plots). In Figure 17, the aromatic line is increasing with spin diffusion time; we are plotting the negative of this polarization change in Figure 18. Note that the rate of polarization change is very similar to that of the intimately mixed blend. We look for behavior similar to that of the heat treated blend, i.e. we look for a break in the slope of the spin diffusion profile following the period of internal equilibration within each phase. The fact that the aromatic protons are in a 13:1 minority, rather than a 5:1 minority as was the case for the aliphatic protons of the blend, means that the phase separation line is closer to zero compared with the line appropriate to the blend. Moreover, what is not so obvious from Figure 18, but a very important point, is that the position of the phase separation line depends strongly on the stoichiometry (aliphatic/aromatic ratio) in the two phases, or, for the blend, on the PEI/PBI stoichiometries in the phase-separated regions. If, for example, one of the phases had consisted of a 60/40 ratio of PEI/PBI and the other phase were a 40/60 mixture, then the spin diffusion experiment could no longer sense the existence of the separate phases because the aliphatic/aromatic ratios for the two phases would have become too similar.

For the asphalt, therefore, we are currently in the position of *not having found any multiple-phase-indicating break in the spin diffusion curves* in spite of the fact that we have observed about a 1000-fold reduction in the initial polarization-per-spin gradient between aliphatic and aromatic spins. Therefore, one way of looking at this result is that *there is no measured length scale typifying variations in aromaticity identifiably larger than that characteristic of intraphase equilibration times.*

Another way of looking at the data is to examine the sensitivity of the measurement and calculate a threshold of composition which would have been detected if the domains are so big that spin diffusion between domains is inconsequential on the T_1 timescale. For a typical asphalt, model 2-phase calculations using realistic proton aromatic fractions (see ahead to Table 5) and typical initial conditions for the magnetization gradients were carried out. [Calculations were based on the following assumptions: a) Two phases coexist and differ from each other in proton aromaticity (or mobility fractions) although, for the purposes of computational simplicity, these intensity differences do not carry over to *lineshape* differences for the individual features, e.g. aromatic, aliphatic, mobile or

immobile protons; b) The sample-average spin polarization (i.e. the total signal integral) is constant over times significantly shorter than T_1 , even though spin diffusion takes place. Moreover, small decreases in total integral attributable to T_1 processes can be corrected for by multiplying the signal by $\exp(\tau_{SD}/T_1)$ where τ_{SD} is the spin diffusion time; c) No spin diffusion is allowed between the two phases, i.e. the phases have large characteristic dimensions (> 100 nm); d) Spin equilibration via spin diffusion is allowed separately in each phase resulting in two distinct polarizations per spin in each phase; e) Initial polarizations per spin can be chosen separately for the aromatic and aliphatic protons in the range from +1 to -1 times the Boltzmann polarization and this choice determines the total integral which one works with; and f) a deviation of 5% or more in the ratio of aromatic to aliphatic intensities is detectable and quantifiable compared to the equilibrium lineshape at a spin-diffusion-lineshape integral of 1.5% of the integral of the Boltzmann signal.]

These calculations showed this threshold to be such that $R_{ra}(\text{phase 1})/R_{ra}(\text{phase 2})$ must be greater than 1.7 and the mass fraction of each phase must be at least 0.15. For the mobility-based experiments, $R_{mi}(\text{phase 1})/R_{mi}(\text{phase 2})$ or $R_{im}(\text{phase 1})/R_{im}(\text{phase 2})$ had to be at least 2 with a similar mass fraction requirement. It was recognition of the latter point which prompted the experiments summarized in Table 4, since the experiments at the higher temperatures were those where it was virtually assured that the proper criteria were met. It was also the model calculations for the chemical-shift-based spin diffusion experiments which underscored to us the importance of controlling the total integral for the spin diffusion experiments (the smaller this integral, the more sensitive the spin diffusion experiment). In addition these calculations helped us recognize that a valid comparison of these experiments for different asphalts required that all experiments be compared at the *same* total integral, hence the data in Table 3 are compiled at a total integral of 1.5% of M_0 .

Since the thresholds in the spin chemical-shift-based spin diffusion experiment require at least a contrast factor of 1.7 in aromatic/aliphatic ratios between phases, one way to assess the meaning of the data from these experiments is to ask whether different chemical fractions in these asphalts can be separated which have at least this level of contrast. In Table 5, we have collected data on the ion exchange chromatography (IEC) column fractions. Included are the NMR-determined proton aromaticities for the whole asphalts and for the strong-acid and neutral fractions from IEC; also given are the corresponding mass fractions. Table 5 shows that there exist fractions in the asphalt whose aromaticities are sufficiently disparate and whose mass fractions are high enough to satisfy the criteria for observing phase structure. However, the larger question is whether the thermodynamics are favorable for the phase separation of any of these components in asphalt. Both the strong acid and the asphaltene fractions are brittle solids when isolated from the asphalt matrix. We have already shown that the asphaltenes and their complement, the malthenes, mix at some level (see Figure 7); likely the same thing can be said for the strong acids which are generally the most aromatic fractions separated by IEC. So, while this unanswered question presents the most serious challenge to the significance of the chemical-shift-based spin diffusion

results, the numbers in Table 5 indicate that fractions like the strong acid fraction, if they comprised a dominant fraction of one of the phases, could withstand at least some degree of dilution before the criterion for the aromatic compositions in the two phases failed.

It is for the foregoing reasons that we view the mobility-based spin diffusion measurements, summarized in both Tables 3 and 4, to be as compelling a proof against large structural organization in asphalts, as is the chemical-shift-based spin diffusion data. Even though the initial gradients in the mobility-based experiments were not as steep as in the chemical-shift-based measurements, yet in the former measurements there was the distinct possibility that the eventual polarization gradient formed between phases, was larger since the probability was higher that all protons in a given domain had excess molecular motion than that all protons were aromatic. Thus, in the mobility-based experiments, one need not have the immediate loss of most of the initial gradient via proton spin equilibration within a molecule.

Since we viewed the proof of the absence of large domains in asphalts as one of our major contributions to the understanding of asphalt structure, we will also mention a few miscellaneous experiments which pertain to this same topic.

Miscellaneous experiments testing for the existence of large domains

The first experiment to mention is summarized in Figure 19. There are six MP spectra shown. In 19A - 19C, the shape change accompanying different irradiation times along the MP spin-locking direction are shown. This relaxation is called T_{1xz} and the relaxation has been shown to be governed by molecular mobility. The rate of relaxation is near maximum for motions in the mid-kilohertz region. These spectra show that aromatic protons in the AAG-1 asphalt have longer relaxation times, on average, than those in the aliphatic region. In Spectra 19D - 19F, a spin-diffusion version of this experiment is shown in which, after the 8 ms T_{1xz} preparation and a storage of the magnetization along the static field direction, spin diffusion takes place. Again, spin equilibrium is reached in a very short time, i.e. 7 ms. This experiment is not so sensitive as the chemical-shift-based spin diffusion experiment is in terms of gradient preparation. However, what makes this experiment potentially more revealing is that the T_{1xz} preparation has a chance of enhancing polarization in a whole region as opposed to the chemical-shift-based preparation which creates polarization gradients between aromatic and aliphatic protons wherever they are found, including those on the same molecule. We did not try this experiment on all of the asphalts; however, we did try it on a few others. Invariably for the others, we could not duplicate the T_{1xz} behavior, i.e. there was little enhancement of the aromatic signal for longer locking times. The exact reason for this remains obscure. Perhaps the other asphalts, having more mobility at 300 K relative to AAG-1, allowed for more spin diffusion during the MP irradiation, thereby preventing the buildup of the polarization gradient.

Another kind of experiment which we carried out on a few samples is illustrated in Figure 20. Both spectra shown fall into the category of T_1 -zero-crossing experiments. For these experiments we test for domains which are larger than spin diffusion distances, i.e. larger than, say, 50 nm. Then if there are two kinds of domains *having different T_1 's*, the polarization in each domain relaxes exponentially with different time constants following an initial inversion of the equilibrium magnetization. Since the initial magnetization is the negative of its equilibrium value, it will pass through zero after about $0.69 T_1$. With different T_1 's in the two domains, this zero-crossing will happen at different times. Thus, when the total magnetization is partially recovered and near zero, there is a good chance that one region will be contributing a positive and the other region a negative signal. Of course, we suppose that there is also a lineshape difference between the spectra of each region. Thus, near the zero crossing, the lineshape has the greatest chance of being distorted from its equilibrium shape. In Figure 20 we illustrate that for the AAG-1 sample, using a MP spectrum and for the AAK-1 sample using an FID spectrum, there is no lineshape distortion from the M_0 shape. Thus, there is no evidence for larger domains in these experiments. One need not have a large difference in T_1 's between two regions in order to detect lineshape distortion, so this experiment further adds to the argument that no large domains exist.

Finally, there was a single experiment which indicated the existence of large domains. This was an experiment carried out at low temperature (200 K) using ^{13}C CP on a non-spinning AAD-1 sample. Again this was a zero-crossing experiment on the protons, with CP used as a probe of aromatic-aliphatic proton polarization ratios (see Figure 1 for spectral regions of assignment). The spectra of Figure 21 labelled 1, 2 and 3 were taken at 200 ms, 500 ms and after full equilibration in the T_1 -zero-crossing experiment, respectively. The zero-crossing lies between the 200 and 500 ms points, thus signal 1 is inverted in the display. Also, in this plot vertical scaling was chosen so that the aliphatic carbon lines were all of the same intensity. (On a per-scan basis, the intensity of lines 1 and 2 is about 20% of that of 3.) The fact that line 2 is more intense and line 1 is less intense than line 3 in the aromatic region implies that there is some phase separation at 200 K (well below road service temperatures) and that it is the more aromatic-rich phase that has the shorter T_1 . We tried to repeat this experiment on the AAG-1 sample and got the same result one time and a no-phase-separation result on a repeat of the experiment. There is some concern about spectrometer stability with respect to radiofrequency amplitudes in these experiments, opening up the possibility that this result is an experimental artifact. Because of our inability to stabilize our spectrometer satisfactorily at low temperature these experiments were abandoned. Therefore, the experimental finding of Figure 21 is only included because it points to the *possibility that phase separation occurs at very low temperatures. It is not presented as a proof at this time.* Low temperature experiments probably require more scrutiny in terms of the questions of phase separation. Although the glass transition and the slowing down of all molecular processes makes any phase separation a very slow process, one should not rule out the possibility that separate phases comprise the thermodynamically stable state at very low temperatures.

A final figure which I would like to include has nothing to do with the question of phase separation. The point of Figure 22 is to show how much more detailed ^{13}C CP-MAS spectra can be from a chemical point of view. These are spectra of the strong acid fractions of asphalts AAD-1 and AAG-1 using a 2.35 Tesla magnet system. These spectra have no spinning sidebands in the displays, i.e. all resonances are real resonances. The aliphatic and aromatic regions are totally separate. The resolution is quite good because the strong acid fraction has much less molecular motion than does the whole asphalt at ambient temperatures. Thus, the CP process works much better and the spectra are a lot more quantitative. The top two spectra are the regular CP spectra and one can see directly that the carbon aromaticity of the AAG-1 strong acids is higher than that of the AAD-1 strong acids. This trend was seen in the proton aromaticities as well (Table 5). Another variation of the CP experiment¹⁷, illustrated by the third spectra down, suppresses rigid methylene and methine carbons and yields spectra of the unprotonated carbons plus a partial methyl carbon profile. Differences between these and the top spectra (middle spectra) represent the protonated carbons along with partial methyl intensity. Points of note are that 1) carboxyl carbons are visible near 180 ppm in the AAG-1 strong acid fraction but not in the AAD-1 fraction, 2) carbon aromaticities of 0.35 and 0.40 for AAD-1 and AAG-1 strong acids agree pretty well with the corresponding solution-state carbon aromaticities of 0.32 and 0.37 for these same fractions given earlier in this report, 3) the fraction of substituted aromatic carbons, relative to the total aromatic carbons, is lower in the AAG-1 strong-acid fraction, and 4) a substantial amount of the unprotonated aromatic intensity is associated with resonances below 130 ppm. One of the unprotonated resonances occurring below 130 ppm is the central carbon in highly fused aromatic structures.

From a knowledge of the fraction of unprotonated carbons in the solid-state spectra, one may calculate, for these strong acid fractions, the ratio of aromatic carbons to aromatic protons, i.e. the ASI or aromatic substitution index which was given for the core asphalts earlier in this report in the high-resolution NMR section. For AAD-1 and AAG-1, the respective high resolution ASI values for the whole asphalts are 2.2 and 2.7 but for the strong acid fractions by solid state NMR are reversed, i.e. 2.7 and 2.1. Thus, even though solution NMR measurements indicate that the strong acid fractions both represent about 35% increases in carbon aromaticity over that of the whole asphalt, the degree of substitution of those strong-acid aromatic carbons in AAG-1 is lower than in the overall asphalt while the opposite is true for the AAD-1 asphalt. If larger ASI values imply a greater degree of ring condensation (and stronger intermolecular π -overlap interactions) and if the strong acid fraction represents molecules which are more capable of association based on polar interactions, then it would seem like the strong-acid fraction of the AAD-1 asphalt combines polar and π -overlap features more effectively for promoting strong molecular association than occurs in its AAG-1 counterpart.

It would be interesting to pursue further high resolution analysis of these fractions in order to try to elucidate more about the structure of the asphalts and their fractions.

Summary and Concluding Remarks

Summary of the NMR findings.

Proton lineshapes at 304 K indicated that the core asphalts differed from one another in their very local molecular mobilities. Moreover, in all asphalts there is a coexistence of protons which have motionally-averaged linewidths of a few kilohertz with those that have more restricted motions on the 10^{-4} s scale and whose linewidths go up to 40 and 50 kilohertz. The distribution of motions is broad but not easily quantified. There seems little warrant for the idea that two strict classes of molecular mobility coexist; rather the lineshapes are more reflective of a continuum of mobilities, as one might expect in a micellar structure. It should be recognized, however, that heterogeneity of molecular motion is not a sufficient proof that the micellar structure exists since significant motional heterogeneity is also seen² by deuterium NMR in homopolymer glasses like polycarbonate where there is little reason to expect micellar structure. In particular, the AAG-1 asphalt was most rigid, followed by AAF-1. The AAA-1, AAB-1 and AAD-1 asphalts are most mobile. Rankings of the core asphalts based on room temperature dynamic shear viscosities at 1.0 rad/s correlate pretty well with rankings of molecular mobility implied by the NMR lineshapes (see Table 1 and Figure 3).

Variable temperature lineshapes were obtained on the core asphalts in the temperature range from 200 K to 340 K. These lineshapes showed the progressive changes in mobility as the temperature was raised. Early motions are probably associated with local conformational motions of the aliphatic molecular fragments. Further narrowing of the lines requires some limited molecular diffusion as well. At 340 K, a significant fraction of the molecules have such translational mobility; however, they coexist with another population (20 - 30%) of protons whose linewidth is still near the rigid lattice limit on the NMR timescale of 10^{-4} s. Lineshapes at 340 K are the most convincing in terms of establishing the notion of a *heterogeneity in the mobility of molecules as opposed to molecular fragments*. This latter point convinces us that it is a worthwhile endeavor to look for 'structuring' and to speak about differences of molecular organization in different regions.

Asphalt physical aging under nitrogen, when monitored by the proton lineshape at 304 K, was insignificant, i.e. corresponded to changes of less than 1 K in temperature. Aging histories included times up to 6 months and temperatures of 253 K, 300 K and 333 K as well as diurnal cycles of 253 K to 298 K and 302 K to 333 K. Initializing conditions for the samples were 413 K for 1 h. Physical aging at other temperatures was not monitored systematically; however, some hysteresis was generally observed at temperatures in the 250 K to 290 K range during variable-temperature experiments. This hysteresis is probably associated with time-dependent free volume collapse in a broad-glass-transition-temperature material, i.e. one in which a wide range of molecular mobility exists. NMR observations are consistent with findings³ that mechanical properties depend on aging time at similar temperatures. It is important to recognize that one cannot, on the one hand, describe asphalt as a structuring material (as one does, for example, in the micellar

theory) and, on the other hand describe it by a single, well-defined glass transition temperature. At best there will be a broad glass transition temperature and time-dependent changes will be observable over a correspondingly broad range of temperature.

According to the NMR lineshapes *at 300 K*, oxidation, either POV or POV preceded by TFO, produces virtually no change. If anything, there seems to be a very slight *increase* in the mobility of the most mobile fraction. This result is counterintuitive since oxidation also increases viscosity substantially. When oxidized asphalts are compared with unoxidized asphalts *at 340 K*, the picture changes slightly. Here the fraction of the least mobile protons is enhanced by about 10% of its otherwise 20 - 30% fraction after oxidation. This effect was not seen at 300 K since most of the oxidized molecules, before oxidation, were immobilized on the NMR timescale in the original asphalts at this temperature. In addition, at 340 K there was also a small enhancement in the number of the most mobile protons as if oxidation immobilized some molecules and in the process, gave a bit more freedom of movement to others. The insight into the influence of oxidation on molecular structure is that the bulk of the molecules are unaffected by the oxidation. These molecules, if anything, gain a very small amount of mobility. On the other hand, a few molecules are slowed down, thereby enhancing the population of the most-rigid molecules. This is a very interesting context in which to ponder the origin of the viscosity increase (typically 7 - 40 fold) which usually accompanies oxidation. If one thinks in terms of the micelle theory and spherical domains, then the origin of the viscosity increase would have to be an increase in the volume fraction of the hard-sphere cores of the micelles since the fluid, peptizing phase is, if anything, becoming more fluid. If we assume that the volume fraction of hard spheres is related to the fraction of the more rigid protons, then we are dealing with an increase in the hard-sphere radius of 3% (10% volume increase) and a volume fraction of about 30%, assuming that the number of micelles does not change. A 7 - 40 fold viscosity increase is more than an order of magnitude larger than is predicted for non-interacting hard spheres in a fluid medium at these volume fractions.¹⁸ *Therefore, it seems reasonable that the more rigid phase is not isolated as hard spheres, but forms a more continuous network.* Using the 'NMR-rigid' proton fraction at 340 K as a predictor of the relative viscosities measured at 333 K was only partially successful since the respective rankings based on each of these measures showed only fair correlation. This only-fair correlation was rationalized by the 'threshold' nature of the NMR-rigid fraction; variations in strengths of molecular interactions within this fraction are not measured.

This paragraph is highly speculative and addresses possible origins for the unique behavior of the AAG-1 asphalt. The NMR-rigid portion, is greatest for AAG-1. This is true in spite of the fact that other measures of molecular association, namely, a low asphaltene content and no significant large-molecular-size fraction in GPC using THF as a solvent, indicate that there are few strongly associating molecules in the AAG-1 asphalt. One possible rationale for these seemingly contradictory observations begins with the recognition that the NMR-rigid protons are those which are rigid on a particular timescale. The number of such protons does not reflect the relative strength of

association between the molecules bearing these protons beyond a threshold which is related to the temperature of the measurement. Thus, one explanation is that the AAG-1 asphalt *has a high degree of chemical uniformity* with the result that the molecules fit together more efficiently and hence have less mobility, *even though the strength of the molecular associations is relatively modest*. The possibility that calcium ions from the lime treatment act as cross-linking agents via interactions with polar sites is dismissed on the basis of a comparison of 297 K lineshapes between the AAG-1 and the same asphalt without lime treatment, ABD. The comparison indicated that the ABD molecules are at least as rigid as the AAG-1 molecules (Figure 6).

In the context of the above discussion, we can also ask the question of why the AAG-1 asphalt has the smallest viscosity increase upon oxidation of all of the core asphalts. If the more rigid network forms a *continuous* phase, then this phase should dominate the viscosity characteristics. In particular, the most strongly interacting molecules within this rigid phase would exert the most influence on viscosity. Conceivably if these same strongly interacting molecules were also oxidized, the strength of association would increase, thereby increasing the viscosity much more effectively than if oxidation had taken place for originally weaker-interacting molecules. In the AAG-1 asphalt, we speculate that moderately strong molecular associations are manifold but very strong associations are missing. Therefore, oxidation of a normal number of sites does not greatly reinforce any already-strongly-interacting network. Moreover, the chemical uniformity hypothesis suggests that each molecule, considering its structure, has greater opportunity to maximize its intermolecular interactions in the unoxidized asphalt compared with its opportunities in a more heterogeneous chemical environment typical of other asphalts; hence, the strengthening of intermolecular interactions as a result of oxidation causes a smaller change relative to the original viscosity. The smaller-than-sample-average aromatic substitution index (ASI) in the strong acid fraction of AAG-1 may also play a role in reducing the number of oxidizable sites, e.g. benzylic sites, for the most strongly interacting fraction.

When molecular mobility of the asphalt in the presence of small (78 - 94 micron) aggregate particles was probed at 300 K via the strength of the dipolar interactions, no change was detected compared with the original asphalts in either samples AAG-1 or AAD-1. The proton lineshapes could not be monitored directly but the echo technique which gives the same kind of information was capable of detecting changes in mobility which would correspond to a 2 K temperature change. So, within that error limit, *no mobility change occurred*. This is not surprising in view of the fact that the interstices between particles are of the order of 10^4 molecular diameters. This is a very long distance to have surface effects propagate. Samples consisted of 4:1 mixtures of asphalt and aggregate; they were initialized at 393 K for 20 m.

A lot of effort was put into spin diffusion measurements. These measurements probed the distance scale of heterogeneities in molecular mobility and aromaticity. According to the micellar model, the core of each micelle ought to be characterized by a lower mobility and a higher aromaticity relative to the surrounding, 'peptizing' medium;

therefore, we expected to get distance scales for the micelles out of these experiments. In order to succeed in determining such length scales in these experiments, certain minimum levels of contrast in the mobility or aromaticity and certain minimum mass fractions had to characterize the different domains (assume two kinds of domains, A and B, for simplicity). Calculations corresponding to the experiments indicated that the ratio of proton aromaticity in phase A relative to phase B had to exceed 1.7 at a mass fraction of at least 0.15 in order for the aromaticity experiment to succeed. The corresponding criteria for the mobility experiment was that the ratio of either mobile or immobile protons in the two phases exceed 2, again at a mass fraction of at least 0.15. It was shown that aromaticities of IEC fractions, particularly the strong acid fractions, have sufficient contrast to satisfy the aromaticity condition even if the strong acid fractions were slightly diluted by the other fractions. It was also judged that the mobility contrast criterion was satisfied, particularly at temperatures slightly above room temperature, judging by the proton lineshapes at these temperatures. The outcome of these experiments, however, showed that *there is no evidence for heterogeneities of mobility or aromatic content on distance scales larger than a couple of molecular diameters, i.e. 2.5 - 4 nm. Moreover, oxidation does not change this claim.* The only evidence for phase separation on a larger scale (>40 nm) came from an experimentally-suspect ^{13}C measurement taken at 200 K. A few other isolated proton experiments, using different approaches with different requirements for the detection of domains, also corroborated the claim of small domain sizes.

Brief comments on these findings

If it weren't for the fact that the proton lineshapes indicated a coexistence of widely differing molecular mobilities, we would be inclined to interpret the spin diffusion data as disproving the micellar theory because the distance scale of motional and compositional heterogeneity is of the same order as the statistical fluctuations in the positioning of the aromatic-rich regions of various molecules or in the distributions of the most aliphatic (mobile) molecules. Given the lineshape observations, however, we are inclined to argue that mobility heterogeneity exists in asphalts on a scale of 2 or 3 molecular diameters *in the thinnest direction*. This leaves room for the possibility that such domains are continuous, as opposed to spherical-micellar in shape, or, if domains are spherical, they are so small that the aliphatic tails of the molecules in the more rigid cores overlap one another in the "peptizing" medium, i.e. the concept of *strongly interacting* hard particles is required.

In fact, one exceedingly speculative idea is that the asphalt has a temperature-dependent microstructure which is doomed to be described by small dimensions because of the fact that each molecule consists of fragments, some of which create associations (polar/aromatic) and some of which (aliphatic) have only weaker dispersion forces at any given temperature. In this picture, asphalt molecules would be analogous to A-B block copolymers where the A and B blocks are incompatible. For such block copolymers, phase separation occurs on a scale with dimensions determined by the block length. The

morphology these block copolymers adopt¹⁹ is that which minimizes surface (interface) area, e.g. lamellar for roughly equal-volume ratios of A and B, followed by rods and then spheres as one of the components becomes a smaller fraction. A temperature-dependent morphology in asphalts may arise because of the chemical heterogeneity (dispersions of A and B block lengths in this picture) and the wide range of strengths of molecular association. If such is the case, at low temperatures the 'more strongly associating domains' may be dominant while at higher temperatures, where thermal effects have broken up many associations, the 'more strongly associating' domains may have become the minority. The large viscosity change with temperature in asphalts may be evidence that one is slowly moving from connected domain morphologies (lamellae) to less connected morphologies (spheres). (In this connection, the lack of any obvious transition points in plots of viscosity versus temperature may raise questions about this theory but we are not convinced that the chemical dispersity of asphalts would make such a transition sharp.) It is clear that the strength of the asphalt matrix will depend less and less on the strongly associating domains as the morphology moves in that direction, i.e. as connectedness of the more rigid region is lost. Again, an essential point in this picture is that the strongly associating domains are limited in size to a molecular diameter or two because each strongly associating molecule drags with it other fragments which do not want to be strongly associating. These more mobile fragments seek to maximize their entropy with other flexible molecules or molecular fragments.

In conclusion, one of the disappointing things to us is that we do not have a better understanding of the differences in molecular structural characteristics of the various fractions of these asphalts which we can then relate to the differences in mechanical properties. While we believe these studies have pointed to the small scale of heterogeneities of microstructure in asphalts, we believe that the connectedness of the strongly associating regions plays a crucial role along with the strength of interaction within these strongly associating regions. One reason why our length-scale measurements looked similar for all asphalts, in spite of the varied performance of these asphalts is that the connectedness of the more rigid domains along with their relative strength of molecular association is more important in determining physical properties than is the length scale of the minimum domain dimension since the latter does not change very much, even though the connectedness might. One avenue of approach might be to analyze fractions more thoroughly by high resolution NMR for 'average' structures, particularly the LMS fractions from GPC. It would be interesting, in conjunction with elemental analysis to see whether there was a strong correlation between the aromaticity or the number of heteroatoms per molecule and the strength of association.

References

1. F.J. Nellenstyn, *J. Inst. Petr. Tech.* 10, 311 (1924) and 14, 134 (1928)
2. H.W. Spiess, *Adv. Polym. Sci.* 66, 24 (1985)

3. D.A. Anderson, *A-002A SHRP Quarterly Report*, Western Research Institute, March, 1990, Task 1.2
4. J.D. Ferry, "Viscoelastic Properties of Polymers", John Wiley & Sons, New York, 1961, Chap. 13
5. P.W. Jennings, *AIIR-14 SHRP Quarterly Report*, March, 1990
6. Data from SHRP Materials Reference Library, Austin, TX
7. J. Schaefer, E.O. Stejskal and R. Buchdahl, *Macromolecules* 10, 384 (1977)
8. R.N. Traxler and H.E. Schweyer, *Proc. Am. Soc. Test. Matls.* 36, 544 (1936)
9. D.A. Anderson, *A-002A SHRP Quarterly Report*, Western Research Institute, September, 1989, Section 1.1.4.
10. J.J. Aklonis and W.J. MacKnight, "Introduction to Polymer Viscoelasticity", John Wiley & Sons, New York, 2nd Edition, 1983, Chap. 4
11. D.A. Anderson, *A-002A SHRP Quarterly Report*, Western Research Institute, March, 1989, Section 1.2.2.
12. E.K. Ensley, *J. Appl. Chem. Biotechnol.* 25, 671 (1975)
13. J.C. Petersen, E.K. Ensley and F.A. Barbour, *Transp. Res. Rec.* 515, 67 (1974)
14. H.Y. Carr and E.M. Purcell, *Phys. Rev.* 94, 630 (1954)
15. J. S. Waugh, L. M. Huber and U. Haeberlen, *Phys. Rev. Lett.* 20, 180 (1968)
16. P. Caravatti, P. Neuenschwander and R.R. Ernst, *Macromolecules* 18, 119 (1985)
17. S.J. Opella and M.H. Frey, *J. Am. Chem. Soc.* 101, 5854 (1979)
18. J. Happel and H. Brenner, "Low Reynolds Number Hydrodynamics", Prentice-Hall, Englewood Cliffs, N.J., 1965, Chap. 9
19. M. Matsuo and S. Sagaye, "Colloidal and Morphological Behavior of Block and Graft Copolymers", G.M. Molau, Ed., Plenum, New York, 1971, pp. 1-19
20. A. Abragam, "Principles of Nuclear Magnetism", Oxford University Press, London, 1961

21. M. Mehring, "Principles of High Resolution NMR in Solids", Springer-Verlag, Berlin, 2nd Edition, 1983
22. S.R. Hartmann and E.L. Hahn, *Phys. Rev.* 128, 2042 (1962)

Figures

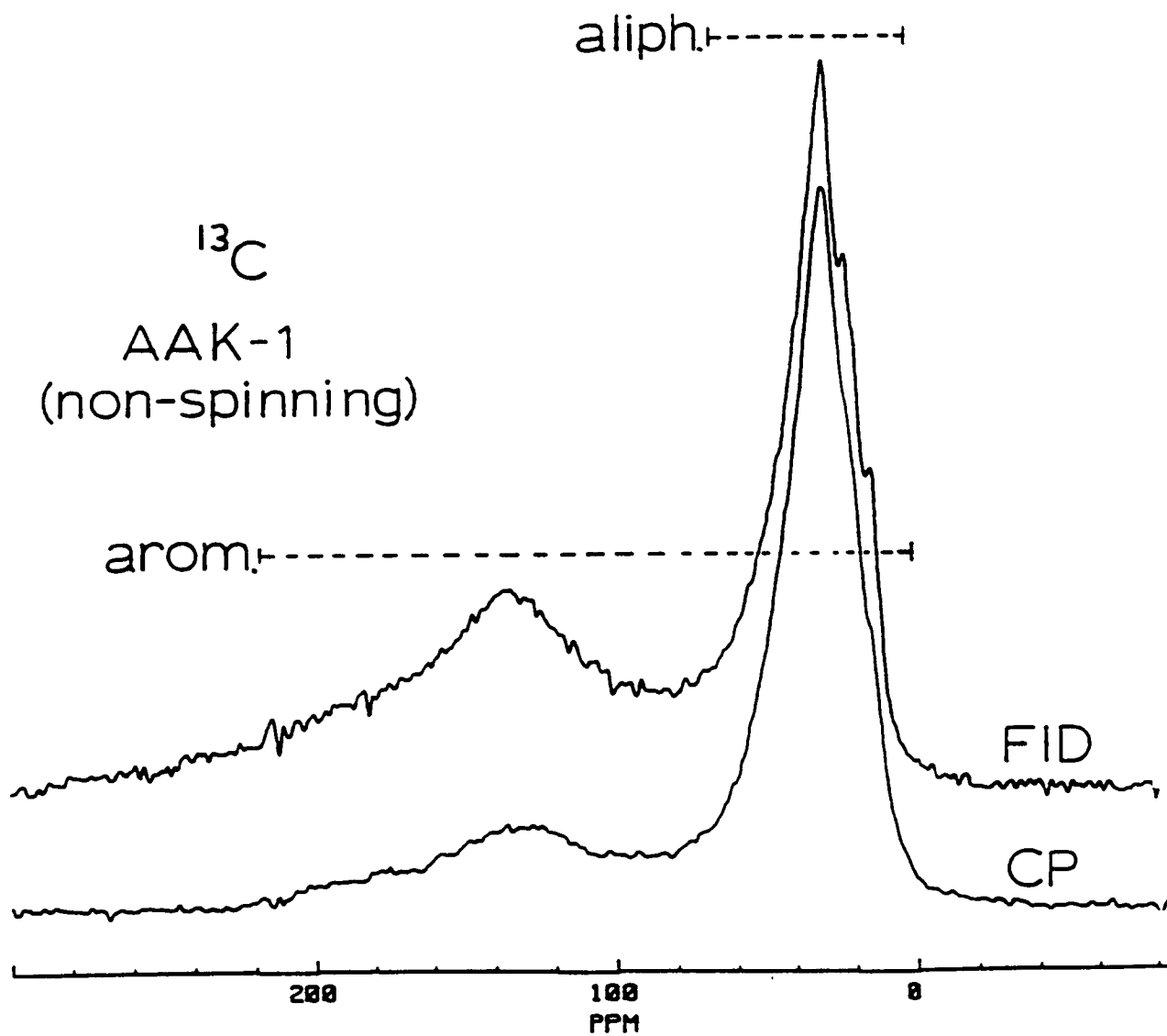


Figure 1. Carbon-13 non-spinning spectra of AAK-1. CP time is 0.2 ms.

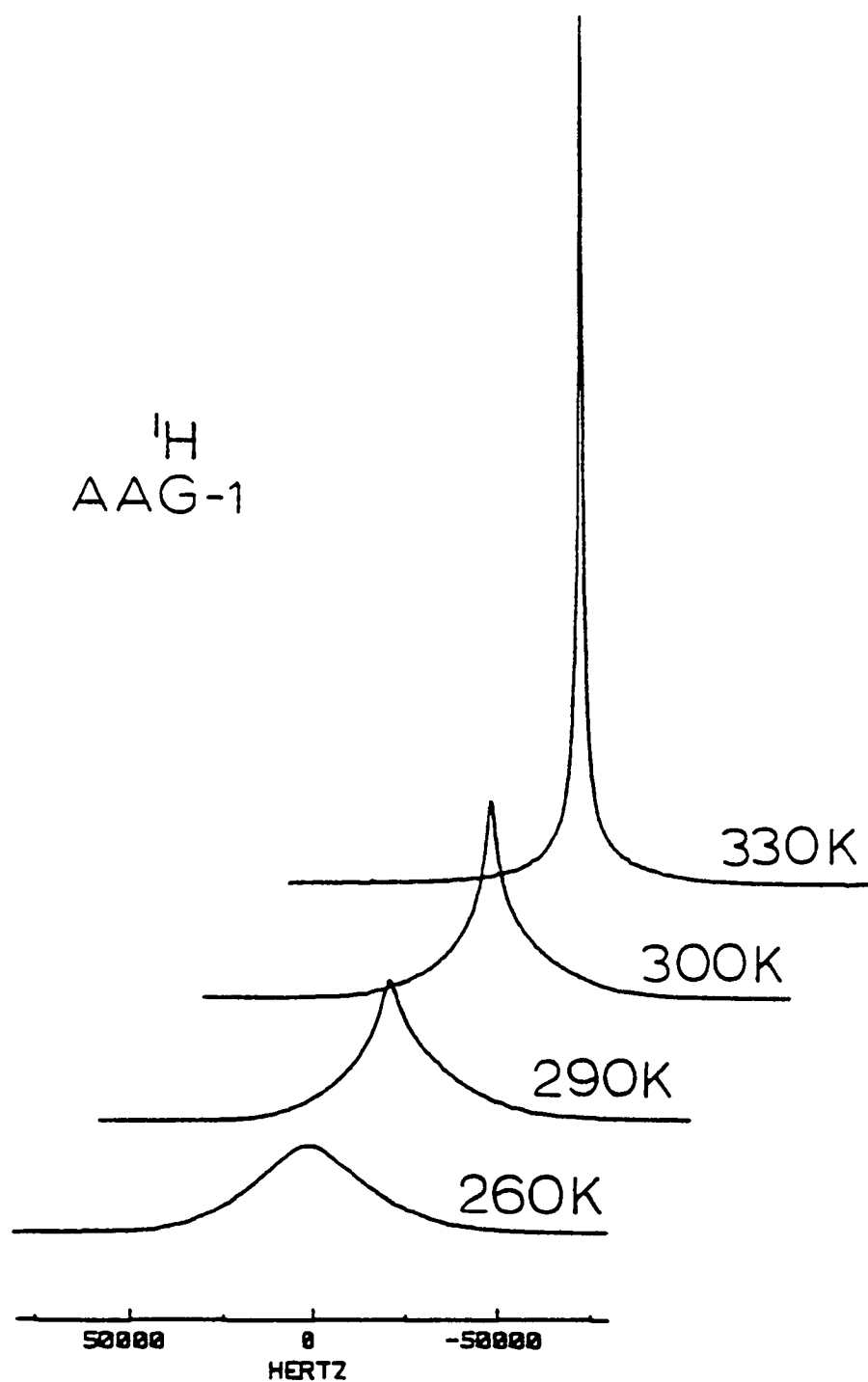


Figure 2. Temperature-dependent proton spectra of AAG-1

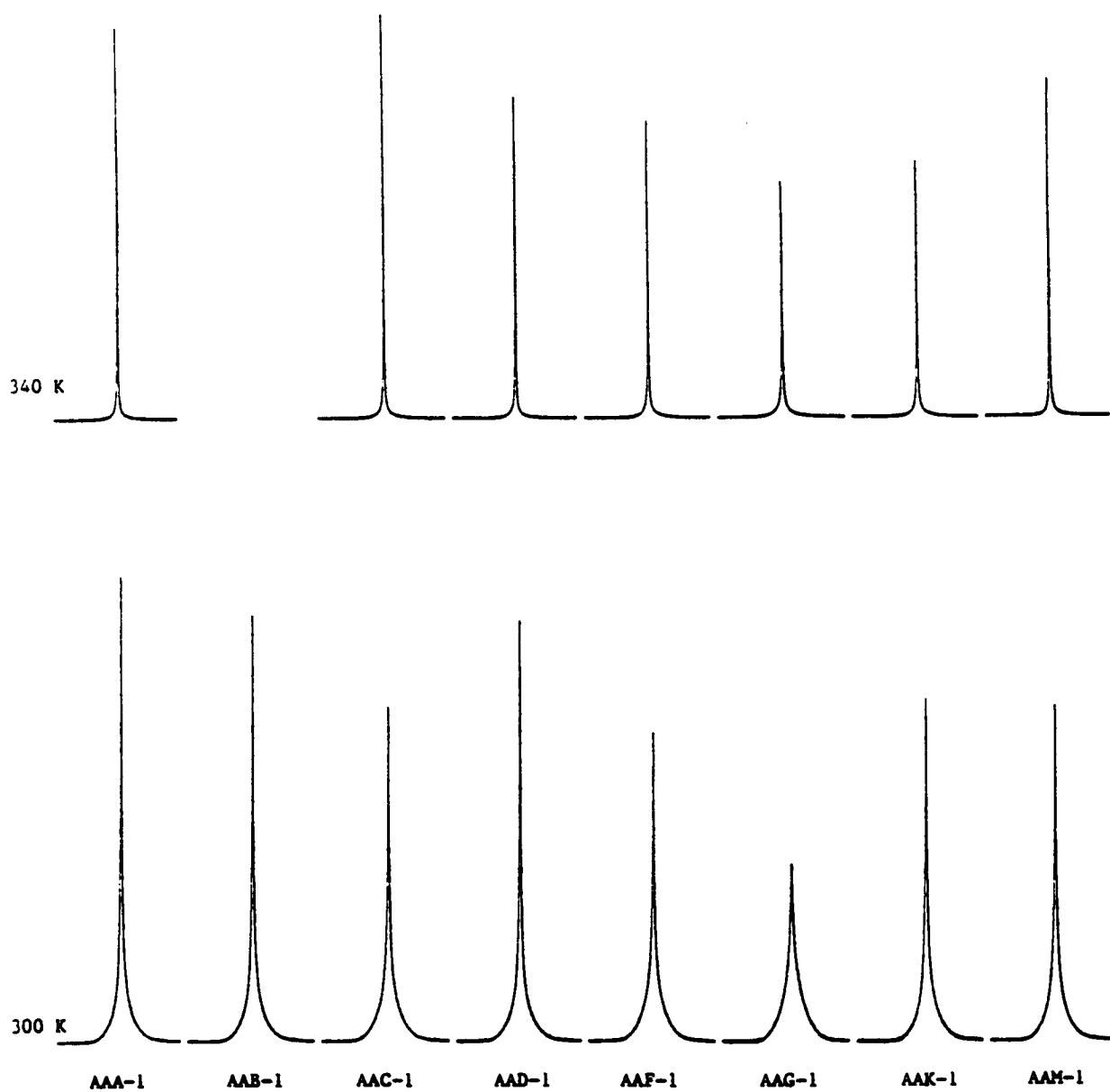


Figure 3. 160 kHz spectral displays of core asphalts; spectra in each group are normalized.

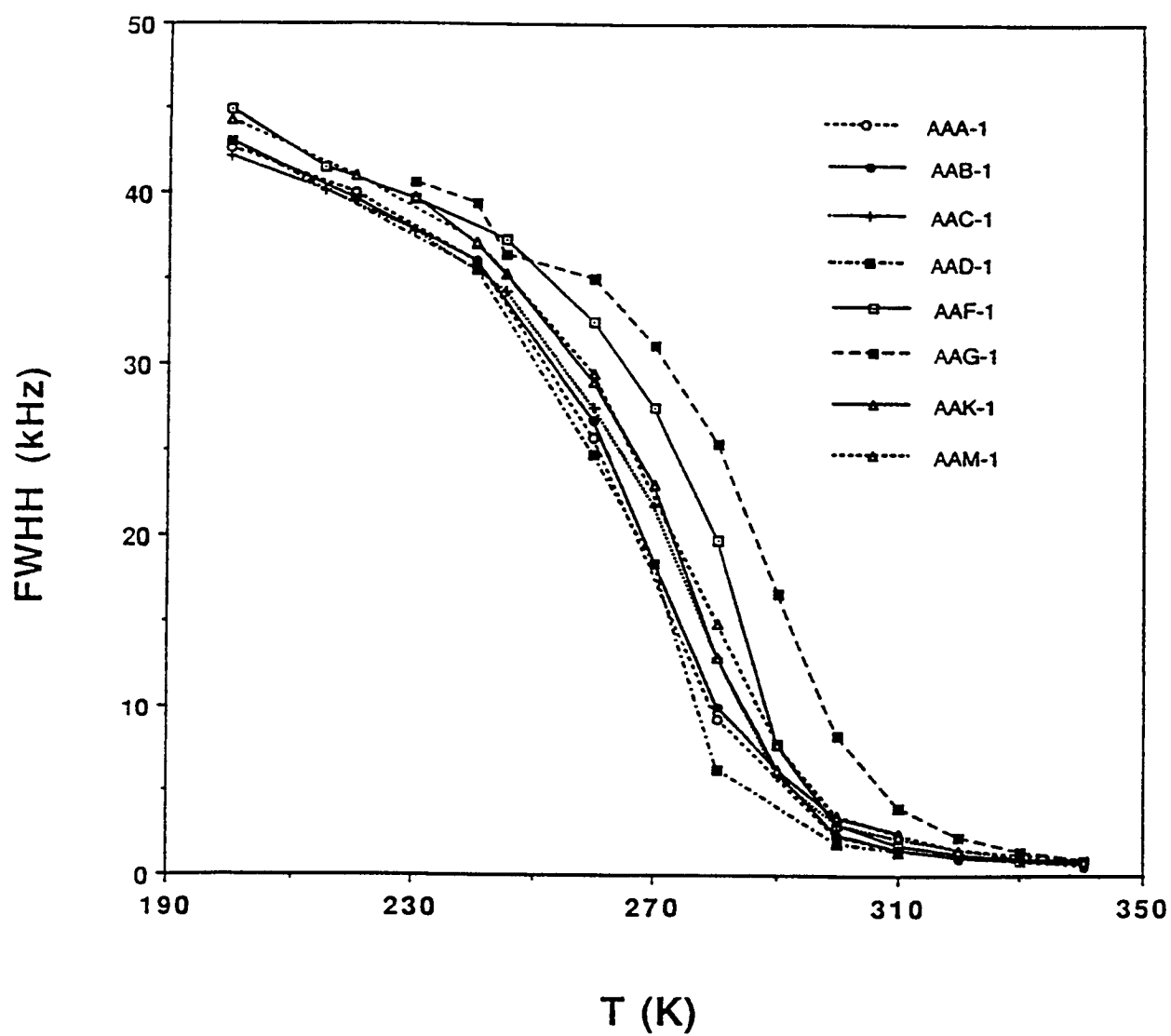


Figure 4. Full width at half height of proton spectra at various temperatures. Points are averages over increasing and decreasing temperature cycles.

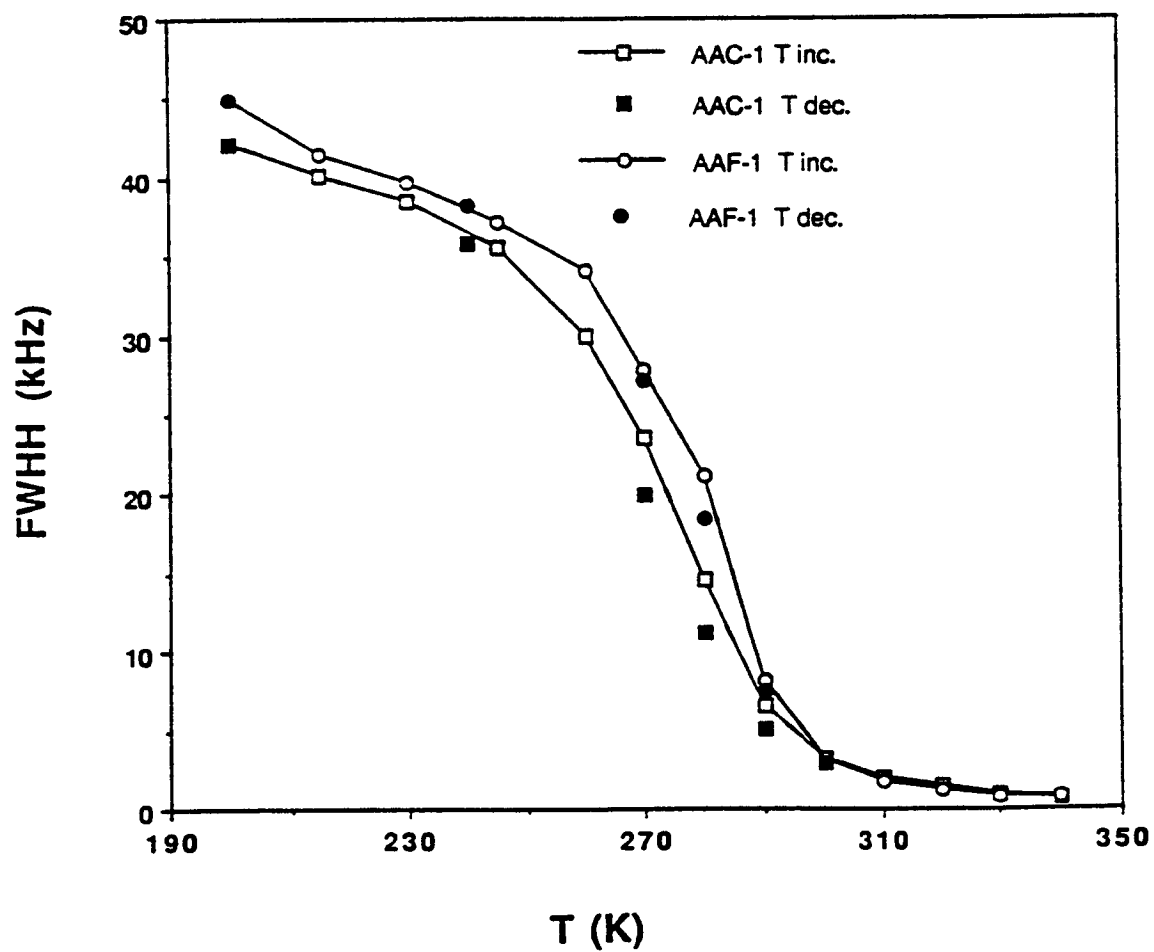


Figure 5. Illustration of hysteresis in linewidth for asphalts AAC-1 and AAF-1

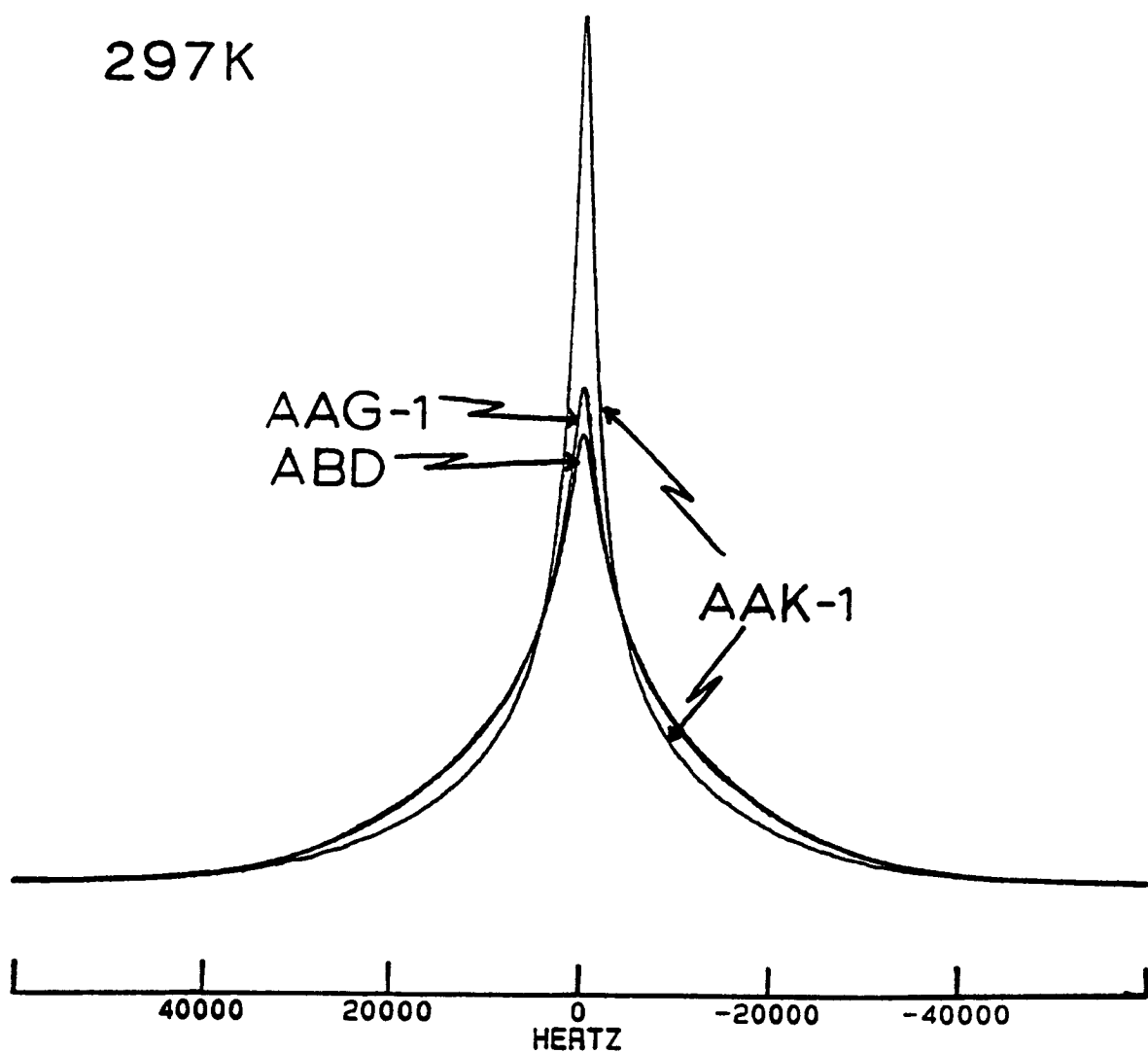


Figure 6. FID proton spectra of the asphalts indicated. Spectra are normalized to the same total intensity to facilitate shape comparison. The similarity of lineshapes AAG-1 and ABD proves that the principal reason for the uniquely lower mobility of molecules in the AAG-1 asphalt is not a result of the lime treatment (ABD is the AAG-1 asphalt without lime treatment).

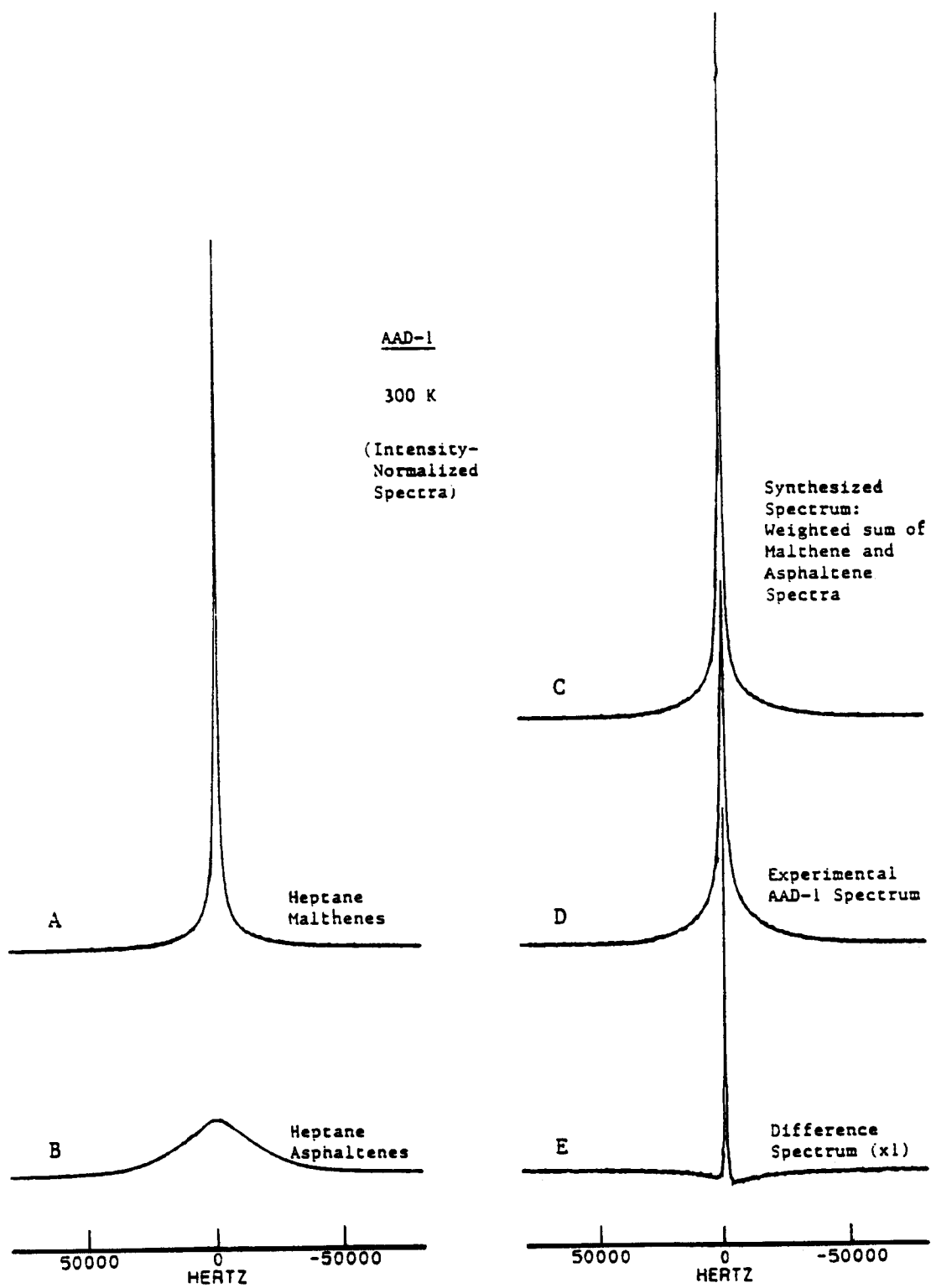


Figure 7. Spectra showing that malthenes and asphaltenes are not separate phases in asphalts

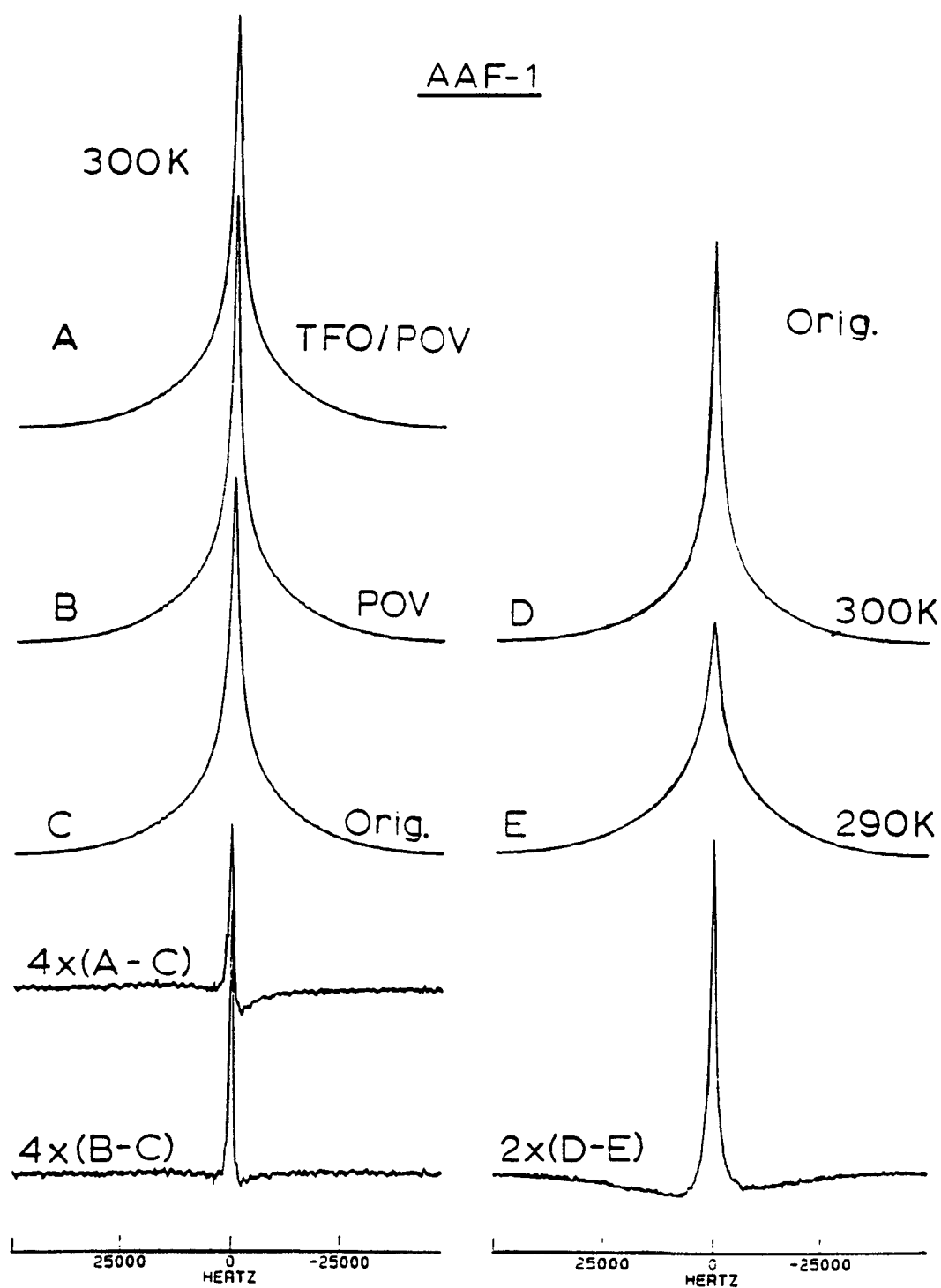


Figure 8. Proton spectra of AAF-1 at 300 K illustrating that the mechanism of viscosity increase through oxidation is accomplished with little change in molecular mobility (spectra A-c) in contrast with molecular mobility change upon decreasing temperature (spectra D and E).

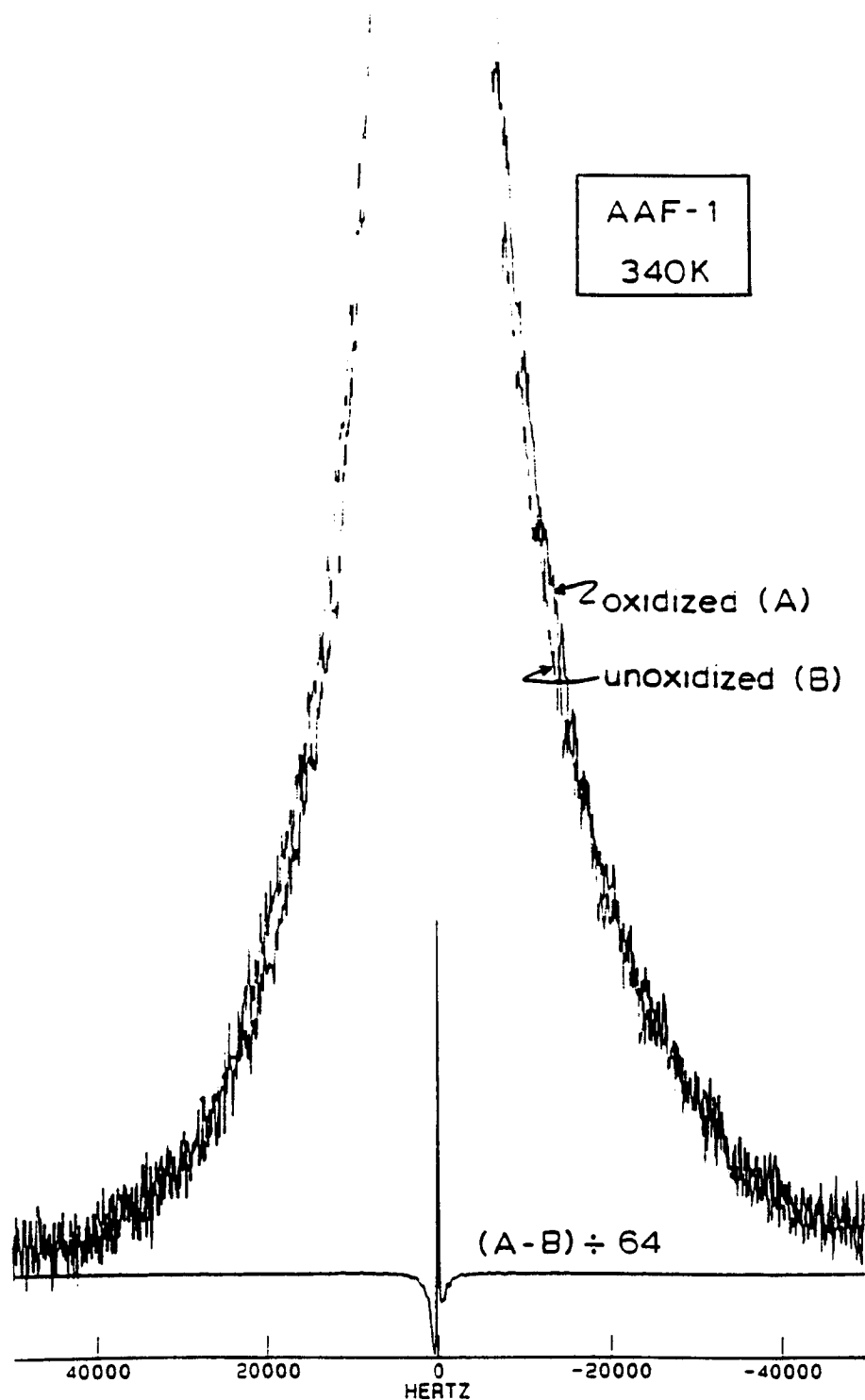


Figure 9. Proton spectra of AAF-1 at 340 K showing that oxidation increases the fraction of most rigid protons (by 10%). Difference spectrum shows that the oxidized material has a slight excess of mobile protons.

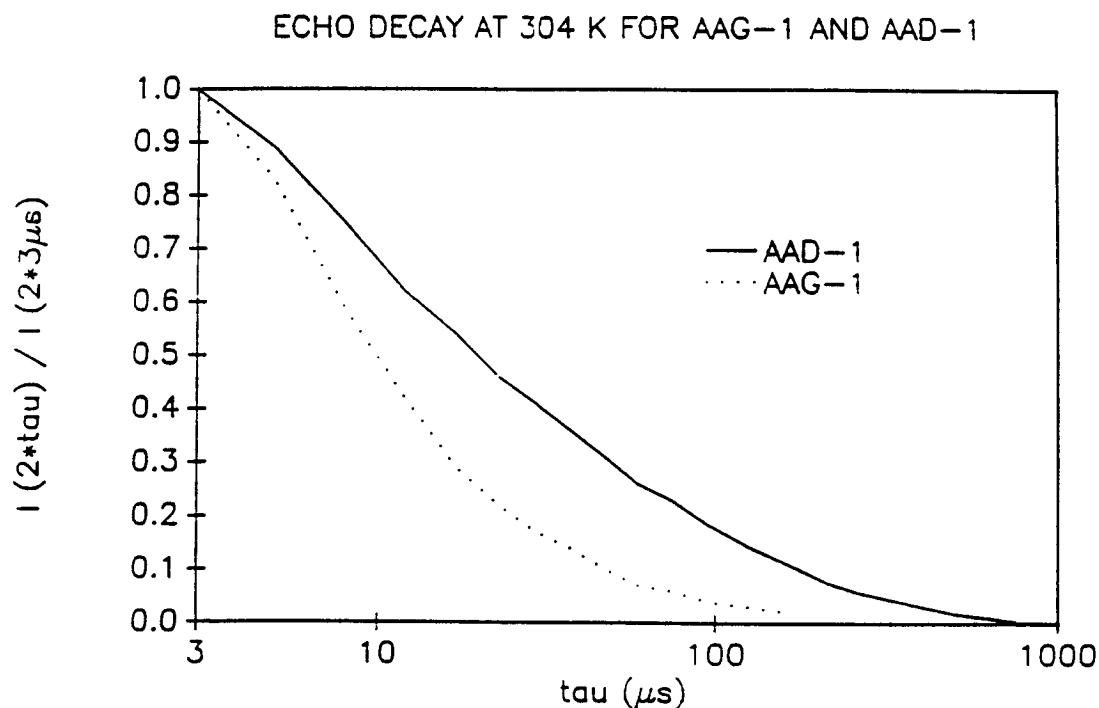


Figure 10. Echo profile showing that D and G have different rates of decay, which is expected based on their linewidth difference

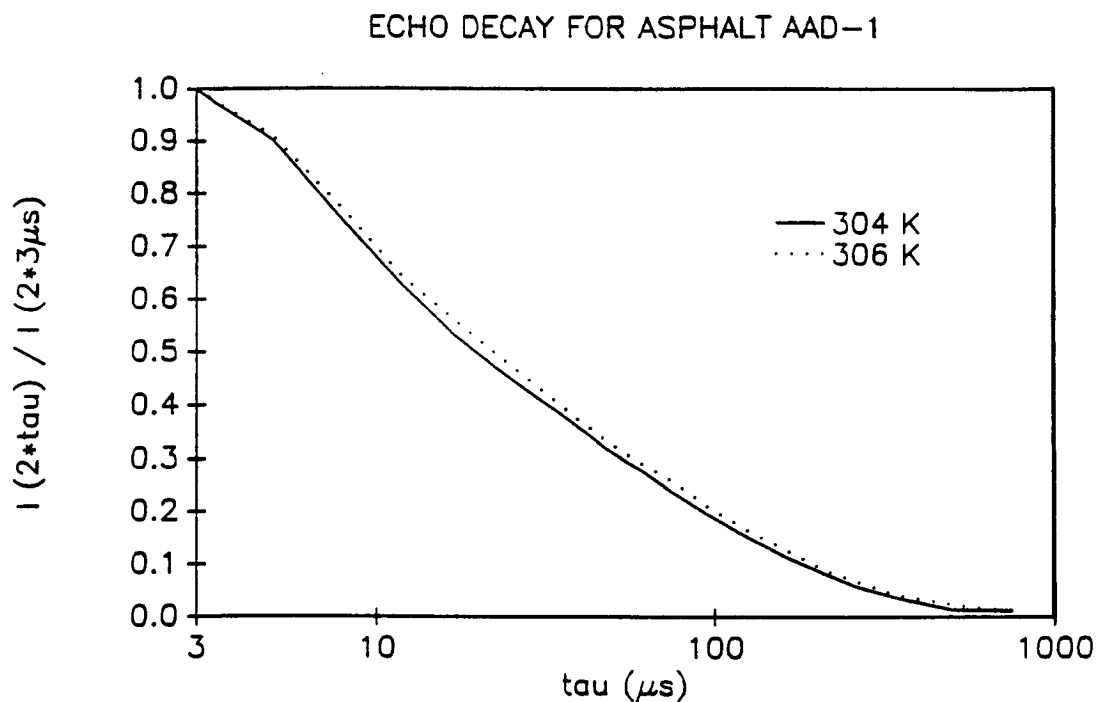


Figure 11. Echo decay illustrating that the profile is sensitive to a change in mobility corresponding to a 2° temperature change

ECHO DECAY AT 304 K FOR AAG-1 PLUS SOLIDS

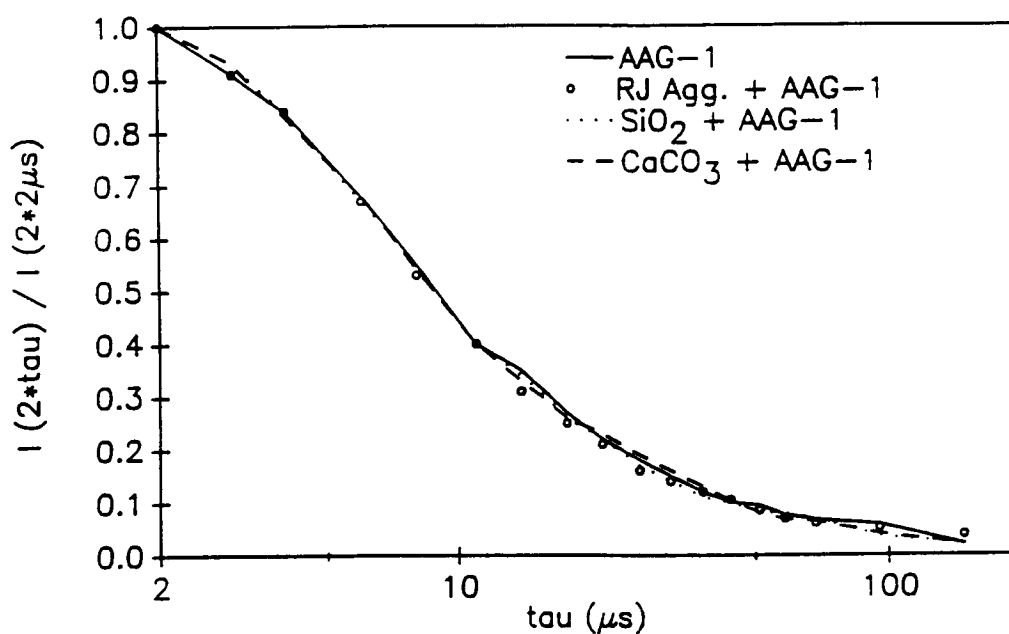


Figure 12. Echo decays for AAG-1 and several solids including the RJ aggregate. Decay uniformity implies molecular motion is not modified by the presence of solid material.

ECHO DECAY AT 304 K FOR AAD-1 PLUS SOLIDS

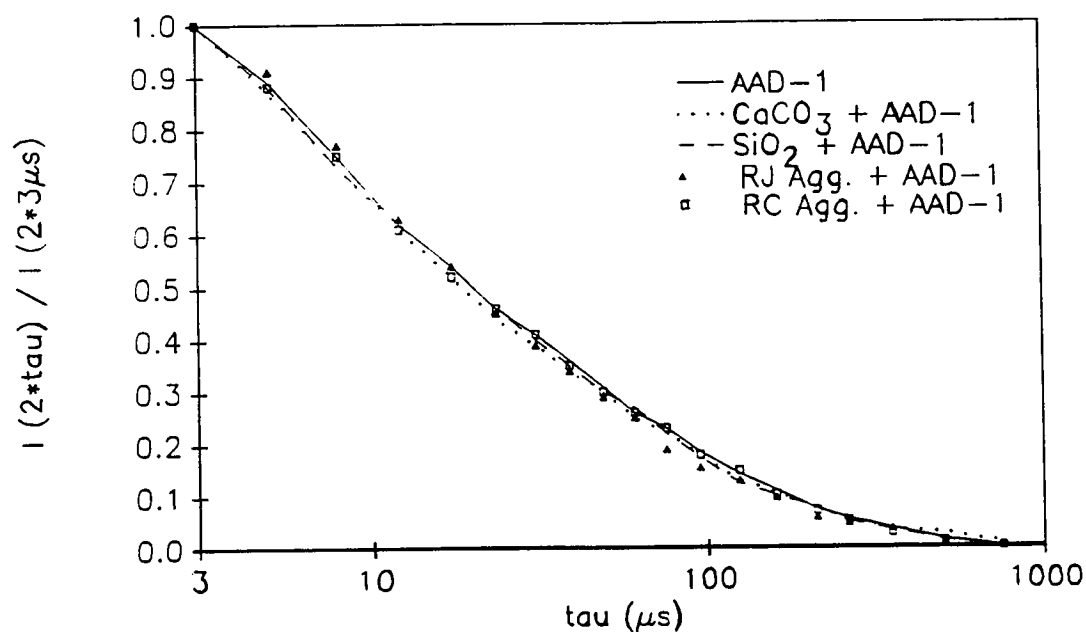


Figure 13. Echo decays for AAD-1 and its mixtures with various solids. There is no evidence that molecular motion is influenced by the presence of the solid.

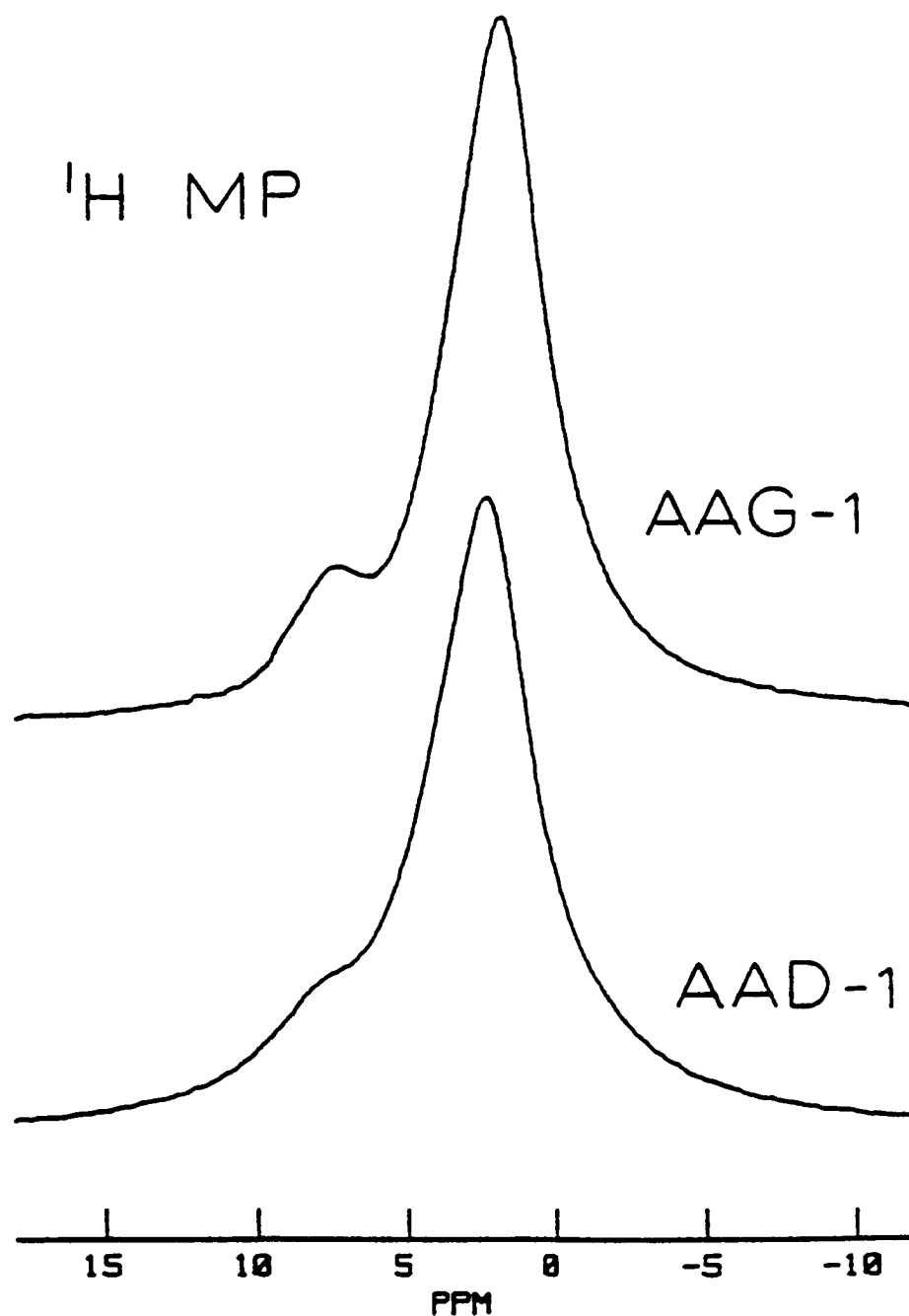


Figure 14. Normalized MP proton spectra of AAG-1 and AAD-1 using the MREV-8 sequence. The resonance near 7 PPM corresponds to aromatics. Resolution is slightly better for AAG-1 since there is less motion in the mid-kilohertz range.

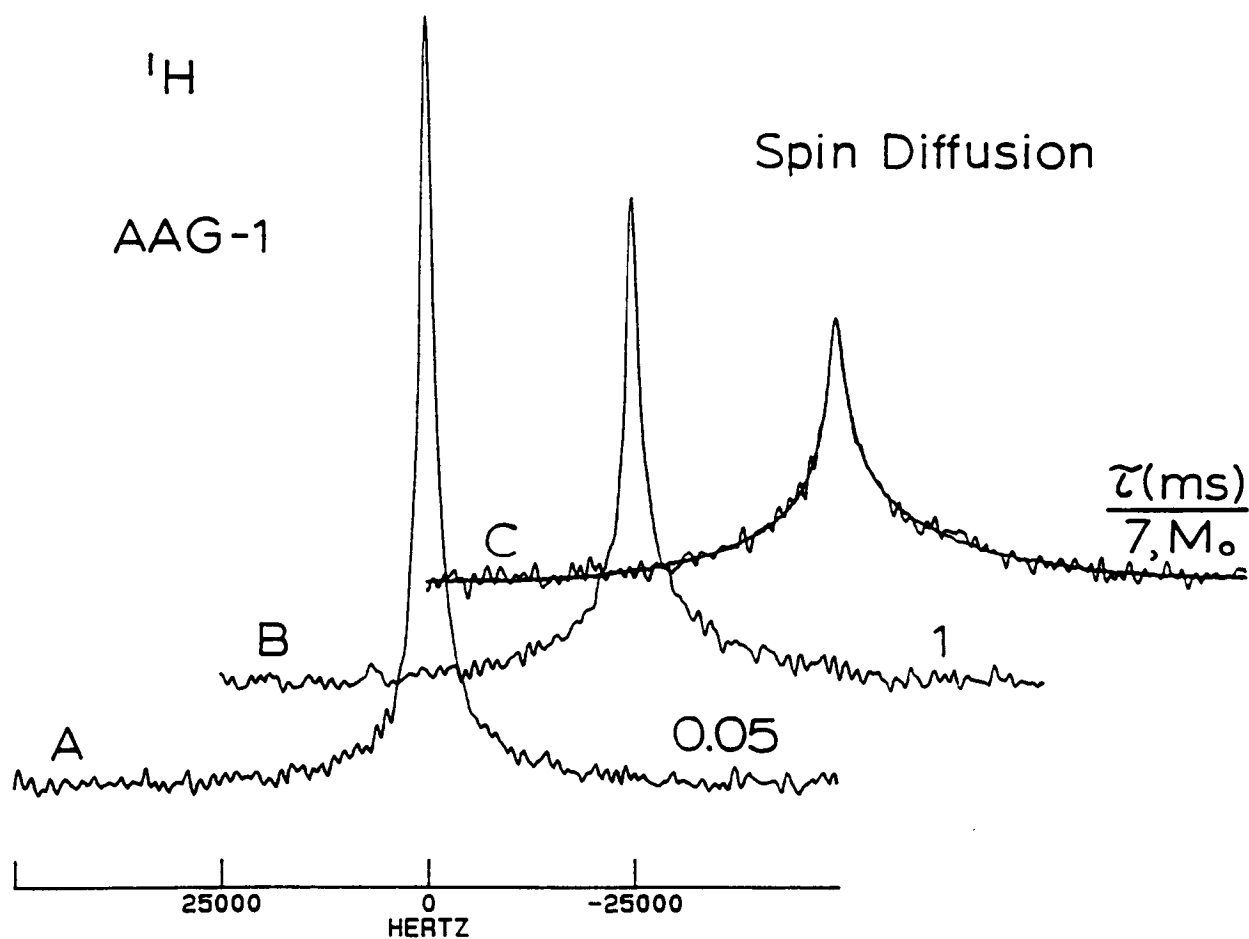


Figure 15. Example mobility-based spin-diffusion spectra of AAG-1. Spectrum A shows that initial polarization is enhanced over the mobile spins; internal spin equilibration is recovered after 7 ms implying that mobility variations occur over distances of approximately 4 nm.

HIGH-MOBILITY-SELECTIVE SPIN DIFFUSION IN ASPHALT AAG-1
(Spectra have equal areas)

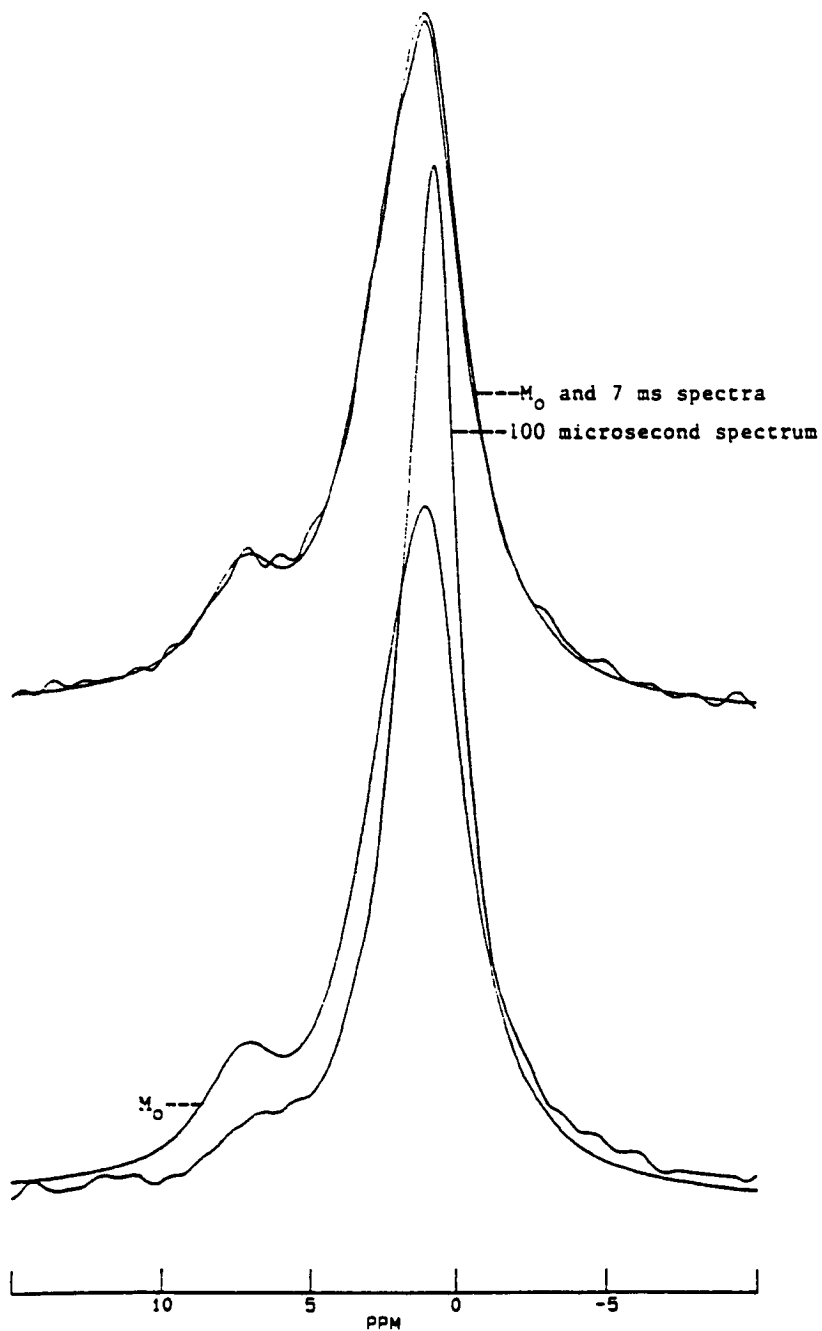


Figure 16. MP spin-diffusion spectrum of asphalt AAG-1. At early spin diffusion times (0.1 ms) where intensity is preferentially associated with mobile protons the MP spectrum demonstrates that mobility is identified with aliphatic-rich protons and a depleted aromatic content.

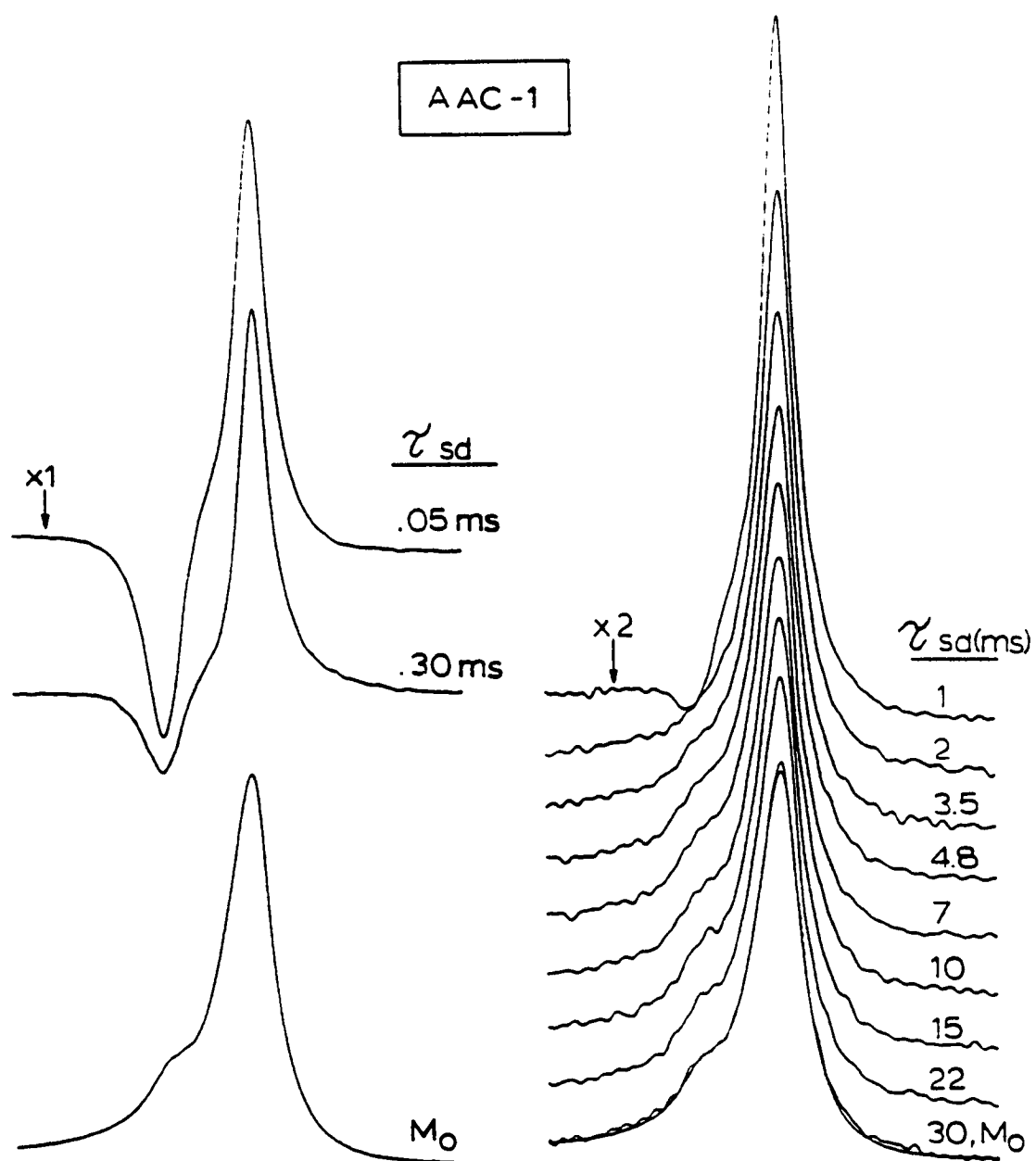


Figure 17. Chemical shift based, MP spin-diffusion spectra of AAC-1. Major lineshape changes occur in the first 2 ms. The spin diffusion spectra have intensities only 2% of the thermally equilibrated signal. The M_0 spectrum is appropriately scaled for lineshape comparison. The implied distance scale of aromatic/aliphatic variations in concentrations is small, ca. 4 nm.

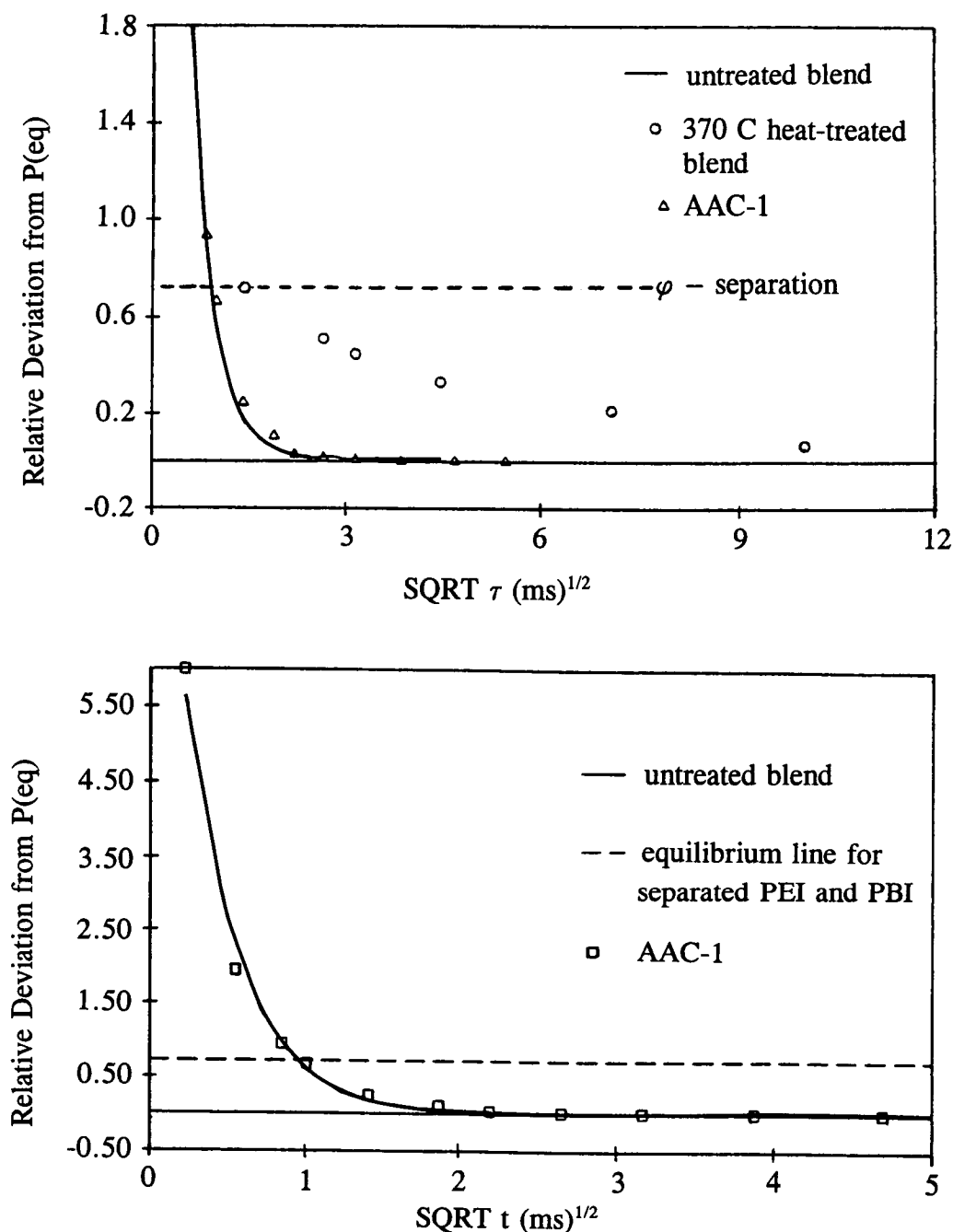


Figure 18. Comparison of chemical-shift-based spin diffusion data from a PBI/PEI polymer blend and asphalt AAC-1. The ordinate in these plots is proportional to the deviations in polarization per spin from internal spin equilibrium. Data corresponds to the behavior of the minority population of spins. The untreated polymer blend is mixed on a molecular scale; the heat treated blend is phase separated. The absence of a break in the asphalt data similar to that observed for the heat treated blend indicates that no domains are identified on a size scale larger than 2 to 3 times the molecular size.

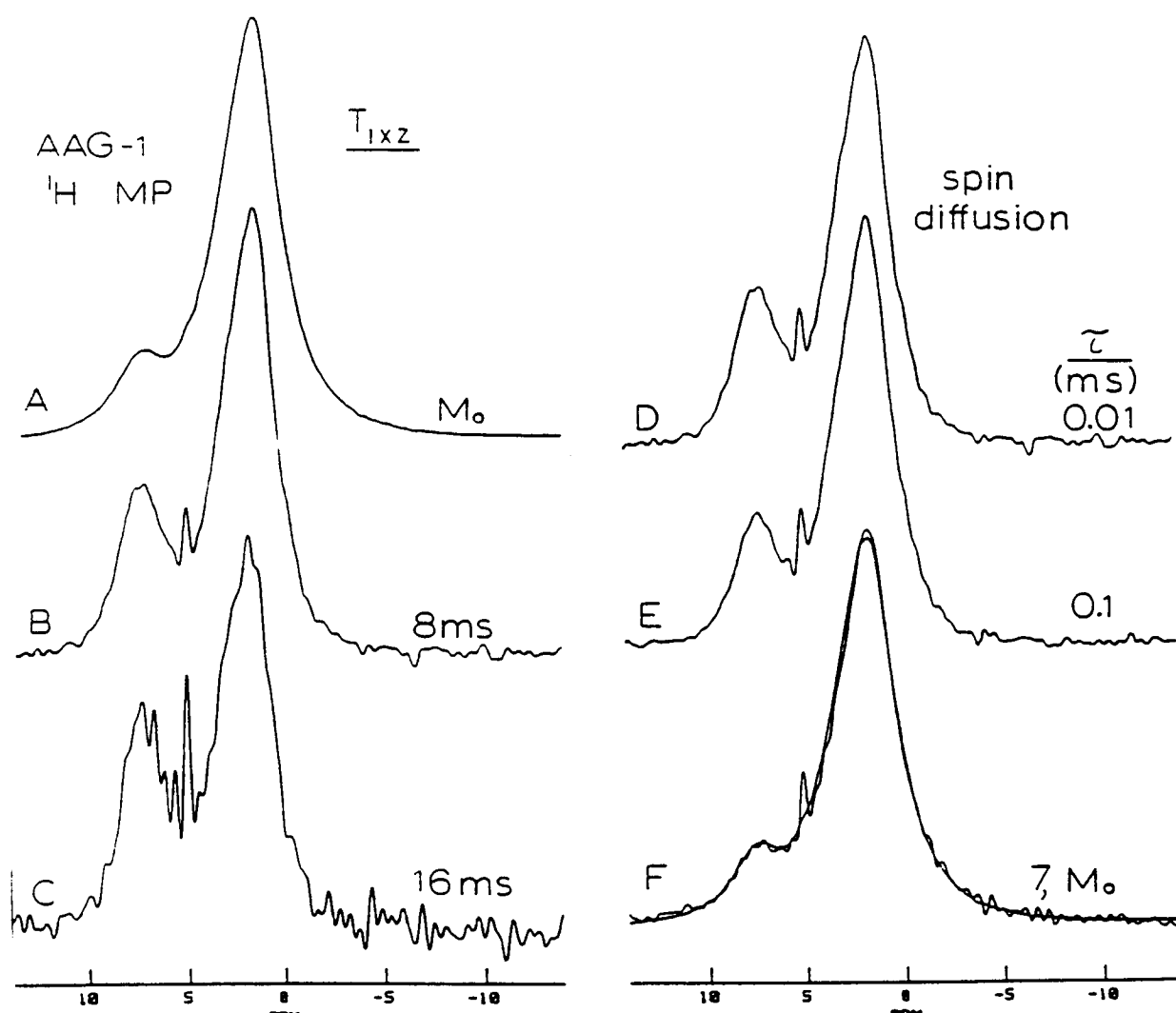


Figure 19. MP proton spectra as a function of MO spin locking in a T_{1xz} experiment (A-C); signals decay with time but are renormalized to the same total intensity for lineshape comparison. Spectra D-F are spin diffusion spectra following an 8 ms spin locking. The spin diffusion times are indicated. Equilibration with the M_0 lineshape at 7 ms reinforces the conclusion that domains are very small.

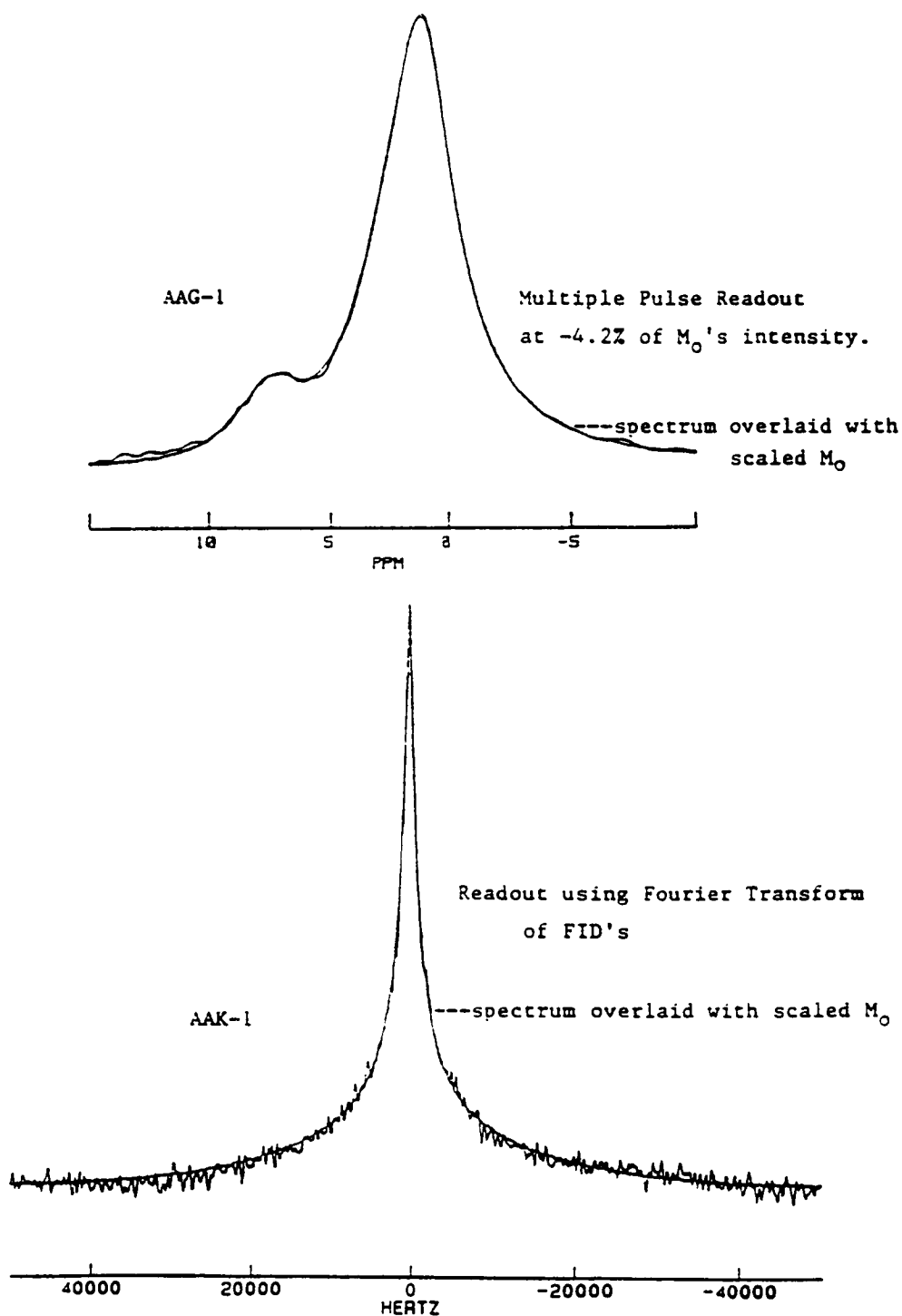


Figure 20. T_1 zero-crossing-spectra for AAG-1 and AAK-1, using MP and FID readouts respectively. These experiments are, in principle, more sensitive to the domain structure than are the chemical-shift-based or mobility-based spin diffusion experiments in the event that domains are large and their levels of contrast are smaller than the thresholds for the spin diffusion experiments.

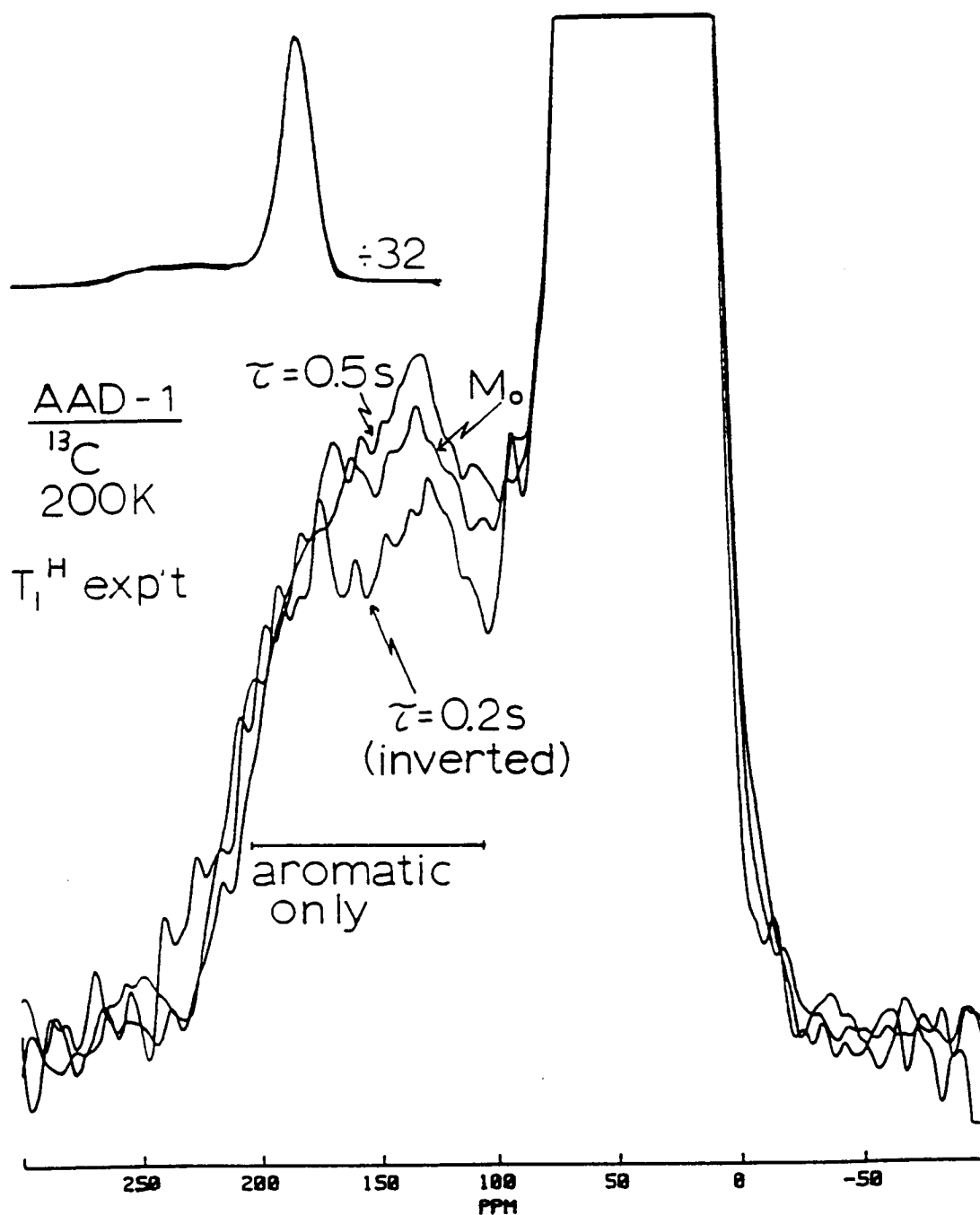


Figure 21. Proton T_1 -zero-crossing experiment at 200 K for asphalt AAD-1 using cross-polarized ^{13}C signals, which distinguish aromatic and aliphatic carbons, as the readout mode for the proton polarizations. The different amplitudes of the aromatic signals imply a large-scale phase separation. This is the only data which gives evidence of phase separation on a large (.40 nm) scale. This data is included for completeness but there is a chance that variations in the aromatic intensity are experimental artifacts rather than an indication of phase separation.

AAD-1 STRONG ACID FRACTION

AAG-1 STRONG ACID FRACTION

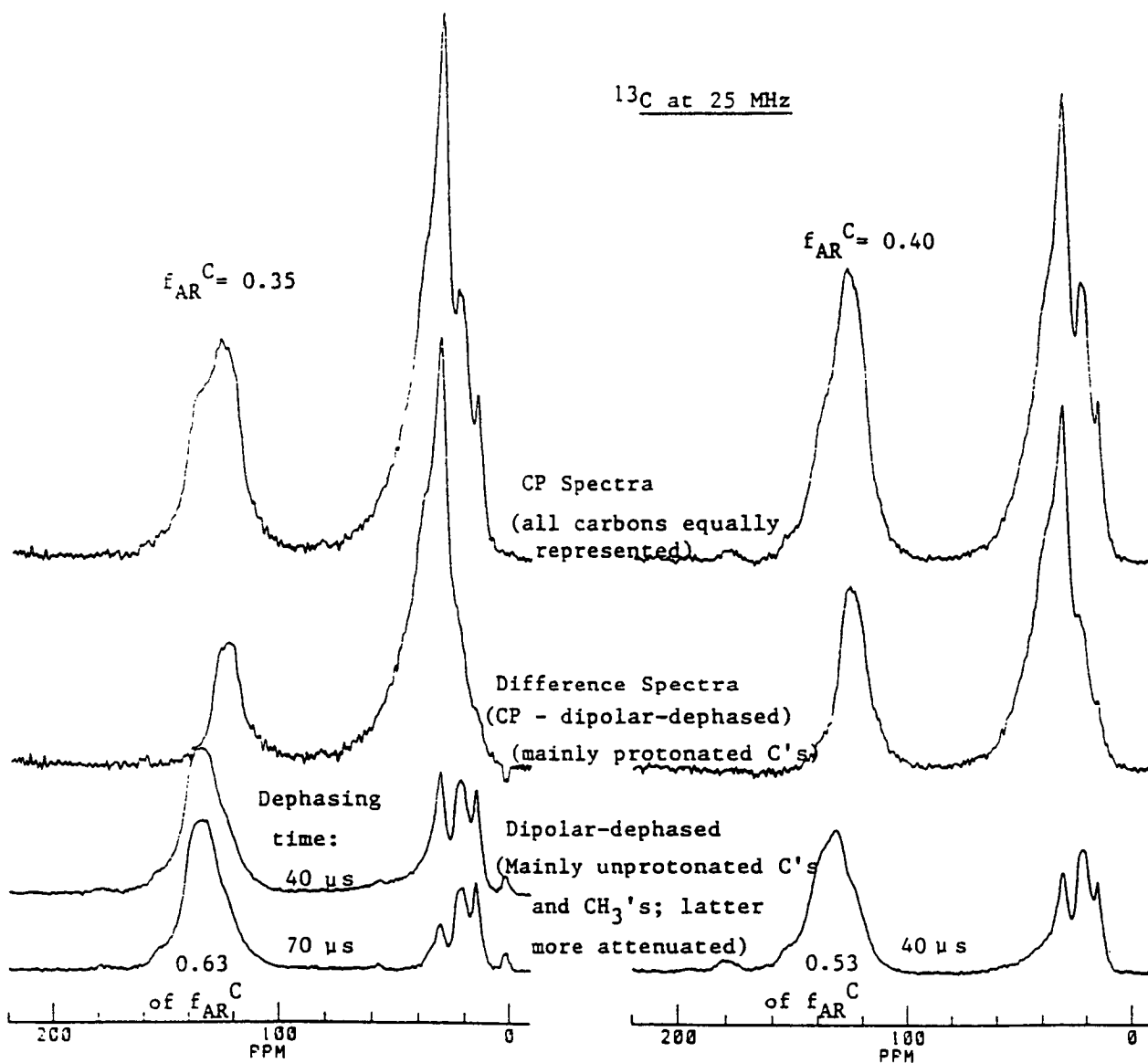


Figure 22. CP-MAS spectra of the AAD-1 and AAG-1 strong acid fractions which are brittle solids and lend themselves to a quantitative observation via ^{13}C NMR. These spectra, among other things, illustrate the level of chemical detail and how one can separate unprotonated from protonated carbons. See text for other deductions.

Tables

Table 1. Viscosities ($\times 10^{-3}$ poises) for the core asphalts at 298 and 333 K and some selected viscosities for oxidized samples.

Sample	η (1 rad/s, 298 K) ^a	η (1 rad/s, 333 K) ^b	η (333 K) ^c	η (333 K) ^d
AAA-1	275	1.24	1.2	0.86
AAB-1	1125	1.51	1.5	1.03
AAC-1	945	1.19	0.98	
AAD-1	406	1.64	1.3	1.06
AAF-1	3078	2.89	2.0	
AAF-1:ox-POV-400 h			80	
AAG-1	3540	3.00	3.0	1.86
AAG-1:ox-POV-400 h			23	
AAG-1:ox-TFO,POV-400 h		19		
AAK-1	1077	4.70	3.3	3.26
AAK-1:ox-POV-400 h			100	
AAK-1:ox-TFO,POV-400 h		73		
AAM-1	1123	2.76	3.3	1.99

^a Dynamic shear viscosities from J.H. Brandthaver et al, Preprints, Div. of Petr. Chem. 35, 376 (1990).

^b Dynamic shear viscosities from WRI SHRP Quarterly Report, June 1990, Table 1.1.2.2.

^c Dynamic viscosity measurement (specific conditions unknown). Ibid. Tables 1.1.7.a-3,4, and 6.

^d Viscosity measurement method unknown. Original data supplied by SHRP Materials Reference Library.

Table 2. Ratios of base proton intensities of various asphalts with respect to the base intensity of asphalt AAG-1 (estimated errors are ± 0.01)

Sample*	R_b at T = 300 K	R_b at T = 340 K
AAA-1	0.63	0.63
AAB-1	0.65	0.53
AAC-1	0.80	0.74
AAD-1	0.70	0.67
AAF-1	0.82	0.80
AAF-1: oxidized (TFO + POV)		0.87
AAF-1: oxidized (POV)		0.89
AAG-1	1.00 (definition)	1.00
AAG-1: oxidized (TFO + POV)		1.05
AAG-1: oxidized (POV)		1.06
AAK-1	0.71	0.82
AAK-1: oxidized (TFO + POV)		0.88
AAK-1: oxidized (POV)		0.87
AAM-1	0.72	0.63

* Oxidized samples have been obtained from WRI. The POV oxidation took place for 300 h at 333 K and 300 psi oxygen pressure; the TFO was carried out at atmospheric pressure at 436 K.

Table 3. Times* (in ms) required, at 300 K, for protons to reach internal spin equilibrium following the production of the polarization gradients indicated.

Asphalt	Mobility-based				Chemical-Shift-Based**		
	Unoxidized (FID)	(MP)	POV (MP)	TFO-POV (MP)	Unoxidized	POV	TFO-POV
AAA-1	7	15	15	7	60	60	60
AAB-1	7	15	15	15	60	60	60
AAC-1	7	15	15	15	60	60	60
					(30 @ 253 K)		
AAD-1	7	15	15	15	30	60	60
AAF-1	7				60	60	60
AAG-1	7	7			30		60
AAK-1	7	7	15	15		60	30
AAM-1	7	(This sample has very magnetic solids in it...iron pyrite?)					

*Times used were 2, 4, 7, 15, 30 and 60 ms. Maximum dimensions corresponding to these times are, respectively, 4, 6, 8 and 11 nm.

**These results were all taken at a total intensity of 1.5% of M_0 .

Table 4. Spin diffusion times for attaining spin equilibrium in a mobility-based experiment at different temperatures using FID-lineshape monitoring.

Temperature	AAD-1	AAF-1	AAG-1
300 K	7 ms	7 ms	7 ms
310 K	30 ms	30 ms	
320 K	60 ms	30 ms	15 ms
330 K	120 ms	120 ms	30 ms
340 K	240 ms	120 ms	30 ms

Table 5. Proton aromatic fractions^a (f_{AR}^H) and mass fractions^b ($m(x)$) associated with IEC separations

Asphalt	Ave. f_{AR}^H	$f_{AR}^H(N)$	$m(N)$	$f_{AR}^H(SA)$	$m(SA)$	$f_{AR}^H(BAL)^c$	$m(BAL)^d$
AAA-1	.073	.051	.596	.118	.174	.096	.230
AAB-1	.076	.061	.569	.136	.150	.074	.281
AAC-1	.064	.045 ^c	.682 ^c	.152	.075	.092	.243
AAD-1	.068	.045	.515	.097	.261	.088	.224
AAF-1	.087	.068	.567	.186	.154	.070	.279
AAG-1	.073	.062	.503	.157	.181	.041	.316
AAK-1	.068	.064	.522	.104	.187	.052	.291
AAM-1	.065	.050	.534	.132	.137	.061	.329

^a f_{AR}^H values are based on NMR data obtained at MSU by Prof. Jennings.

^b Mass fraction data is supplied by WRI for the strong acid (SA) and neutral (N) fractions.

^c Data in the last two columns are deduced, not measured; 'BAL' means balance, i.e. not SA or N.

^d The neutral fraction includes the 13.8% waxes which were separated prior to the IEC fractionation

Appendix A. Solution NMR Spectroscopy

Refinery source whole asphalts (AAA-1, AAB-1, AAC-1, AAD-1, AAG-1, AAK-1 and AAM-1), known as the SHRP Core Asphalts, were supplied by the SHRP Materials Reference Library. Samples from these core asphalts which had been fractionated by ion exchange chromatography (IEC) or were oxidized by pressure oxygen vessel (POV) procedure or by POV preceded by thin film oven (TFO) process, were submitted by SHRP A-002A contractors at Western Research Institute. All samples were stored and handled according to the standard protocol of the MRL. Oxidized asphalts were held in a freezer prior to use.

1. ^1H -NMR Spectroscopy

Sample size for ^1H -NMR analysis was 20 mg asphalt diluted to 1.0 ml with deuterated methylene chloride (CD_2Cl_2). Samples were held in a thin-walled 5 mm O.D. NMR tube. No relaxation agent was used for ^1H -NMR analyses. Data acquisition was 20 minutes per sample. The spectra were internally referenced to CD_2Cl_2 at 5.32 ppm.

The instrument used was the Bruker AC-300 spectrometer at 75,469 MHz with continuous ^1H broadband decoupling. Data were collected using the following parameters:

01 transmitter offset frequency	5449.190 Hz
SI spectrum size	32,000 points
SW sweep width	7812.5 Hz
PW pulse width	6.0 μ sec
RD relaxation delay	122 μ sec
AQ acquisition time	2 sec
NS number of scans	64
02 decoupler offset frequency	off

2. ^{13}C -NMR Spectroscopy

Sample size for ^{13}C -NMR analysis was about 100 mg in 0.5 ml CDCl_3 . Samples were held in a thin-walled 5 mm O.D. NMR tube. Approximately 5 mg of Cromium

(acetylacetonate)₃ [Cr(acac)₃] was added to each sample as a relaxation agent. Data acquisition required 8-12 hours per sample. The spectra were internally referenced to CDCl₃ at 77 ppm. To calculate specific amounts of O-methylated entities, a measured amount of tetramethylsilane (TMS, δ = 0.00 ppm) was added to some samples.

The instrument used was the Bruker AC300 spectrometer at 75,469 MHz with continuous ¹H broadband decoupling. Data were collected using the following parameters:

01 transmitter offset frequency	6137.164 Hz
SI spectrum size	32,000 points
SW sweep width	17857.145 Hz (236.6 ppm)
PW pulse width	4.0 μ sec
RD relaxation delay	3.0 sec
AQ acquisition time	0.918 sec
NS number of scans	8,000 to 12,000
02 decoupler offset frequency	4900 Hz

Aromatic hydrogen and carbon contents, expressed as percent of total hydrogen and carbon, were determined for whole, oxidized, and fractionated asphalts by high resolution proton and carbon-13 NMR spectroscopy. The measurement procedure consisted of: (i) manual phasing of each NMR spectrum; (ii) integration of the aromatic ¹H (1 - 5 ppm); ¹³C(109.8 - 159.7 ppm) and aliphatic ¹H(6 - 10 ppm); ¹³C(5.6 - 66.5 ppm) areas; and (iii) repetition of (i) and (ii) several times for calculation of an average aromatic/aliphatic ratio \pm one standard deviation. Statistical analysis via Murphy's Gap Test for sample uniqueness was afforded by replicate NMR experiments on : (i) three samples of each core asphalt for aromatic hydrogen; (ii) two samples of AAB-1, AAD-1, and AAG-1 for aromatic carbon; and (iii) a sample of AAA-1, AAB-1, and AAD-1 by a second operator for aromatic carbon.

3. Purification of tetrahydrofuran

It is critically important that tetrahydrofuran (THF) used in the following reactions is dry and peroxide-free. Only freshly distilled and tested THF was used.

HPLC grade THF (99.9%; Fisher) was dried by distillation from sodium and benzophenone in a nitrogen atmosphere. Sometimes several hours of refluxing were necessary to dry the THF. The distillate was tested for peroxide with Merkoquant peroxide test paper. Peroxide levels \geq 1.0 ppm were not acceptable. All reactions involving THF were carried out in shaded fume hoods.

Other methods of drying THF were sometimes used for particular reactions. All drying procedures took place in a N₂ atmosphere. Distillation from lithium aluminum hydride (LiAlH₄) was used for procedures (m), (o), (q). THF was also dried over calcium

hydride and sodium hydride and filtered over sodium hydride for procedure (c). For procedure (f) THF was dried over sodium hydride and filtered. In the second part of the methoximation procedure (o) THF was distilled first from cuprous chloride, then from LiAlH_4 , and for procedure (r) distilled THF was passed through anhydrous calcium chloride before asphalt was dissolved in it.

4. Short-term phase transfer methylation (16,17,18)

Asphalt (0.100 g) was dissolved in 100 ml of freshly distilled THF in a 250 ml Erlenmeyer flask equipped with a magnetic stir bar. 0.2 ml of aqueous tetrabutylammonium hydroxide, TBAH (40% wt; Aldrich) was slowly added, dropwise, and the mixture was stirred under nitrogen at room temperature for 20 minutes. Then 0.20 ml of a 45% (v/v) solution of carbon 13 enriched iodomethane (99.4 atom % ^{13}C) in carbon tetrachloride was added to the reaction flask and stirred overnight, under nitrogen, at room temperature.

Any THF remaining the next morning was removed by roto-evaporation at 30°C. The residue was dissolved in 100 ml of chloroform and then rigorously extracted, first with several aliquots of a 1-5% (wt) aqueous solution of sodium nitrate (total volume 1l) and then by several 150-200 ml aliquots of distilled water (total volume 4R.). During the course of the extraction small aliquots of the aqueous phase were tested for the presence of ionic iodide with the addition of a few drops of aqueous (21%) silver nitrate (Alfa). No iodide was detectable after 6-7 washings.

Chloroform was removed by roto-evaporation at 30°C and the residue dried for an additional 0.5 hr. at 70°C on the roto-evaporator.

Finally the product was dried at 70-80°C and ≤ 1 mm Hg for 2 hr. on a high vacuum pump.

5. Long-term phase transfer methylation of asphalt

Asphalt (0.500g) was dissolved in 150-200 ml of freshly distilled THF in a 250 ml Erlenmeyer flask equipped with a magnetic stir bar. Aqueous 40% (wt) TBAH (1.0 ml) was slowly added dropwise and the mixture was stirred under nitrogen at room temperature. After 3-5 hr, 0.20 ml of a 45% (v/v) solution of [^{13}C]-iodomethane (99.4 atom% ^{13}C) in carbon tetrachloride was added to the reaction flask. The solution was stirred overnight, under nitrogen at room temperature. Any THF remaining the next morning was removed at 30°C on a rotoevaporator. The product was dissolved in 150-200 ml of chloroform, then rigorously extracted first with several aliquots of a 1-5% (wt) aqueous solution of sodium nitrate (total volume 1l) and then by several 150-200 ml aliquots of distilled H_2O (total volume 4l). During the course of the extractions, small aliquots of the aqueous extract were tested for the presence of ionic iodide with the

addition of a few drops of aqueous (21%) silver nitrate (Alfa). No iodide was detectable after 6-7 washings.

Finally, the solvent was removed at 30°C on a roto-evaporator and the product was dried at 70-80°C and ≤ 1 mm Hg for 6-24 hr on a high vacuum pump.

The above procedure was performed three times on the sample.

6. Methylation of asphalt with sodium hydride and [^{13}C] - iodomethane (22,23)

Asphalt (0.405g) and sodium hydride (0.16g; 6.66 mmol) were dissolved in freshly distilled THF in a 250 ml Erlenmeyer flask. The solution was stirred under nitrogen at room temperature for 3 hr. [^{13}C]-Iodomethane 45%(vol) in CCl_4 (0.2 ml) was added and the mixture was allowed to react overnight, under nitrogen at room temperature. Any THF remaining the next morning was allowed to evaporate under nitrogen.

The residue was dissolved in 150 ml of chloroform (Baker A.R. 98.9%) and the mixture filtered into a 500 ml separatory funnel. Extraction and drying of the product was as described in the Short-Term Phase Transfer Methylation.

7. Double methylation of asphalt with sodium hydride and [^{13}C]-iodomethane

Asphalt that had been previously O-methylated with sodium hydride and [^{13}C]-iodomethane (0.260g) was dissolved in 150 ml freshly distilled THF. An excess of NaH was added and the mixture was then stirred and filtered under nitrogen. Anhydrous magnesium was added to the filtrate. This mixture was again filtered under nitrogen and allowed to react with the NaH overnight, under nitrogen at room temperature.

Four drops of HCl (aq.) were added to remove excess NaOH. An excess of NaH was again added to the reaction mixture. This was stirred under nitrogen for 3 hr. [^{13}C]-Iodomethane/ CCl_4 (0.20ml) was added and the mixture was stirred under nitrogen at room temperature for 20 hr.

The residue was dissolved in 150 ml of chloroform and stirred for 0.5 hr. The measured pH was 7-8. HCl (aq.) 10%(vol) was added until the pH measured was < 7 . The organic layer was extracted and dried as described in the Short Term Phase Transfer Methylation procedure.

8. Methylation of asphalt with [^{13}C]-diazomethane (30)

Precautions on the handling of Diazald and diazomethane should be reviewed before beginning this methylation.

Asphalt (0.0200 g) was dissolved in 30 ml of freshly distilled THF in a 100 ml round bottom flask equipped with a magnetic stir bar. The flask was attached to a Mini Diazald (Aldrich) apparatus, purged with nitrogen gas and cooled in a sodium chloride-ice bath (-21.3°C). Potassium hydroxide (0.4 g), distilled water (2.5 ml), carbitol (10 ml) and anhydrous ethyl ether (10 ml) were added to the reaction vessel of the mini diazald unit equipped with a stir bar and heated to $65\text{--}80^{\circ}\text{C}$ on a water bath. [^{13}C]-Diazald (99% ^{13}C) (0.0200 g) was dissolved in 50 ml of ethyl ether and very slowly added to the reaction vessel through a separatory funnel. The [^{13}C]-diazomethane/ether distillate was condensed via a dry ice/acetone cold finger into the asphalt solution over a period of 30 minutes.

Solvent was removed from the asphalt first under a stream of nitrogen, then on a roto-evaporator at 30°C .

The procedure was performed a second time on the same sample. The final product was dissolved in deuterochloroform, washed several times with distilled water and dried in vacuo.

9. Reduction of asphalt with sodium borohydride

Asphalt AAG-1 (0.495 g) was dissolved in pyridine which had been dried over lithium aluminum hydride/calcium hydride and filtered into a 250 ml Erlenmeyer flask. Sodium borohydride (2.5 g; Baker A.R.) was added and the mixture was stirred under nitrogen overnight.

The mixture was washed first with distilled water, then with 50 ml of a 2% (wt) aqueous NaOH solution. Benzene was added to separate the organic phase. The organic layer was extracted several times with 10% (vol.) aqueous HCl and then with distilled water. Finally solvent was removed from the product on a roto-evaporator.

10. Reduction of asphalt with lithium aluminum hydride

Lithium aluminum hydride was mixed with 100 ml of freshly distilled THF in a 3-neck, 500 ml round bottom flask equipped with a reflux condenser, a nitrogen gas inlet and a magnetic stir bar. A solution of asphalt AAG-1 (0.516g) in 150 ml freshly distilled THF was slowly added (over a period of 2 hr) to the slurry of lithium aluminum hydride. This mixture was stirred under nitrogen at room temperature for 3 hr. An additional 0.634 g

of LiAlH_4 was added and the mixture was allowed to react under the same conditions overnight.

The LiAlH_4 was hydrolyzed by the addition of 3.0 ml of a 10% (vol) aqueous sulfuric acid solution, followed by several ml of distilled water.

An aqueous solution of sodium chloride (1.3% wt) and 200 ml benzene were added to the reaction mixture. This was filtered and the filtrate extracted several times with an aqueous NaCl solution (total volume 1l) and then several times with a 1.1% (wt) solution of sodium carbonate.

Solvent was removed from the organic layer on a roto-evaporator.

11. Asphalt O-methylated with iodomethane, reduced with lithium aluminum hydride, O-methylated with [^{13}C]-iodomethane and reduced with lithium aluminum hydride

Asphalt AAG-1 was O-Methylated with 0.8 ml TBAH (aq.) and 0.35 ml of iodomethane (45% v/v in CCl_4) according to the Long Term Phase Transfer Methylation procedure previously described.

The O- ^{12}C -methylated asphalt was dissolved in 200 ml of freshly distilled THF and added slowly, dropwise, to a slurry of 0.53g LiAlH_4 in 100 ml THF. The flask was equipped with a reflux condenser and the mixture was stirred, under nitrogen for 6 h. Fresh LiAlH_4 (0.2g) was added to the reaction mixture and stirred overnight, under nitrogen at room temperature.

Distilled water was added, dropwise, to the reaction mixture to neutralize the excess LiAlH_4 . 50 ml of aqueous NaCl (1%) was added, dropwise, then 200 ml of benzene. The mixture was filtered into a separatory funnel and extracted with several aliquots of a 1% aqueous solution of NaCl (total volume 3l). Benzene and THF were removed by roto-evaporation.

The product was again methylated by the Long Term Phase Transfer Methylation procedure this time using 0.8 ml TBAH (aq. soln) and 0.35 ml of [^{13}C]-iodomethane (45% v/v in CCl_4).

Finally the product (0.067g) was reduced a second time. The product was dissolved in freshly distilled THF and 1.073 g LiAlH_4 was added. The flask was fitted with a reflux condenser and the mixture was stirred under nitrogen for 21 h.

Distilled water was slowly added, dropwise, to neutralize the excess LiAlH_4 , then dilute NaCl was added as before. Finally 100 ml benzene was added. The salted residue was

filtered and washed with benzene through a sintered glass funnel and transferred into a separatory funnel.

The organic layer was extracted several times with 1% NaCl (aq.) and then distilled water. The solvents were removed by roto-evaporation.

12. Methoximation of asphalt

Oximation of Asphalt Asphalt (0.517g) was dissolved in 150 ml of dry THF and held under N₂. Hydroxylamine hydrochloride (0.705 g; 10.14 mmol; ALD 99% ACS) was dissolved in 10 ml distilled H₂O and added dropwise, over a period of 20 min., to the asphalt solution. The mixture was stirred under N₂ at room temperature for 2 hr. Sodium hydroxide (0.420 g; 10.50 mmol) was dissolved in 7 ml distilled H₂O and this solution added dropwise, over a period of 20 min to the reaction mixture cooled in an ice bath. The mixture was warmed to room temperature and allowed to react under a stream of nitrogen overnight. The residue was dissolved in 100 ml chloroform, extracted several times with distilled water and dried in vacuo.

O-Methylation of Oximated Asphalt The oximated asphalt was dissolved in 200 ml dry THF. TBAH (aq.) (1.0 ml total) was added in 0.1 ml aliquots over a period of 4 hr. The reaction mixture was kept at room temperature under nitrogen. [¹³C]-iodomethane/CCl₄ (0.2ml; 45% v/v solution) was added and the mixture was stirred under a stream of nitrogen overnight.

The residue was dissolved in chloroform, extracted and dried as described in the Short Term Phase Transfer Methylation procedure.

13. Phosphorylation of asphalt with CDMPOPS

Asphalt (0.100 g) was azeotropically dried three times with benzene and then dissolved in 30 ml of dry THF in a 100 ml round-bottom flask. Dry distilled triethylamine (0.08 ml) and (2R, 4R, 5S)-2-chloro-3, 4-dimethyl-5-phenyl-1,3,2-oxazaphospholidine 2-sulfide (CDMPOPS) (0.0972 g) were added to the asphalt solution in a glove bag filled with nitrogen gas. The mixture was refluxed at 65°C under N₂ for 72 hr and dried in vacuo.

14. Phosphorylation of asphalt with ethylene chlorophosphite

Asphalt (0.065 g) was dried azeotropically three times with benzene, then in vacuo at 40°C for 2 hr. The product was cooled at room temperature in a desiccator over calcium chloride, then dissolved in 2.5 ml of deuteriochloroform (99.8 atom % ²H; Norell Inc.).

Dry, distilled ethylamine (0.2 ml; 99+%; Aldrich) and distilled ethylene chlorophosphite (0.2 ml; Lancaster Synthesis) were added to the asphalt solution in a 10 mm o.d. NMR tube in a glove bag containing anhydrous $\text{CaCl}_2/\text{P}_2\text{O}_5$ and filled with dry nitrogen passed through concentrated H_2SO_4 and potassium hydroxide.

Appendix B: NMR Basics for Data Interpretation

There are excellent books by A. Abragam²⁰ and M. Mehring²¹ which will offer much more detailed descriptions of each of the subjects briefly described below.

1. Dipolar Interaction

The dipolar interaction is the most important interaction to understand in order to view, with a critical eye, the results contained in this report. The proton lineshapes which are observed are centered at a frequency which is determined by the applied, external magnetic field, B_0 . This follows from the fact that all protons are characterized by a precession frequency which is exactly proportional to the strength of the magnetic field at each nucleus; the proportionality constant being the same for all protons. In a solid, each nucleus also experiences perturbing magnetic fields from other nuclei, which are themselves magnetic dipoles. The dipolar Hamiltonian, H_D , describing the energy of interaction for a proton spin pair, I_1 and I_2 , is

$$H_D = kr^{-3} (1 - 3 \cos^2\theta) (3I_{z1}I_{z2} - I_1 \cdot I_2) \quad (1)$$

where k is a collection of constants involving the gyromagnetic ratio of the two protons, r is the internuclear distance between protons, θ is the angle between the applied magnetic field and r , and z is defined as the direction along this applied field so that I_z 's are then the projections of spins along this direction. The important points to be noted in Equation 1 are: a) the dipolar interaction is very short range, falling off as r^{-3} so only the nearest few nuclei dominate this 'local' field; b) the term containing θ , when averaged over all angles on the surface of a sphere, becomes identically zero, implying that two spins in an isotropically rotating molecule (like a liquid) experience no dipolar field because the rotation is sufficiently fast; and c) for protons, I_{z1} and I_{z2} only take on the values $\pm 1/2$ and with nearly equal numbers in both states so that dipolar broadening is symmetric.

In Figure B-1 we illustrate, using some experimental lineshapes, that lineshapes depend on the structure of molecules and that motion, when it occurs fast enough, is capable of partially averaging (i.e. narrowing) these resonances. Spectra of linear polyethylene (LPE), polystyrene (PS) and poly(benzobisthiazole) (PBZT) are shown in Figure B-1,

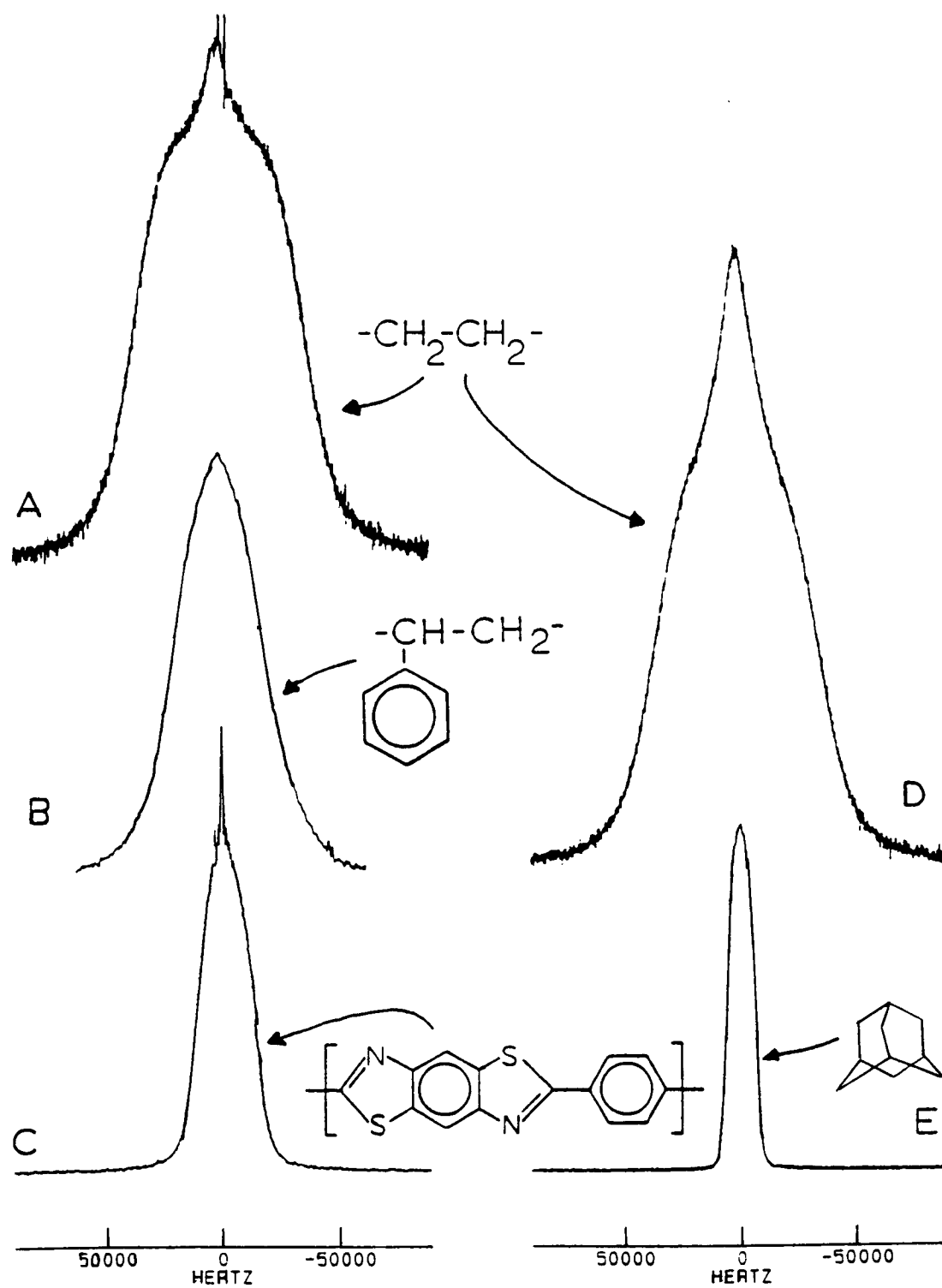


Figure B-1. Proton spectra illustrating the influence of proton distribution and motion

indicated as *A*, *B* and *C*, respectively. These materials are presented in decreasing order of proton density. Thus, we would expect that the linewidth would also follow the same trend. In particular, in organic materials, the closest proton pairs are those on the same carbon ($r = 0.18$ nm). Thus, for rigid molecules, linewidths would decrease as one went from methyl (CH_3) to methylene (CH_2) to methine (CH)-type protons. In actuality methyl resonances are comparable to methine resonances above liquid nitrogen temperatures since methyl groups typically rotate rapidly about their axes of symmetry. Thus, the main (rigid-lattice) contributions to the lineshapes in *A*, *B*, and *C* in Figure B-1 have linewidths (fullwidths at half height), respectively, of 75, 43 and 25 kHz, corresponding to the diminishing importance of methylene protons. PBZT in 1C, is an extreme case because, in addition to the absence of methylene protons, the CH protons are unusually isolated, there being two ortho-pairs on one aromatic ring ($r = 0.25$ nm) and one pair in para-substitution on another aromatic ring ($r = 0.50$ nm).

The second point to be illustrated in Figure B-1 is the effect of molecular motion on the lineshape. The LPE samples in *A* and *D* of Figure B-1 are the same material but two different preparations. The first is pressure crystallized, with the result that almost 95% of the material is crystalline. In *D*, the sample is the as-received pellets and crystallinity is about 70%. The non-crystalline (NC) resonances are responsible for the narrower features in the center of the spectra. These features have linewidths in the range of 11 - 16 kHz. The linewidth reduction is a result of fast *anisotropic* motion of the NC methylene segments. From the literature² we know that the correlation time for NC molecular motion at ambient temperature is shorter than 10^{-8} s and that this motion is predominantly 3-bond motion. The NC linewidth is determined more by the anisotropic character of the motion than by the correlation time of the motion in the sense that an order of magnitude change in correlation time would not be noticeable but any change in the anisotropic character of the motion, i.e. the angles over which motion is averaged, would affect the linewidth. (Incidentally, all spectra were taken at ambient temperature except for *B* (202 K).) In *E*, the adamantane molecule represents a contrasting case where this very spherical molecule rotates *rapidly* and *isotropically*, but stays on its own lattice site in the crystal. Therefore, the observed linewidth represents interactions exclusively between protons on *different* molecules. The linewidth is still 12 kHz in width, which reflects the sheer numbers of protons on neighboring molecules as opposed to the strength of the dipolar interaction between any intermolecular pair of spins.

Figure B-2 depicts, in a very approximate way, the change of intramolecular dipolar linewidth as a function of correlation time, for different kinds of protons, assuming methyl group rotation. The lineshape narrows over a range where the correlation time for molecular motion is within an order of magnitude faster or slower than the inverse of the second moment, M_2 , of the lineshape, expressed in radians. The linewidth at very short correlation times is dependent on the exact nature of the anisotropic motion. If motion is isotropic, linewidths (e.g. *E*) can still be of the order of 10 kHz, and further narrowing does not occur unless translational diffusion at correspondingly rapid rates is simultaneously occurring over distances of at least the order of 1 nm. If the latter

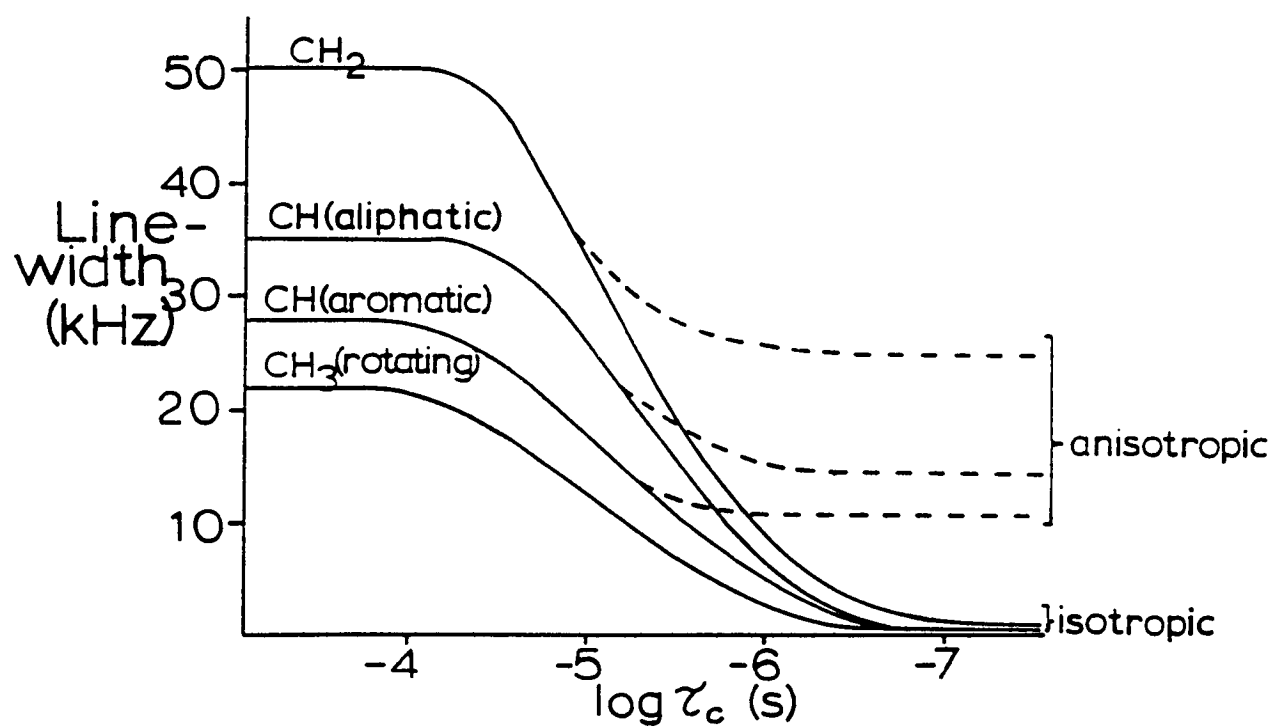


Figure B-2. Typical proton linewidths versus correlation time for isotropic and particular anisotropic motion

translational diffusion is present, along with isotropic motion, linewidths can easily fall into the 1 kHz category, or below.

2. Chemical Shift

The chemical shift arises primarily because the electron cloud surrounding each nucleus is capable of slightly modifying the external applied field. Moreover, since the electron cloud is usually not identical from proton site to proton site, nor is the cloud generally spherical in shape, it follows that nuclei at different sites in the molecule have slightly different resonance positions (different isotropic chemical shifts); they also have anisotropic chemical shifts (chemical shifts which depend on the orientation of the molecule in the magnetic field). For protons the isotropic chemical shift range is rather small, 8 - 10 ppm. Major groupings of isotropic shifts are such that, using tetramethyl silane as a reference at 0 ppm, aliphatic protons on carbons not attached to aromatic rings lie in the 0 - 2 ppm range. Aliphatic protons on carbons attached to aromatic rings generally are found in the 2 - 4 ppm range, and protons on aromatic carbons generally fall into the 6.5 - 8 ppm region. Hydroxy protons are often in the 4 - 5 ppm range while carboxylic acid protons can be found over quite a range of values, often at shifts substantially higher than 8 ppm. The range of anisotropic chemical shift values is generally about 4 - 7 ppm for an aliphatic proton. In liquids, the anisotropic shifts are averaged to zero by isotropic molecular motion in a manner similar to the averaging of the dipolar interaction.

^{13}C nuclei have much larger chemical shift ranges, about 200 ppm for both isotropic and anisotropic effects. Thus, the richness of chemical information is potentially much greater for ^{13}C spectra compared with proton spectra.

3. Magic Angle Spinning

In principle, this method takes advantage of the fact that both the dipolar and chemical shift interactions are second rank tensors of order zero, defined with respect to the static magnetic field (B_0) direction. If spinning is fast with respect to both of the interactions, it is easy to show mathematically that when a sample spinning axis is oriented such that it makes an angle ($54^\circ 44' = \arctan \sqrt{2}$) with respect to B_0 , then both the dipolar and chemical shift interactions are averaged to zero. In practice, magic angle spinning (MAS) is usually too slow to average the strong dipolar interactions, but it does a good job on the chemical shift interactions. In fact, for the latter interaction one need not spin faster than the interaction in order to see a resonance at the isotropic chemical shift. However, if spinning is slower, then other absorptions called spinning sidebands appear, displaced from the central resonance position by the spinning frequency.

4. Magnetization

The magnetization is the population excess in a given spin state relative to another spin state. NMR signals arise from population *differences* between energy levels connected by the magnetic dipole operator, I_x , where the x axis is defined to be perpendicular to the static field (z) direction. The energy levels giving rise to these population excesses have energy differences in the millidegree Kelvin range. Thus, the population differences at ambient temperatures are of the order of 1 in 10^5 . As a result, the NMR signals are usually quite weak, particularly for ^{13}C since its isotopic abundance is only 1.1%. (Protons are 100% naturally abundant.) Computer-aided signal averaging is the usual method for enhancing signal-to-noise ratios.

5. Relaxation

This is the process by which a non-equilibrium magnetization returns to its normal Boltzmann population. Relaxation is generally determined by the characteristics of molecular motion. T_1 is the time constant for reequilibration along the static field B_0 . It is determined by motions whose components lie in the mid-MHz range, near the resonance frequencies of the nuclei themselves. T_{1e} is the time constant for reequilibration of populations quantized (or 'locked') along the rf field, B_1 . Since these energy levels are separated by spacings about three orders of magnitude less than those along B_0 , this relaxation is sensitive to motions about three orders of magnitude slower, i.e., the mid-kHz range. (It is important to recognize that in a solid where motions are typically slow, the presence of motions with components in the kHz range is much more likely than motions with components in the MHz range, therefore, T_{1e} is generally much shorter than T_1 .) A typical range for T_1 in solids is 0.1-1000 s, and for T_{1e} , 0.1-1000 ms. The relaxation time T_2 is not a relaxation time associated with energy levels. It is a description of the time constant for the persistence of magnetization in the observation plane of detection (normal to B_0). As such, in a solid it is often inversely proportional to the dominant interaction experienced by the nucleus being observed, e.g., the dipole-dipole interaction or the chemical shift interaction.

6. Spin diffusion

This is the process of magnetization transport between like spins in the presence of a magnetization gradient. In this paper spin diffusion will refer mainly to proton-proton spin diffusion. The basis for the process is the existence of dipolar couplings in an organic system. There is a term in the Hamiltonian of Equation 1 whereby, if I_{z1} is $+1/2$ and I_{z2} is $-1/2$, then these two spin states will exchange on a timescale of the inverse of the dipolar coupling between the two spins. The notion that each spin is coupled to several other spins and not just one allows this 'spin-exchange' to form the basis for spin diffusion, which is no more than a phenomenological averaging over several spin-exchange events. It is also assumed in spin diffusion that the entire solid is a coupled

network in that there are no islands of spins isolated by barriers. It is known that spin exchange is by no means a random process so that on a microscale (a scale of molecular dimensions) it is probably inappropriate to speak of diffusion, yet because of the many-body nature of the spin-spin interactions, the diffusion equations are a good approximation.

Spin diffusion proceeds most efficiently when the spins are quantized along B_0 . By comparison, the diffusion constant describing diffusion when the magnetization is quantized along a large, resonant B_1 radiofrequency field is half as big. The observation of spin diffusion effects requires that magnetization gradients be established within the system. The production of such gradients requires some kind of inhomogeneity to be present in the system. For example, in a phase-separated polymer blend, one phase may be more mobile than the other. Thus, relaxation should be more efficient in one phase than the other. Consequently, as relaxation proceeds, gradients would tend to appear. Spin diffusion would then tend to resist the establishments of strong gradients in a mixed system. With diffusion constants in the range quoted above, we can estimate the distances over which proton magnetization might propagate in times characteristic of T_1 or T_{1e} . A formula which can be used to estimate a mean squared displacement, x , is

$$x^2 = 4Dt/3 \quad (2)$$

where t is the diffusion time and D is the spin diffusion constant which, for rigid organic systems, will usually lie in the range of $3 - 6 \times 10^{-12} \text{ cm}^2/\text{s}$. A D of about $5.5 \times 10^{-12} \text{ cm}^2/\text{s}$ is probably appropriate for rigid asphalt molecules.

7. Cross-polarization

This is the process (abbreviated CP) in which unlike spins which are dipolar-coupled to one another can transfer magnetization from the spin system of higher order (or higher polarization per spin) to that of lower order. In the usual so-called spin-lock CP strong resonant rf fields are applied to the proton and ^{13}C spin systems. The magnetization is initially ordered along the proton rf field and then part of this order is transferred to the ^{13}C nuclei in a level-crossing experiment. The net result is that when the so-called Hartmann-Hahn condition²² is fulfilled, the carbons respond as if they were protons. In this process, the total order is redistributed by spin diffusion among the carbons and the real protons. In this way, the carbons gain a polarization approximately four times larger than their corresponding Boltzmann polarization. Two important advantages arise out of the use of the CP method: first, signal enhancement and second, the carbons (with their greater resolution in the solid state) can be used to monitor the local proton magnetization. The disadvantage of the method is that cross-polarized ^{13}C signal strengths can be distorted. The reasons for these variations are manifold, but some of the more common ones are unequal T_{1e} 's in a sample, differences in CP efficiencies between protonated and unprotonated carbons (the necessary dipolar couplings are weaker for the latter), and nearly isotropic motion in some regions of a sample (giving

very weak dipolar couplings). In a polymer system below the glass transition temperature, the principal source of intensity distortion is the difference in efficiencies between protonated and unprotonated carbons. It usually takes about 200-500 μs to generate full intensity for a protonated ^{13}C signal and about 1-3 ms for an unprotonated ^{13}C signal.